Durham E-Theses

Guest-host effect of dyes in polymer dispersed liquid crystals

Masutani, Akira

GUEST-HOST EFFECT OF DYES IN POLYMER DISPERSED LIQUID CRYSTALS

A thesis submitted for the degree of

Doctor of Philosophy

By

ira Masutani

University of Durham

Department of Physics

October 2002

ABSTRACT:
GUEST-HOST EFFECT OF DYES IN
POLYMER DISPERSED LIQUID CRYSTALS
BY AKIRA MASUTANI

The guest-host (*GH*) effect of a tetracyanoquinodimethane (*TCNQ*) dye in nematic liquid crystals (*LC*) and polymer dispersed liquid crystals (*PDLC*) has been studied and compared with commercial azo and anthraquinone dyes. The adduct (*MORPIP*) is a conjugated molecule with a high dipole moment of 15 Debyes.

E7 LC doped with MORPIP was found to give a dichroic ratio of 2.34 and an order parameter of 0.31; these values are lower than for the other dichroic dyes, typically 0.6 - 0.78. However, MORPIP showed a useful property when doped in LC and PDLC samples. The rise time of E7 was decreased by 21% when doped with 0.3 wt% MORPIP. It was suggested that MORPIP increased the dielectric anisotropy of E7 and hence reduced the rise time. Nevertheless, no change in dielectric anisotropy was observed. This observation favours a model in which the dipolar dopant reorients rapidly in the applied field and drives the reorientation of the surrounding LC. The effects of the dyes incorporated in PDLCs were also studied, in order to explore their suitability for use in a colour reflective display. Dichroic PDLCs were made using the photo-initiated phase separation method. 0.37 wt% MORPIP doped PDLCs showed a 45% faster response to an applied electric field than that of the undoped PDLCs. However, the contrast ratio of the dichroic PDLCs was not sufficiently high for display use due to insufficient scattering and dye trapping.

Two new fabrication methods were developed to overcome this problem. One method involved the preparation of a network type PDLC into which a doped LC was dispersed. Another method involved the preparation of voids by removing the LC from the PDLC. In both methods, subsequent re-filling of the doped LC into the pre-made polymer matrix improved the contrast ratio and reduced the decay time of the dichroic PDLC.

Declaration

I hereby declare that the work presented in this thesis has not been previously submitted for any degree and is not being currently submitted in candidature for any other degree.

Signed...... *A. Mountain* ...

Candidate

The work reported in this thesis was carried out by the candidate. Any work not carried out by the candidate is acknowledged in the main text.

Signed......

Ph.D. Supervisor

Signed......

Ph.D. Supervisor

Signed...... *A. Mountain* ...

Candidate

Statement of Copyright

The copyright of this thesis rests with the author. No quotation from it should be published without his prior written consent and information derived from it should be acknowledged.

To my wife Nahoko and my daughter Ayaka

ACKNOWLEDGEMENTS

Not to us, O LORD, not to us but to your name be the glory,

because of your love and faithfulness.

Psalm 115:1

TABLE OF CONTENTS

LIST OF FIGURES

LIST OF TABLES

Chapter 1: Introduction

1.1.Introduction

Polymer dispersed liquid crystal (PDLC) film [1-4], which consists of micron-sized
liquid crystal (LC) droplets dispersed in a polymer matrix, shows an
interesting optical property based on voltage-controlled light scattering by
nematic droplets. PDLC is believed to be one of the most promising display
modes to overcome some problems faced by the *liquid crystal display (LCD)*
technologies of today. The main problems associated with conventional LCD
are the achievement of bright colour, the limits on both the size and cost, and
a short battery life. Some work [5-8] has led to the belief that the combination
of coloured dyes with PDLC would yield a bright flexible full-colour paper-
like display.

The main objectives of this work are; firstly to investigate the interactions
between liquid crystals and dyes, particularly with a highly dipolar dye
synthesised within the University of Durham and secondly to fabricate a
dichroic PDLC of commercial standard. The exact requirement for the
standard is stated in later Section 1.4.4.2, where a prototype of the paper-like
display target is explained.

This chapter lays the foundation of this work by describing the historical
development, trends, controversies and breakthroughs in the field of liquid

crystals and PDLCs, along with a description of their strengths and weakness, application, and justification and both strength and weaknesses. Chapter 2 contains an account of the basic characterisation of the dyes used in this work. Chapter 3 discusses the interactions between highly dipolar dyes and the liquid crystals, in which an improvement in liquid crystal switching speed was demonstrated [9]. Chapter 4 introduces the fabrication procedures of the PDLCs, and problems encountered with the preparation of dichroic PDLCs. Two new PDLC fabrication techniques [10] are proposed, which result in the increased contrast and decreased turn-off time.

1.2. LC History

In 1888, an Austrian botanist Friedrich Reinitzer [11] reported an observation of liquid crystalline behaviour for the first time. In his experiment, Reinitzer increased the temperature of a cholesteryl benzoate crystal to measure the melting point of the compound probably because benzoate compounds has sharp melting point. During this experiment, he watched the crystal change into a "hazy liquid" at 143.5 °C. As the temperature increased further to 178.5 °C, he observed that the material changed again into a clear, transparent liquid.

A year later, a German physicist Otto Lehmann [12] investigated the "hazy liquid" under a polarising microscope, and observed that the material exhibited a property known as *birefringence* (Section 1.3.2). A birefringent material has the ability to rotate linearly polarised light, and, at that time,

birefringence was believed to be a property exclusive to certain crystals such as calcite or quartz. Lehmann called the "hazy liquid" by the term *"Liquid Crystal"* - the term indicating that the substance has one or more phases between the solid and liquid phases. He concluded that when a solid melted into a liquid crystal state, it lost positional order but some orientational order remained (Figure 1-1).
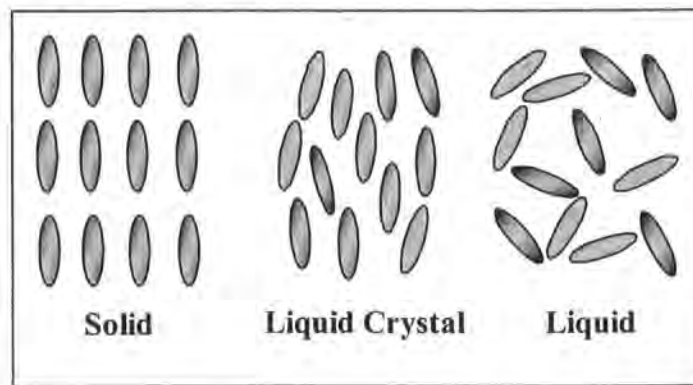
Figure 1-1. Schematic figure of solid, liquid
crystal and liquid phases.

While early papers [13-18] described a variety of new phenomena, materials and devices, the field of liquid crystal display technology only began to expand in the 1970s after the discovery of stable compounds such as methoxybenzylidene-p'-n-butylaniline (MBBA) [19, 20] and widespread adoption of the *twisted nematic* (TN) effect [21] (Section 1.4.2).

1.3. Physical Properties

1.3.1. Types of Liquid Crystal

There are two types of liquid crystal phases known as *thermotropic* and *lyotropic liquid crystals*. Thermotropic liquid crystals are most commonly used for display applications. They form a stable liquid crystal phase over a particular temperature interval. For example, the thermotropic liquid crystal E7 used in this work, exhibits liquid crystal properties only between -10 and 61°C [22]. On the other hand, a lyotropic liquid crystal forms a liquid crystal phase when mixed with a solvent. Lyotropic liquid crystals can be found in plants and animals, and play a vital part in the activities of living materials, such as living tissues, cell membranes, tendons, muscles, nerves, proteins, etc. Industrial applications of lyotropic liquid crystals are: soap, emulsion, detergents, oil recovery, food industry, etc. As lyotropic liquid crystals are not used for display applications, this work is only concerned with thermotropic liquid crystals.

Thermotropic liquid crystal materials [23-27] generally have a rod-like molecular structure with a rigid long axis (e.g. biphenyl) and flexible tails (e.g. alkyl chains). They may also contain groups with permanent dipoles (e.g. CN groups) and easily polarisable substituents (e.g. chlorinated substances). Depending on those parameters and the temperature, thermotropic liquid crystal materials can have several phases within the liquid crystal phase. In

1922, Friedel [28] classified liquid crystals broadly into three categories: *nematic,*
cholesteric and *smectic.* These phases are schematically illustrated in Figure 1-2.
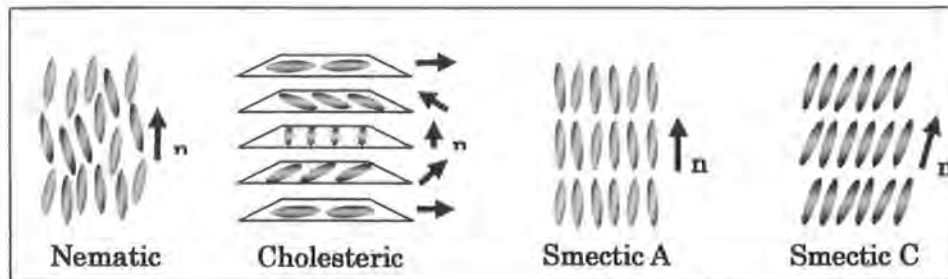
Figure 1-2. Nematic, cholesteric and smectic
phases of liquid crystal.

The most commonly occuring phase is the nematic in which the molecules do
not hold a positional order but maintain a preferred orientational direction.
The average alignment direction of the liquid crystal molecules is indicated by
the *director, n.*

The cholesteric liquid crystal phase [23-27] is typically composed of nematic
molecules with a chiral-induced twist in the directors. This leads to the
formation of a structure with very thin nematic-like layers where the director
in each layer is twisted with respect to those above and below, i.e. the
directors form a continuous helical pattern about the layer normal.

Smectic liquid crystals [23-27, 29] have at least twelve different phases such as
smectic A, B, C, etc., with the phases being labelled not according to any
microscopic properties, but rather by the chronological order of their
discovery. In this state, the molecules not only point along their director, but

also tend to align themselves in layers. In the smectic A phase, the director is perpendicular to the layer plane. In the smectic C phase, the molecules in each layer are tilted at a certain angle to the layer normal. The viscosity and the temperature range for a smectic phase is much higher than that of a nematic liquid crystal.

All liquid crystals used in this work are of the nematic type. They are the most appropriate LCs for the investigation of the interaction between dyes and liquid crystals, called the *Guest-Host (GH) effect*, because other types of LCs have additional inter molecular effects which may complicate the matter. The LC used for the fabrication of the PDLCs were also nematic. All references made to liquid crystals from here on refer only to nematic liquid crystals unless otherwise specified.

1.3.2. Optical Anisotropy (Birefringence)

The directional order within liquid crystals leads to the condition known as *anisotropy* which means that material properties vary with direction, i.e. are not isotropic. It is the existence of these anisotropic properties which give rise to a variety of phenomena not observed in the isotropic liquid state and which make these materials interesting to study and to use in applications.

The anisotropic nature of liquid crystals gives them an anisotropic optical property known as *birefringence*. This means that the refractive indices along the ordinary (n_o or $n_\perp$) and extraordinary (n_e or $n_{//}$) axes of the material are

different (Figure 1-3). The refractive indices of the E7 liquid crystal used for this work (Section 2.3.1), are $n_\perp = 1.5216$ and $n_{//} = 1.7462$ [22]. The birefringence is defined as $\Delta n = n_{//} - n_\perp$. Typical nematic liquid crystals have a birefringence of between 0.01 and 0.45. The birefringence of E7 is 0.23 [30]. Although $n_\perp$ is largely independent of the liquid crystal molecular structure (usually 1.5), a strong dependency on the molecular structure is observed for $n_{//}$. This is because the refractive index increases with the increase in molecular length. While the width (along the x- or y-direction) of rod shaped molecules does not vary much, there is a much greater variation in the length (along the z-direction) of the molecules.
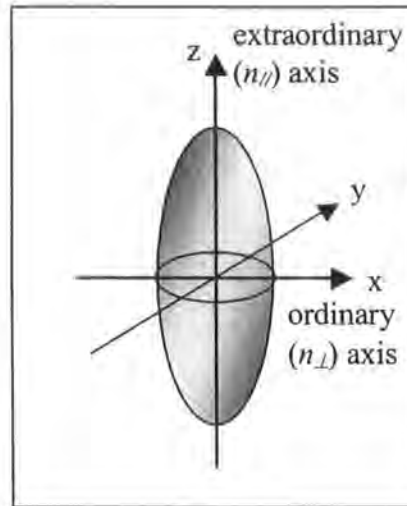
Figure 1-3. Schematic diagram of a liquid
crystal molecule.

The bonds in LC molecules are covalent. Such multiple bonds enhance molecular rigidity and are commonly found in the rod-like structure required for LC behaviour. The optical polarisability is mainly due to the presence of

delocalised π-electrons participating in chemical bonds. The π-electrons are more polarisable, i.e. can be displaced over a longer distance.

The extraordinary refractive index, $n_{//}$, is higher for compounds containing double or triple bonds compared to the compounds consisting of only single bonds. Therefore, a very effective way to increase $n_{//}$ and thereby Δn is to include triple bonds in the system to increase the polarisability of the molecule. Such an addition also adds rigidity to the structure. An example of this can be seen in Table 1-1 [31].
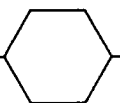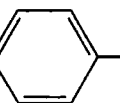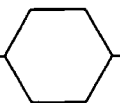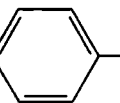
Structure	$n_\perp$	$n_{//}$	Δn
C_5H_{11}—⬡—C_2H_4—⬡—CN	1.498	1.615	0.117
C_5H_{11}—⬡—C≡C—⬡—CN	1.499	1.696	0.197

Table 1-1 Refractive indecies improvement for
liquid crystal with a triple bond.

The existence of benzene rings also helps to increase $n_{//}$. Also, different terminal polar molecules influence the molecular polarisability since these are associated with different degrees of polarisable electron density: e.g., fluoro- or alkyl substituents contribute much less to the birefringence than cyano groups do. Generally, $n_{//}$ decreases as the wavelength increases and slightly decreases as the temperature increases.

1.3.3. Alignment
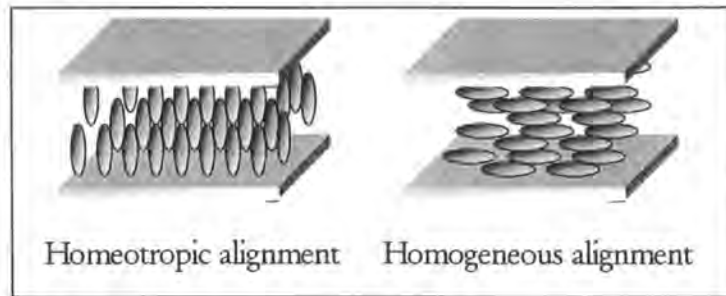
Figure 1-4. Homeotropic and homogeneous
alignment.

The image quality of a LCD is dependent on the display mode used, and each mode relies on appropriate liquid crystal alignment. One method used for aligning liquid crystals involves coating the top and the bottom glass substrate with a polyimide, PTFA or PVA based film, and rubbing it with a cloth [32]. Simplistically, this can be thought of as forming grooves on the polyimide film with dimensions of the order of nanometers, and the liquid crystals align with the direction of the grooves. For parallel alignment, both top and bottom substrates are rubbed anti-parallel to each other. When the liquid crystal is aligned parallel in such glass substrates, the alignment is called *homogeneous* (or *planar*). It is also possible to force the liquid crystal to align perpendicular to the substrate by using surface-active agent layers [33-35], termed *homeotropic* alignment. Both alignments are schematically shown in Figure 1-4. Such alignments are useful in determining the anisotropic properties of liquid crystals.

1.3.4. Order Parameter

A common characteristic of the liquid crystal is the tendency for the molecular axes to align along the same director direction, n. To quantify the degree of order present in a material, an *order parameter* of the liquid crystal (S_L) is defined as [23]:

$$S_L = \frac{1}{2}\left\langle 3\cos^2\theta - 1\right\rangle$$

Equation 1-1

where θ is the angle between the director, n, and the long molecular axis of the molecule (Figure 1-5), $\langle\cos^2\theta\rangle$ is the average value of $\cos^2\theta$ for all of the liquid crystal molecules. For an isotropic liquid, the average order parameter is equal to zero while a perfectly ordered crystal equals one; for a liquid crystal it ranges between 0.3 and 0.9. Since temperature will have large impact on molecular motions, S_L will be strongly temperature dependent.
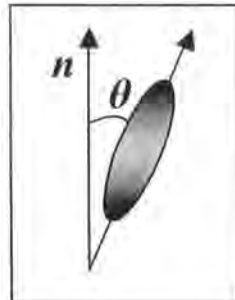
Figure 1-5. Deviation of a single molecule at a
time from its average director.

1.3.5. Elastic Constants

The elastic constants of a liquid crystal are associated with the restoring torques which become apparent when the system is perturbed from its

equilibrium configuration. The electric or magnetic field induces the initial

perturbation, and the balance between the electric (or magnetic) and elastic

forces determines the static deformation pattern of a liquid crystal. A

deformation state can be expressed by the combination of three *elastic*

constants: splay, twist and bend denoted as K_{11}, K_{22} and K_{33}. They are related to

the three different possible deformations as shown in Figure 1-6.

Splay K_{11} Twist K_{22} Bend K_{33}
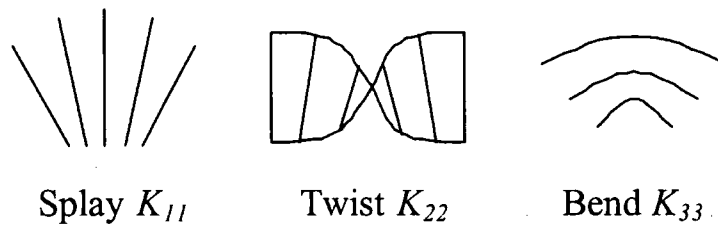
Figure 1-6. Elastic deformations: splay, twist
and bend.

Frank showed that the internal free energy density, F, of a perturbed liquid

crystal is given by the equation [36]

$$F = \frac{1}{2}\left[K_{11}(\nabla \cdot n)^2 + K_{22}\{n \cdot (\nabla \times n) + q_0\}^2 + K_{33}\{n \times (\nabla \times n)\}^2\right] \qquad \text{Equation 1-2}$$

where the Frank elastic constants, K_{11}, K_{22}, and K_{33}, are positive numbers, and

q_0 is an arbitrary constant for a given liquid crystal. At the relaxed state of the

liquid crystal, $F = 0$, so the splay, twist, and bend terms must be zero. For the

twist state to be zero, either q_0 must equal zero, or $n \cdot (\nabla \times n)$ must equal $-q_0$.

The former indicates that the liquid crystal is nematic, and the latter indicates

that the liquid crystal is cholesteric with a twist of π/q_0.

As can be seen from the equation, the free energy density is a quadratic function of the curvature strains with the elastic constants appearing as factors of proportionality. This expression is very reminiscent of the internal mechanical energy of classical mechanical systems, e.g. a loaded spring with $F_{el}=1/2(kx^2)$, where F_{el} is the elastic energy and k being the elastic constant of the spring. These restoring forces for LC are very weak in comparison with the restoring forces of solids, e.g. Hooke's law. The typical magnitude of the elastic constants is in order of 10^{-12} N. The small value indicates that the liquid crystal can be controlled easily by electric or magnetic fields.

The bending constant, K_{33}, is larger than the others, while the twist constant is the smallest. A large elastic constant increases the minimum voltage required to switch the liquid crystal, but it can reduce the time taken for the liquid crystal to relax back to equilibrium, while not affecting the turn-on time.

Each constant is an intrinsic property of the liquid crystal material. Unfortunately, a predictive theory enabling an estimate of magnitude of the elastic constants for a given molecule does not exist. Instead, one has to rely primarily on experimentally obtained data.

1.3.6. Dipole Interaction

In dipolar molecules, positive and negative charges are slightly displaced even without an external electric field. This is called a *permanent dipole*, and its size, *dipole moment*, μ, can be expressed as

$$\mu = qd \qquad\qquad \text{Equation 1-3}$$

when the charge $+q$ and $-q$ is separated by the distance d. The dipole moment points from the negative charge to the positive charge. The magnitudes of dipole moments are still commonly reported in the non-SI unit _debye_, D, where $1\,D = 3.33564 \times 10^{-30}$ Cm. Dipole moments of small molecules are typically about 1 D.

All molecules in liquid crystals generally contain covalent bonds formed by the overlap of electron clouds. A covalent bond formed by atoms of different electronegativities has an unbalanced distribution of charge, as atoms or groups with high electronegativity (e.g. CN, F) have a strong attraction for shared electrons. This shift of electron distribution forms a permanent dipole moment.

If no electric field is present, the permanent electric dipoles are randomly oriented, and hence the liquid crystal possess no net dipole even when the liquid crystal molecules are aligned. However, when the electric field is applied, the dipoles experiences forces and rotate to line up with the electric field. Even if a molecule does not have a permanent dipole, it can still be influenced by an electric field. In a high frequency of typically above kHz regime, additional dipoles are induced by the applied electric field, which causes a distortion of the electron clouds and a redistribution of the electrons. While not as strong as permanent dipoles, orientation with the AC external field may still occur. This will be explained in the next section.

(a) When $\mu_1 \parallel \mu_2 \perp r_{12}$

(b) When $\mu_1 \parallel \mu_2 \parallel r_{12}$
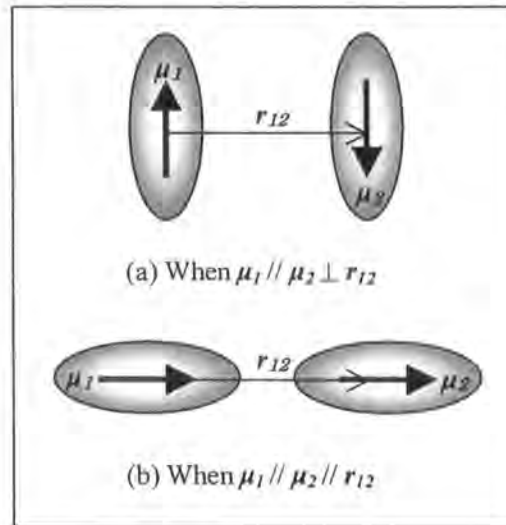
Figure 1-7, Molecular orientation at minimum
interaction potential energy.

The potential energy of interaction between two polar molecules , such as liquid crystal molecules, or a liquid crystal molecule and a highly dipolar dopant, is a complicated function of their relative orientation. When two molecules with dipole moments μ_1 and μ_2 with positional vectors $\mathbf{r}_1$ and $\mathbf{r}_2$ are close together, the dipole experiences force. The potential energy associated with this force is:

$$V_{12} = \frac{\left\{ \boldsymbol{\mu}_1 \cdot \boldsymbol{\mu}_2 - 3(\boldsymbol{\mu}_1 \cdot \mathbf{r}_{12})(\boldsymbol{\mu}_2 \cdot \mathbf{r}_{12})/r_{12}^{\ 2} \right\}}{r_{12}^{\ 3}} \qquad \text{Equation 1-4}$$

where $\mathbf{r}_{12} = \mathbf{r}_1\text{-}\mathbf{r}_2$, and $r_{12} = |r_{12}|$ is the distance between the dipoles. This force is called the *dipole interaction*. If a molecule possess an electric dipole, the molecular interaction depends not only on the distance $\mathbf{r}_{12}$, but also on the direction of $\mathbf{r}_{12}, \mu_1$ and μ_2. Hence the molecule experiences the force such as to minimise the potential energy from the dipoles (Figure 1-7).

1.3.7. Electric Polarisation

Polarisation is an important basic property of a material when dealing with the effects of electric fields both static and alternating. The interaction with electric fields is particularly important for LCs for switching. Even when the LC is electrically neutral, polarisation occurs when external electric field is applied. This induced polarisation causes the LC to orient. In general, there are three types of polarisations which can be classified as *electric polarisation*, *ionic polarisation* and *orientation polarisation*.

Electric polarisation occurs when an electron is displaced slightly within an atom due to external electric field as shown schematically in Figure 1-8. The size of the polarisation is determined by the multiplication of the distance of the displacement, *l*, and the amount of charge displaced, *q*,

$$P = ql$$

<div align="right">Equation 1-5</div>

The distance of the displacement, *l*, is determined by the balance of the Coulomb force between a nucleus and an electron, and the force due to an external electric field. A larger electric polarisation can be achieved for the molecules with covalent bonds, because π-electrons are more delocalised compared to electrons from σ-bonds. It is important to note that when the molecule is not spherical in shape, the polarisation is anisotropic. For example, for a macromolecule with covalent bonds along its chain, the polarisation along the long chain direction will be bigger than that perpendicular to the

chain direction. This is the case for most rod-like LCs, and origin of their anisotropic properties.
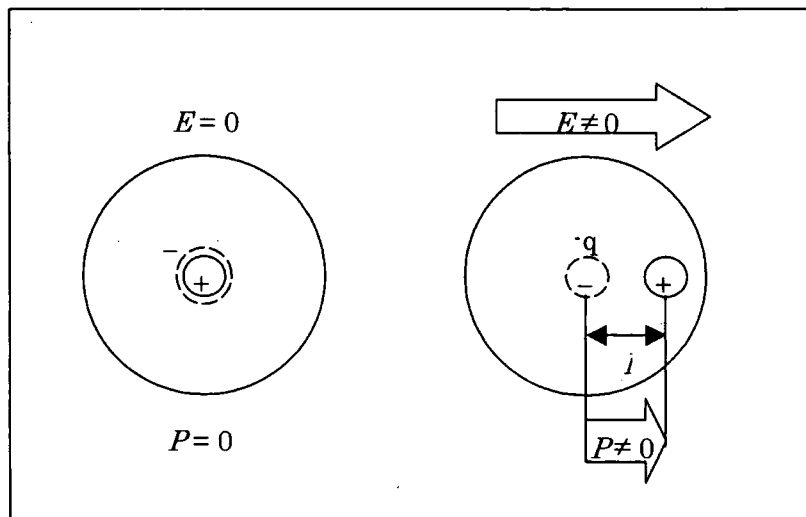
Figure 1-8. Schematic diagram of the electron polarisation

Ionic polarisation, sometimes called atomic polarisation, occurs when positive and negative ions are displaced slightly within a material due to an externally applied electric field (Figure 1-9). The displacement is determined by the balance of the force due to an electric field and the Coulomb force between positive and negative ions. This type of polarisation is larger for materials with ionic bonds, and for soft materials where atoms can move easily. Since ionic bonds have directional characteristics, and the distance between ions can differ, ionic polarisation can also be anisotropic depending on the material structure.
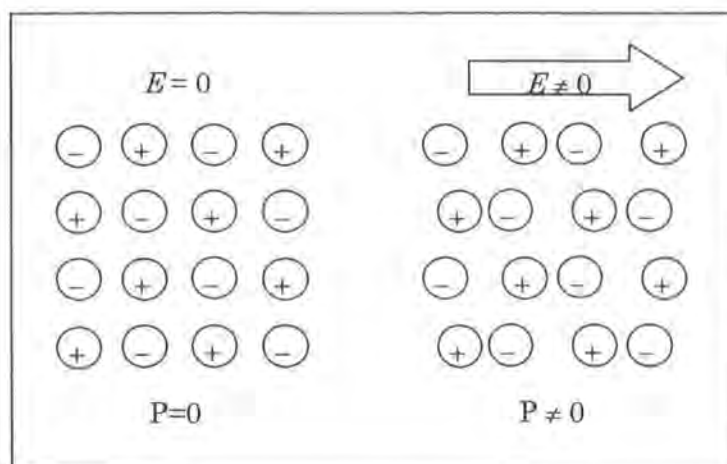
Figure 1-9. Schematic diagram of ionic
polarisation

Orientation polarisation occurs when randomly oriented dipolar molecules orients in one direction when an external electric field is applied. The polarisation applies to LC molecules and dipolar molecules. This type of polarisation also possesses anisotropy.

All three polarised states induced by an external electric field return to the unpolarised state on removal of the electric field. The speed of the response to the ON and OFF of the electric field differs depending on which type of polarisation is involved; electric polarisation responds very fast (10^{-16} s) to the electric field, then ionic polarisation (10^{-15}-10^{-12} s), and orientation polarisation responds more slowly (10^{-12}-10^{-10} s). This difference can be observed when an AC electric field is applied. Electron polarisation can respond up to the very high frequencies of visible light (10^{15} Hz), ionic polarisation can respond up to a lower infrared frequency (10^{14}-10^{11} Hz), and orientation polarisation can barely respond up to microwave frequencies (10^{11}-10^{9} Hz).

The degree of electron redistribution can be described by the *permittivity*, ε, which is the ratio of the electric displacement (D, sometimes called electric flux density) in a dielectric medium to the applied electric field strength (E), i.e. $\varepsilon = D/E$, this indicates the degree to which the medium can resist the flow of electric charge. In electromagnetic field, polarisation, P, E and D has the following relation:

$$P = \varepsilon_0 \chi E$$

<div align="right">Equation 1-6</div>

$$D = \varepsilon_0 E + P = \varepsilon E$$

<div align="right">Equation 1-7</div>

where χ is electric susceptibility and ε is dielectric permittivity. Since in MKS units, the dielectric constant of vacuum is ε_0, the dielectric constant of a material, ε, can be expressed as

<div align="right">Equation 1-8</div>

$$\varepsilon = \varepsilon_0 \varepsilon_r$$

where ε_r is a relative dielectric constant. It can vary from 1 (in a vacuum) to 4000 (for ferroelectrics).

As polarisation is frequency dependent, so is χ and ε. It is important also to note that P is directly proportional to the applied electric field (i.e. non-linear effects are not considered here). As there is anisotropy in polarisation, there is also anisotropy in χ and ε.

In the liquid crystal field, ε_r is called the *dielectric constant*, and this varies from 5.2 to 19.0 for E7 depending on the axis along which it is measured. The difference between the dielectric constant parallel to the long molecular axis,

$\varepsilon_{//}$, and that perpendicular, $\varepsilon_{\perp}$, is termed *dielectric anisotropy*, $\Delta\varepsilon$: i.e. $\Delta\varepsilon = \varepsilon_{//} - \varepsilon_{\perp}$. This is another important property of liquid crystals. When the dielectric anisotropy of the liquid crystal is positive, the induced dipole causes the molecules to align along an applied external field. Similarly when the dielectric anisotropy of liquid crystal molecules is negative, the molecules align perpendicular to the external field.

1.3.8. LC Response to Alternating Electric Field

When an electric field **E** with field strength E is applied to a liquid crystal with $\Delta\varepsilon$, and the angle between the liquid crystal director (n) and the applied electric field is φ (Figure 1-11), the liquid crystal experiences an electric energy of

$$
\begin{aligned}
f &= -\frac{1}{2}\varepsilon_0\Delta\varepsilon\mathbf{E}^2 \\
&= -\frac{1}{2}\varepsilon_0\varepsilon_{//}\mathbf{E}^2 - \left(-\frac{1}{2}\varepsilon_0\varepsilon_{\perp}\mathbf{E}^2\right) \\
&= -\frac{1}{2}\varepsilon_0\varepsilon_{//}\left(E\cos\varphi\right)^2 - \frac{1}{2}\varepsilon_0\varepsilon_{\perp}\left(E\sin\varphi\right)^2 \\
&= -\frac{1}{2}\varepsilon_0\varepsilon_{\perp}E^2 - \frac{1}{2}\varepsilon_0\left(\varepsilon_{//} - \varepsilon_{\perp}\right)\left(E\cos\varphi\right)^2 \\
&= -\frac{1}{2}\varepsilon_0\varepsilon_{\perp}E^2 - \frac{1}{2}\varepsilon_0\Delta\varepsilon\left(n\cdot\mathbf{E}\right)^2
\end{aligned}
$$

Equation 1-9

Since the first term does not depend on the direction of the director n (where n is a unit vector), the electric energy due to the director orientation can be expressed as

$$f = -\frac{1}{2}\varepsilon_0 \Delta\varepsilon (n \cdot \mathbf{E})^2$$

Equation 1-10

Thus when $\Delta\varepsilon > 0$, it is energetically favourable for the liquid crystal to align parallel to the electric field, and when $\Delta\varepsilon < 0$, the liquid crystal aligns perpendicular to the electric field. Generally, the values of $\Delta\varepsilon$ range from –6 to +50 for liquid crystal materials [31], and the E7 liquid crystal used in this work (Section 2.3.1) has a value of 13.8.

It is known that the higher the $\Delta\varepsilon$, the shorter the turn-on time, known as *rise time* τ_{rise}, for liquid crystal molecules to align with respect to the applied field. This relation is given by the Equation 1-11 [37] where γ is the rotational viscosity of the liquid crystal. The equation will be discussed further in Section 3.2.3.

$$\tau_{rise} = \frac{\gamma}{\varepsilon_0 \Delta\varepsilon (E^2 - E_0^{\;2})}$$

Equation 1-11

Also, it is known that the higher the $\Delta\varepsilon$, the smaller the minimum voltage, *threshold voltage*, required to change the orientation of liquid crystal molecules. This is given by the following equation [38]:

$$V_0 = \pi\sqrt{\frac{K_{ii}}{\varepsilon_0 \Delta\varepsilon}}$$

Equation 1-12

Where V_0 is the threshold voltage and K_{ii} is the appropriate elastic constant depending on the initial alignment. Since $V = Ed$, Equation 1-12 follows to

$$E_0 = \frac{\pi}{d} \sqrt{\frac{K_{ii}}{\varepsilon_0 \Delta \varepsilon}}$$

<div align="right">Equation 1-13</div>

where E_0 is the threshold electric field.
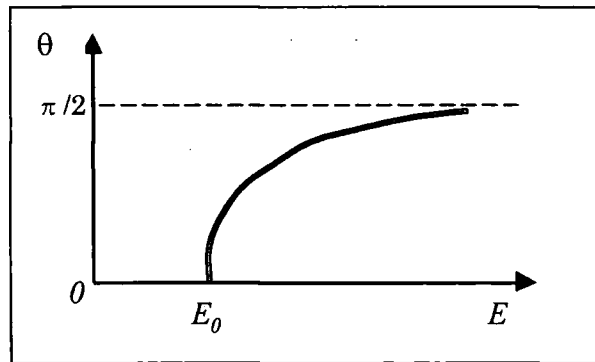
Figure 1-10. Director orientation change with electric field.

This effect of LC responding only above a threshold electric field E_0 is known as the *Freedericksz transition* [39], which is schematically shown in Figure 1-10. θ is an angle between the initial alignment (x-direction) and the director of the liquid crystal.

Equation 1-13 is based on the following assumptions: (1) there is strong anchoring between the molecules and the cell surfaces, (2) the steady state is considered, and (3) the field in the sample is taken as uniform [37]. When an electric field, **E** is applied to the z-direction, the free electric energy is

$$f = \frac{1}{2} K_{ii} (n \cdot \nabla \times n)^2 - \frac{1}{2} \varepsilon_0 \Delta\varepsilon (\mathbf{E} \cdot n)^2$$

$$= \frac{1}{2} K_{ii} \left(\frac{d\theta}{dz} \right)^2 - \frac{1}{2} \varepsilon_0 \Delta\varepsilon E^2 \sin^2 \theta \qquad \text{Equation 1-14}$$

For a cell with thickness d, the free energy, F, becomes

$$F = \int_0^d f dz$$

Equation 1-15

By using variational calculus [40], the system is minimised at

$$K_{ii} \frac{d^2\theta}{dz^2} + \varepsilon_0 \Delta\varepsilon E^2 \sin^2 \theta \cos\theta = 0$$

Equation 1-16

This gives an elliptic integral when expressed as a Jacobian elliptic function [37, 41], and expanded as a series. The first two terms of the expansion are

$$E = \frac{\pi}{d} \sqrt{\frac{K_{ii}}{\varepsilon_0 \Delta\varepsilon} \left(1 + \frac{1}{4} \sin^2 \theta_m + ... \right)}$$

Equation 1-17

Therefore, there is a threshold field, E_0, which must be exceeded before a deformation occurs. From inspection of Equation 1-17,

$$E_0 = \frac{\pi}{d} \sqrt{\frac{K_{ii}}{\varepsilon_0 \Delta\varepsilon}}$$

Equation 1-18

can be obtained.

There are many types of Freedericksz transition depending on the initial liquid crystal alignment and the direction of applied electric field. Figure 1-11 (a), (b) and (c) represent a splay, twist and bend Freedericksz transition respectively. In this work, the splay transition (a) was of main interest.

Freedericksz transitions can also occur with magnetic fields, but as this is not relevant to this work, it will not be discussed further.
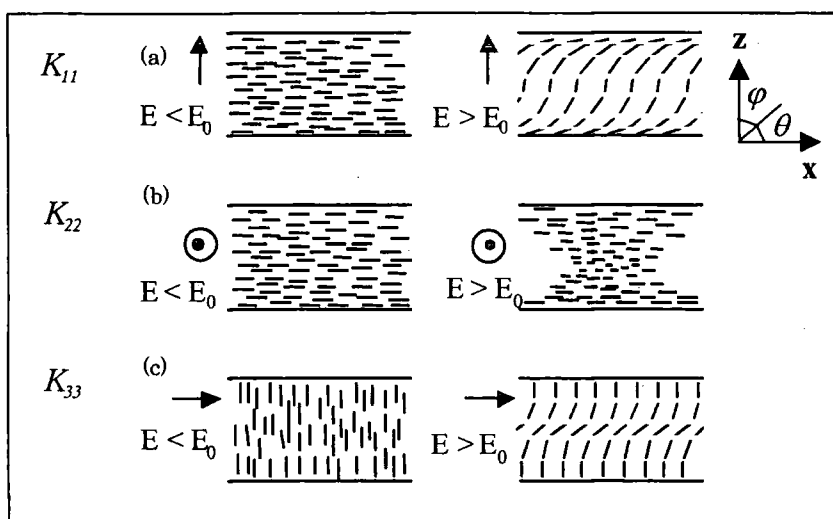
Figure 1-11. Three types of Freedericksz transition.

1.4. Applications

1.4.1. Guest-Host Displays

Dichroic dye molecules added to liquid crystal host materials tend to line up with the liquid crystal director. This effect of dye alignment is known as the *Guest-Host (GH) effect* [42]. Switchable absorbers or switchable polarisers can be produced from this, because it is possible to rotate the guest dyes, by rotating the host liquid crystal and hence control the light absorption by the dye. Displays that incorporate dyes have also been made, and they are called *guest-host (GH)* liquid crystal displays. The degree of dye alignment with the

liquid crystal alignment depends on the dye's molecular structure. More details of the GH effect will be discussed later in Section 3.2.1.

1.4.2. Twisted Nematic Displays

The *twisted nematic (TN)* effect is by far the most widely used effect for LCDs. A nematic liquid crystal with positive dielectric anisotropy is sandwiched between a layer of transparent conducting material called *indium tin oxide (ITO)* and a rubbed polyimide layer to obtain alignment. The electrodes are separated by a thin spacer, and before filling, they are assembled with directions of alignment at 90° to each other. The result is a helical liquid crystal film with a 90° twist in the director across the cell (Figure 1-12). The plane of polarisation of linearly polarised light propagating parallel to the helical axis follows the twist of the phase, and as a result, the polarisation of the light also turns by 90°. When an electric field is applied, the helical arrangement disappears and the liquid crystal molecules aligns parallel to the field and normal to the substrate. In this situation, the polarisation of the light remains unchanged and the light transmission through the TN cell is negligible. After removal of the field, the liquid crystal relaxes back to its initial state.

Improvement of TN display technology progressed from simple pocket calculator displays to high information content displays in a mere twenty years. TN displays have advantages of being thin, light weight and consuming less power compared to CRT. They have typical response times of 1-10 ms, with a

contrast of 350, and a colour purity of 60%. Nevertheless, the TN effect suffers from some basic drawbacks such as its poor brightness and narrow viewing angle due to the polarisers required.
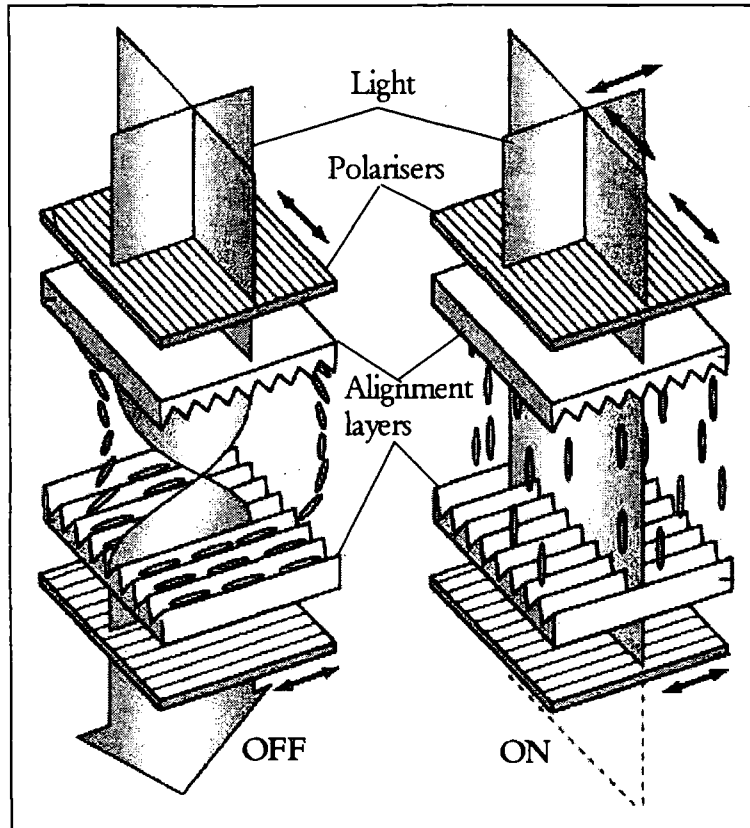
Figure 1-12. Mechanism of TN display.

1.4.3. Ferroelectric LC Display

A chiral smectic C liquid crystal molecule with a permanent dipole perpendicular to its long axes shows ferroelectric properties. When such a liquid crystal is contained in a thin cell with a gap of 1-2 μm, the interaction between the liquid crystal and the cell walls induces the helix next each other, i.e. their permanent dipoles point in the same direction and their molecular

axes align along their directors. In such texture, there are only two states possible so that they have the ferroelectric ordering (Figure 1-13).
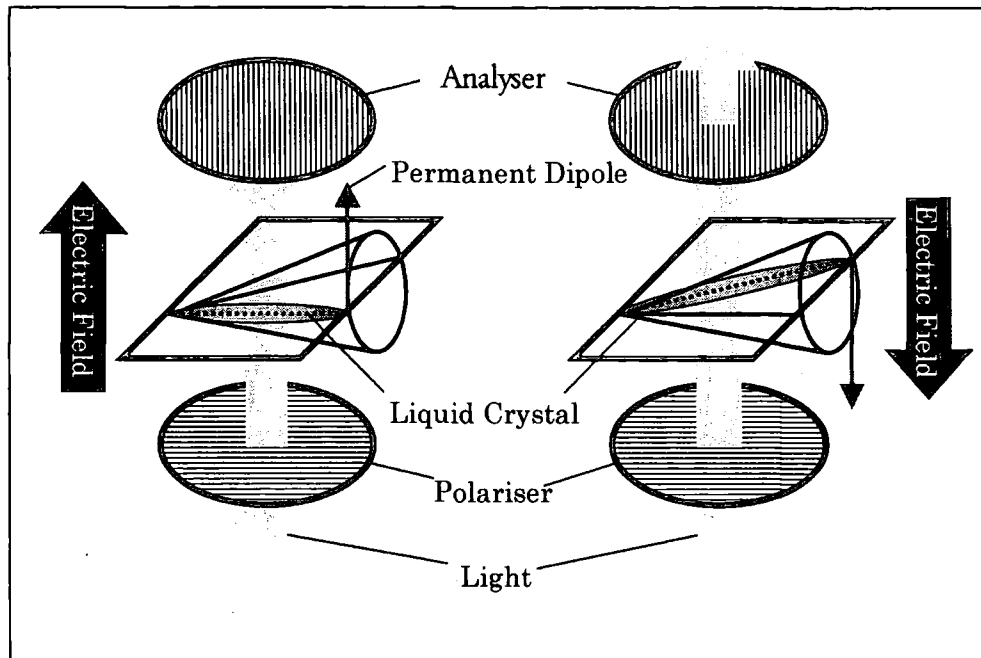
Figure 1-13. Two states of ferroelectric liquid
crystal.

Each of the two states possesses an electronic polarisation perpendicular to the cell walls. If an electric field is applied opposite to the direction of the permanent dipole of the smectic liquid crystal, the response is such that the dipole rotates by 180°, thus changing the bulk director direction. By sandwiching the cell between a pair of cross polarisers and aligning one polariser parallel to a liquid crystal director, it is possible to achieve blocking and transmitting states. For optimum operation, the conic angle separating the two states must be 45° and the optical retardation of one state is 180°. This type of display is called *surface stabilised ferroelectric liquid crystal* (SSFLC).

Since the removal of electric field does not affect the LC orientation, a SSFLC

is said to be bistable and possesses memory. The switching times for these

displays are typically of the order of 10 μs. This is faster than other LCDs by a

factor of one hundred to one thousand. This is because (1) the LC possesses

ordered permanent electric dipoles, and (2) an electric field forces both the on

and off transition.

1.4.4. PDLC Displays

In 1976, Hilsum demonstrated the changing of a liquid crystal composite

from an opaque to a transparent state for the first time [43]. He used micron

sized glass beads dispersed in a nematic liquid crystal, but because of the low

contrast, the device was not developed for display applications [44]. However,

the concepts are still investigated today using micron sized polymer particles

[45].

In 1982 Craighead *et al.* published a device where the second medium is a

polymer [46]. They made use of a microporous filter, filling the micron-size

pores with a nematic liquid crystal of positive dielectric anisotropy and

sandwiched the film between a layers of ITO. The contrast and the switching

times were not impressive and the device was also not developed for display

applications.

Fergason developed a material developed for commercial display applications

in 1985 [1, 2]. He applied encapsulation procedures to create micron-size

liquid crystal droplets inside a polymer. The material was prepared using a water-based emulsion. These materials have been successfully developed for a variety of displays and have been studied extensively by the Taliq and Raychem Corporations.

A year later, Drzaic developed phase separation procedures to obtain a dispersion of liquid crystal droplets inside a polymer [3]. He reported that liquid crystal-polymer composites could be obtained by drying an emulsion of liquid crystals in an aqueous solution of polyvinyl alcohol. These materials were soon developed for smart window applications.

In the same year, Doane introduced a second class of composites called PDLCs by inducing phase separation in a homogeneous mixture of a liquid crystal and an epoxy prepolymer [4]. Since then, the types of polymers that can be used have been greatly extended and a variety of procedures for adjusting droplet morphology and display fabrication methods have been introduced.

PDLCs are also of interest to basic physics because of new kinds of physical phenomena brought about by the confinement of a nematic liquid crystal to small submicron-size droplets. Enhanced surface-to-volume ratio, large nematic deformations and problems associated with surface forces (called *anchoring*) at a polymer wall are providing new areas of study in the field of surface mediated phenomena [4, 44, 47-50].

1.4.4.1. Principles of Operation

A PDLC consists of liquid crystal droplets dispersed uniformly in a transparent polymer matrix. A thin PDLC film (typically 10-25 μm thick) is sandwiched between glass or plastic substrates coated with a very thin layer of ITO (typically 20-30 nm).
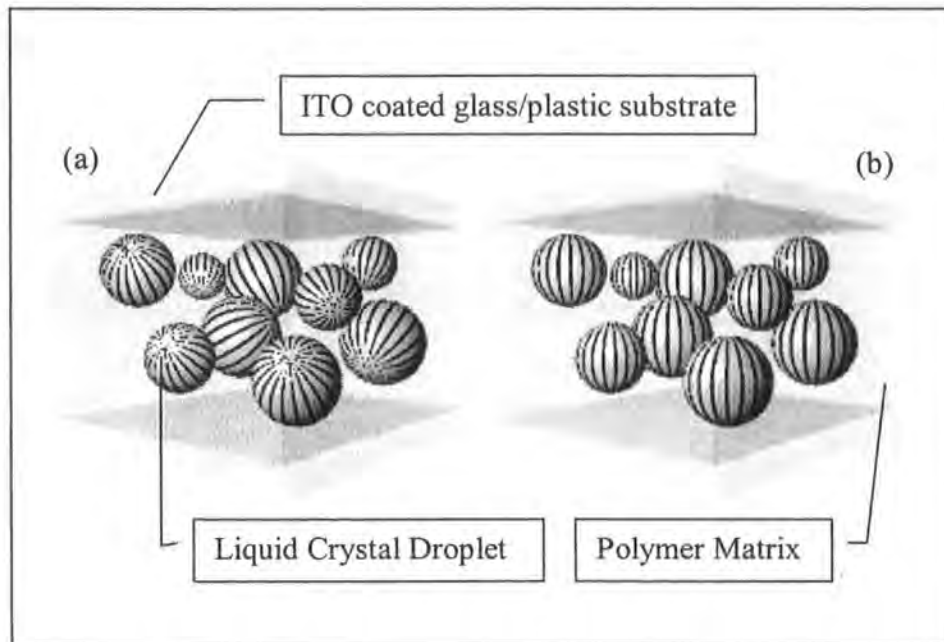
Figure 1-14. PDLC in the off-state (a) and on-
state (b).

Initially the directors of the individual droplets are pointing in different directions as shown in Figure 1-14 (a). The directors are represented as stripes in the figure [51]. Due to the large mismatch of refractive index (more than 0.01) of the liquid crystal and of polymer, the film appears milky white in the absence of an applied voltage (i.e. at off-state) because of light scattering. The diameters of the liquid crystal droplets are comparable to the

wavelength of visible light ($\leq 1 \ \mu m$). Since these diameters are small compared with the film thickness, a light ray will be scattered many times before emerging from the film.

When a sufficiently high voltage (50-100 V_{RMS}) is applied across the PDLC (i.e. at the on-state), the directors of the droplets align with the field as shown in Figure 1-14 (b). The film becomes transparent provided the ordinary refractive index of the liquid crystal within the droplets is close to the index of the polymer matrix material, in other words the refractive index mismatch is less than 0.01. When the electric field is removed, the liquid crystals recover their initial orientations because of anchoring. The degree of the off-state scattering depends on the size of the refractive index mismatch, number density of the liquid crystal droplets, and the thickness of the PDLC film.

1.4.4.2. Advantages and Targets

Displays described previously suffer from many drawbacks. The strong demand for bright, large area, direct view LCDs able to reproduce high definition coloured pictures for personal computer terminals, television screens and large area information boards, requires the development of new electro-optical effects. PDLCs are one of the promising candidates to achieve these requirements [3, 49].

The biggest advantage of PDLCs compared to other LCDs is their brightness. The on-state is close to 100% transparent because no polariser is required.

The lack of polarisers also means that a wider viewing angle is possible [52-54]. Additionally, no alignment layer is required and the thickness of the PDLC is not as crucial as the other LCDs, simplifying the manufacturing process. Also the polymer matrix of PDLC adds extra mechanical stability. These factors allow the display to be flexible, large-scale, simple and cost effective to fabricate. Today, *reflective displays* are becoming popular because they consume less power, as backlighting is not required. PDLC films incorporating dichroic dyes can be used to produce high performance reflective displays using either glass or plastic substrates. Currently, dichroic PDLC films can already be found in many control panel applications for office equipment and appliances [5].
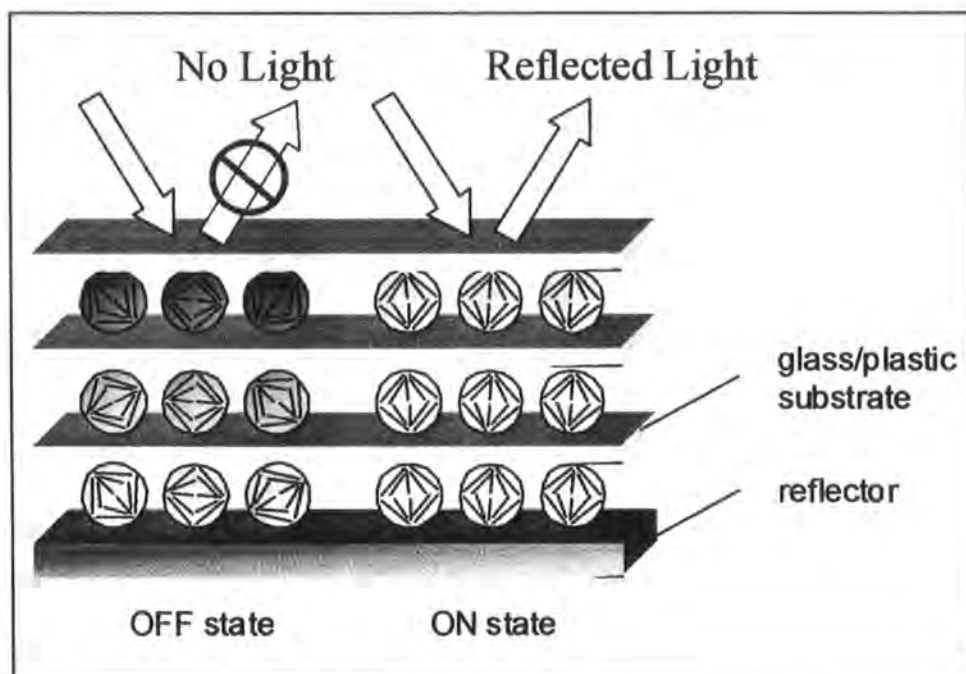
Figure 1-15. Three layered reflective-type
dichroic PDLC display.

Target aim for reflective dichroic PDLC
Response (rise + decay) time of less than 0.1 s
Threshold voltage of less than ± 5 V
On-state reflectance of more than 74% = transmittance of more than 86% = absorbance of less than 0.15
Off-state reflectance of less than 10% = transmittance of less than 31% = absorbance of more than 1.17
Contrast Ratio, CR ($reflectance_{MAX}/reflectance_{MIN}$) of more than 5 = CR ($transmittance_{MAX}/transmittance_{MIN}$) of more than 2.23 (=√5)

Table 1-2. Target aims for reflective-type
dichroic PDLC samples.

For this work, a targeted device and aims for commercial standard reflective-type dichroic PDLCs were given by Sony [55] who is the sponsor of this work. Three layered dichroic PDLCs display with subtractive colour mixing as shown in Figure 1-15 is expected to allow the development of full colour reflective displays. Each layer consists of LC droplets doped with cyan, magenta or yellow dyes. Also, the four property targets are listed in Table 1-2. It should be noted that the transmittance and reflectance are not defined in a usual way. This will be discussed further in Section 4.1.

The response time of less than 0.1 s enables a use of the display for a video application, and the maximum threshold voltage of less than $\pm$ 5 V is required to keep the power consumption low. On-state reflection of more than 74% is necessary for the brightness (or whiteness) of the display, and off-state reflection of less than 10% is expected to give enough colour ("blackness" for a black and white display). The values measured in this work will be continually compared with these target values.

The dyes used for such displays are important, hence the required dye properties are discussed and characterised first in the next chapter.

Chapter 2: Dye Characterisation

2.1. Introduction

Following the motivation and the fundamental background of this work in the previous sections, this chapter describes the properties of dichroic dyes required for GH display and their experimental characterisation. The dyes employed in this chapter include a highly dipolar MORPIP chromophore, D2 azo dye, D16 anthraquinone dye, and B2 black dye which is a mixture of azo and anthraquinone dyes. Each dye used is described in detail, and their dichroic ratios, order parameters, and photostabilities are compared experimentally.

2.2. Properties of Dyes

2.2.1. Introduction

Dichroic dyes have a large transition moment along one molecular axis. This leads to higher absorption along this axis rather than the others. This property makes the dichroic dye useful when mixed with liquid crystal material. As dyes tend to align with the liquid crystal, it is possible to control how much light the dye absorbs by controlling the liquid crystal rotation.
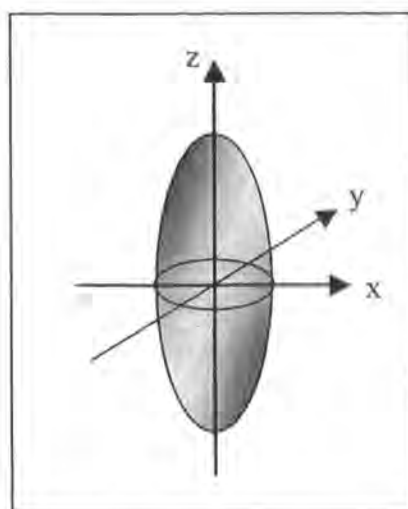
Figure 2-1. Schematic diagram of a dichroic
dye.

Dyes termed *pleochroic* (or *positive dichroic*) [56-60], have their transition moment along the long molecular axis (z-direction in Figure 2-1), and thus absorbs the portion of E vector of light which is along this axis. In contrast, dyes termed *negative dichroic dye* have their transition moment along the short molecular axes (x- or y-direction in Figure 2-1). Hence the negative dichroic dyes absorb the E vector of light which is perpendicular to their long molecular axis [61]. Most dyes used with liquid crystals are pleochroic dyes because they exhibit higher dichroic ratios and order parameters compared with the negative dichroic dyes.

Normally dyes have a narrow absorption spectrum, and the wavelength of the maximum absorption is designated as λ_{max}. The colour that is observed is basically the light which is not absorbed by the dye. By mixing several dyes with different λ_{max}, it is possible to make *black mixtures* [62, 63]. This is shown

schematically in Figure 2-2. This is the main black dye called Black-2 (B2) which was used in this work, and it consists of 13 different azo and anthraquinone dyes [64].

[Formulation]		
Color / Dye No.		Conc.(wt%)
Yellow	LSY-116	0.84
	LSY-120	0.61
	LSY-108	0.77
Red	LSR-405	0.49
	LSR-406	0.50
Blue	LSB-278	1.14
	LSB-350	1.29
	LSB-349	0.41
Cyan	LSB-318	1.02
	LSB-335	1.12
Violet	LSR-463	1.27
	LSR-464	1.29
	LSR-426	0.58
HOST		88.47
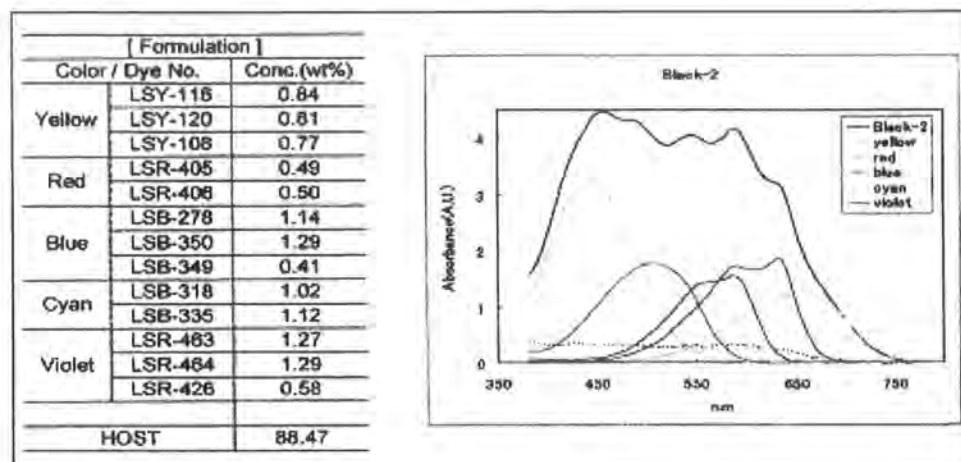
Figure 2-2. Absorption spectra of the B2 black
dye.

In selecting a dye for GH displays, colour, compatibility and stability of the dye in the liquid crystal must be considered [56, 65-69]. Good colour and hue comes from an appropriate λ_{max} and a narrow spectral width with high extinction coefficient, dichroic ratio [56], order parameter [56] and solubility [70, 71]. Good compatibility of the dyes with the liquid crystal (e.g. low influence on the viscosity), with the surface alignment materials, and mutual compatibility when using multiple dyes, are necessary. Good stability comes from high purity, high electrical resistivity (non-ionic nature), high photochemical, electrochemical and thermal stability (Section 2.2.5) [60, 72-76]. Photochemical instability can lead to *fading*.

2.2.2. Dichroic Ratio and Order Parameter

For display applications, high contrast is important. One of the factors that affects the contrast is the order parameter (Section 1.3.4) of the dye in the liquid crystal. It is the only parameter that when increased, both the contrast ratio and the transmittance also increase.

The dye order parameter is heavily dependent on the liquid crystal host. Usually the dye order parameter (S_D) increases with an increase in the host order parameter (S_L) and vice versa. In this work, S_D was measured for different dyes employed in the host material E7 (Section 2.3.1).

The direction of each dye molecule deviates from the director due to thermal fluctuations in the same way as individual liquid crystal molecules deviate from their own director [56, 57, 60]. The impact of thermal fluctuations is different for dye and liquid crystal molecules depending on their molecular structure. Elongated dyes are also found to withstand thermal fluctuations better at higher temperatures and hence show less variation in S_D. Elongated dyes are also found to have high S_D, while shorter dyes have lower S_D compared with the host order parameter, S_L [56].

For elongated pleochroic dyes, the direction of transition moment and the long molecular axis of the dye is almost parallel, thus the order parameter can be determined experimentally from the Equation 2-1 [77-80]:

$$S_D = \frac{D-1}{D+2} = \frac{A_{//} - A_{\perp}}{A_{//} + 2A_{\perp}}$$

Equation 2-1

where $D = A_{//}/A_{\perp}$ is termed the *dichroic ratio* of the dye, and $A_{//}$ and $A_{\perp}$ are the absorbance of the light polarised parallel and perpendicularly to the director of the dye, respectively. The director of the dye in the host liquid crystal coincides with the director of the host [56, 57, 60]. Consequently, $A_{//}$ and $A_{\perp}$ of the dye can be measured experimentally by placing an aligned dye doped liquid crystal sample parallel and perpendicular to the light polarisation, as demonstrated in Section 2.4.2.

2.2.3. Structure

A number of intensive investigations of dyes with different chemical classes have been carried out in the past [58, 81-83]. Mainly azo [56-58, 61, 65, 84-87] and anthraquinone [56-58, 66, 67, 73, 86, 88] dyes were employed. The azo dyes often have a poor photochemical stability, whereas most of the anthraquinone dyes have inadequate dichroic ratios and solubility [73]. One azo and one anthraquinone dye were used in this work for the comparative study of the highly dipolar dye.

Besides these dyes, methine [81, 82, 89, 90], azomethine (Schiff's bases) [81, 83, 89-91], merocyanine [81, 83], napthoquinone [92],benzoquinone [83], tetrazine [93, 94], hydroxyquinophthalone [95], perylene [95], azulene [96], organometallic [68, 97] and other types of dyes [83] have also been

investigated. Attempts have also been made to synthesize dyes with liquid crystal phases [93, 94, 98].

2.2.4. Solubility

To realise bright and pure colours in the GH liquid crystal displays, a high solubility of the dye in the liquid crystal (>1 wt%) [99] is essential. The solubility of dyes differs in different hosts. Usually, dye molecules contain several phenyl rings and conjugated linking groups so that their melting points are high (>100 °C). Owing to the high melting point, the dye's solubility is generally limited to about 2-5 wt%; a higher concentration causes phase separation from the liquid crystal mixture. Additionally, an increase in dye concentration increase in the viscosity of the host.

2.2.5. Stability

For display applications, dyes must have high chemical, photochemical and electrochemical stability. Electrochemical stability implies that dyes should not phase separate in liquid crystal mixtures under "field-on" conditions. A mixture of non-ionic pure dichroic dyes and pure stable liquid crystal material must have sufficiently high resistivity (>10^{11} Ωcm) to keep the current consumption of the display low. However, even the purest form of non-ionic dichroic dyes may increase the electrical conductivity of the liquid crystal mixture, possibly due to interactions such as liquid crystal - dye charge

transfer [66, 83]. Also, small amounts of impurities, such as water, present in liquid crystal mixtures may have reactivity to dichroic dyes.
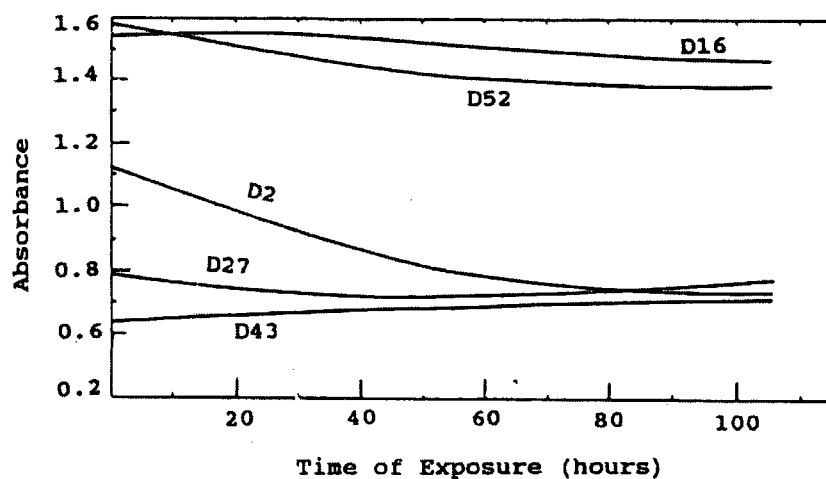
Figure 2-3. Change in absorbance of dyes on
exposure to Hanovia Arc Tube.

Photostability is one of the most important considerations in determining the use of dichroic dyes in LCDs [65, 67, 73-76, 81-83, 86, 100]. The fading mechanisms [76, 100] are known to be influenced by the chemical structure of both the liquid crystal and the dye, concentration of the dye, temperature, and the presence of moisture and oxygen. Deterioration after long exposures to light results in loss in absorbance, reduction in dichroic ratio and order parameter, increase in electrical conductivity, dissociation of the dye, loss of alignment, dye segregation, loss of solubility and, formation of voids and gas bubbles [101]. Deterioration of the absorbance and order parameter of dyes can be seen in Figure 2-3 and Figure 2-4 respectively. These measurements were carried out by Pellatt *et al* [73]. They used a stable Merck (formerly

BDH) mixtures E7 or E9 as host, and dichroic cells were exposed for up to

1500 hours from a low power UV lamp (Hanovia UVS 500 Arc tube type

509/10 with quartz tube, 500 W).

D2 and D16 dyes, which can be found in both figures, are commercially

available dyes from Merck, and they were employed in this work to compare

the stability of the highly dipolar dye MORPIP (Section 2.4.3). D2 is an azo

dye which is known to be less stable compared to the anthraquinone dye D16.
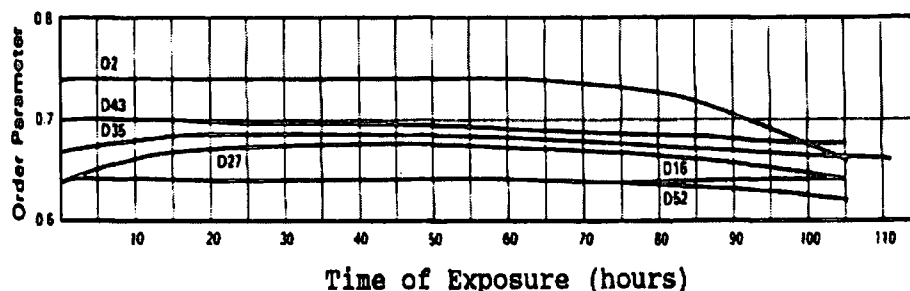
Figure 2-4. Change in order parameter of dyes
on exposure to Hanovia Arc Tube.

It is known that the degradation can be reduced by the use of an UV cut-off

filter on the display [86]. This can be achieved by putting a plastic layer

containing UV absorbing particles or by deposition of a UV absorbing thin

oxide film on the glass. The filter can increase the photostability of the azo

dyes by 25-30 times [102]. This makes the stability of azo dyes comparable to

that of stable anthraquinone dyes [102]. The UV curable epoxy resins are also

found to absorb UV light significantly even in the cured state, which would

be an additional advantage of the PDLC made by the UV curing method (Section 4.2.1).

2.2.6. Highly Dipolar Dye
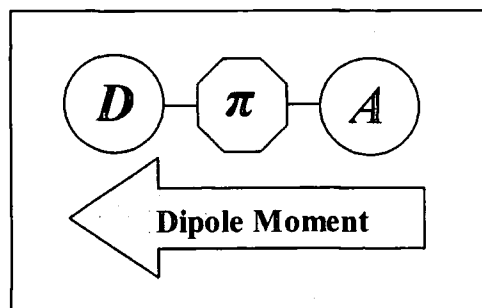
Figure 2-5. Schematic diagram of a dipolar
molecule.

Dyes with high dipole moments usually consist of electron acceptors, A, (e.g. NO_2, CN), and electron donors, D, (e.g. NH_2) separated by an extended π-conjugated sequence (-π-) as shown in Figure 2-5 [103-105]. The delocalisation of the electrons in the π-conjugated sequence allow electrons to move freely between the acceptor and donor groups. Additionally, when such molecules are planar in shape, this results in a higher dipole since sufficient 2ps hybrid orbital overlap is required for delocalisation of π-electrons. The exact structure and nature of the highly dipolar dye used in this work will be discussed in Section 2.3.2.

2.3. Materials

2.3.1. Liquid Crystal
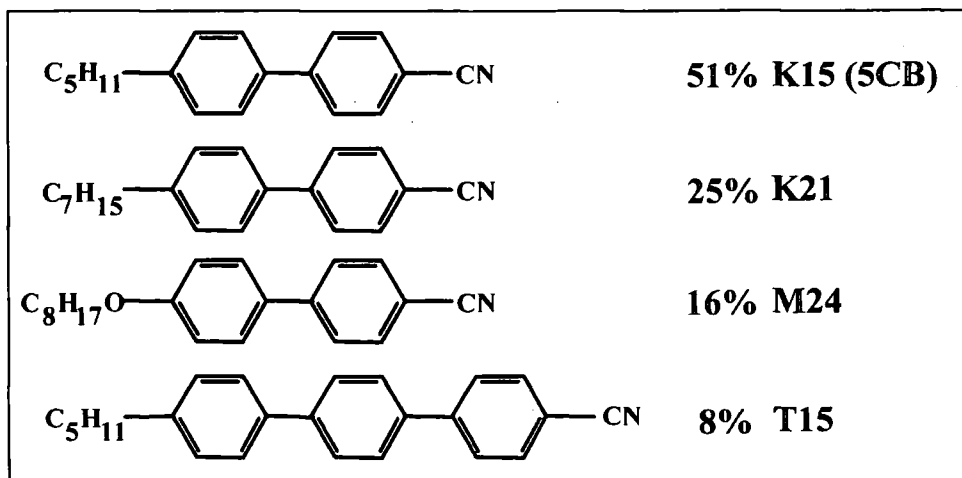
Figure 2-6. Molecular structure of E7 (BL001)
and 5CB.

E7, or BL001, is one of the most commonly used nematic liquid crystals for

PDLCs. Its properties have been widely studied [106, 107]. E7 consists of

K15 (5CB; 4-pentyl-1-4'-cyanobiphenyl), K21 (4-heptyl-4'—cyanobiphenyl),

M24 (4-octyloxy-4'-cyanobiphenyl), and T15 (4-pentyl-4'-cyanoterphenyl).

The proportions of liquid crystal molecules that form E7 are shown in Figure

2-6. Due to this mixing of several liquid crystals, E7 has a broad liquid crystal

phase of between -10 and 61°C and a high boiling point of 200°C. E7 liquid

crystal was purchased from Merck Ltd UK, and the values quoted below are

from the manufacture's data sheet unless otherwise stated.

The dielectric anisotropy, $\Delta\varepsilon$, is 13.8 ($\varepsilon_{//}$=19.0, $\varepsilon_{\perp}$=5.2, 1 kHz, at 20 °C), the

density is 1.0 g/ml, and the resistivity is 5 x 10^{10} Ωcm. The ordinary refractive

index ($n_o = n_{\perp}$) of the liquid crystal is 1.5216 and extraordinary refractive

index ($n_e = n_{//}$) is 1.7462 (589 nm at 20 °C). This ordinary refractive index

matches the refractive index of the polymer (n_p), enabling the PDLC to

become transparent when a voltage is applied. The liquid crystal's

extraordinary refractive index differs from the polymer refractive index by

0.22. This refractive index mismatch results in PDLC scattering.

2.3.2. Highly Dipolar Dichroic Dye
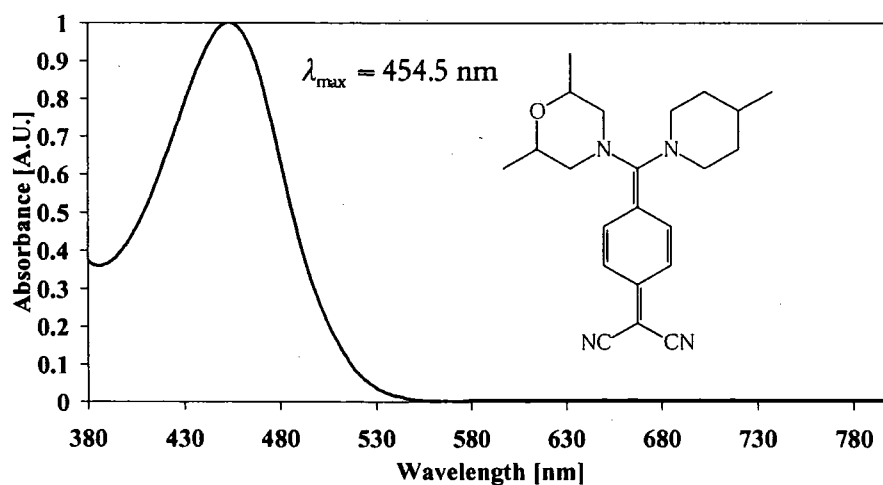
Figure 2-7. Chemical structure and the
normalised absorbance of MORPIP when
doped into E7 liquid crystal.

A derivative of 7,7,8,8 tetracyanoquinodimethane (*TCNQ*) called *MORPIP*

[108] was used as a highly dipolar dye in this work. Its full chemical name is 7-

(2,6,dimethylmorpholino)-7-(4-methylpiperidino)-8,8-dicyanoquinodimethane, and the structure is shown in Figure 2-7. This was measured when the alignment direction is parallel to the polarisers. Its absorbance was normalised to 1. It has a dipole moment of 15 ± 1 Debyes [108]. It is a conjugated yellow chromophore with absorption typically in the range of 350-500 nm (λ_{max} = 454.4 nm in E7) and that absorbs UV light in E7. The peak absorption changes with different solvents [109]. The absorption spectra was taken with a MORPIP doped E7 in a homogeneous alignment cell. The extinction coefficient is 0.22×10^4 in 5CB. The decomposition temperature is over 260°C. The molecule was synthesised within the University of Durham [110] and was chromatographically purified. The structure of the dye was confirmed by NMR, and mass spectroscopy and the purity was estimated by the thin layer chromatography method.
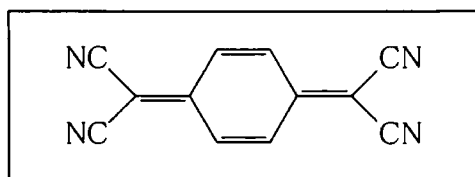
Figure 2-8. Molecular Structure of TCNQ.

The large dipole moments of TCNQ adducts result from the strong electron affinity of TCNQ enabling intramolecular charge transfer within its resultant adducts [111]. TCNQ (Figure 2-8) [112-118] forms stable charge transfer salts due to the high electron affinity due to the presence of the four strong electron accepting cyano groups and its planar nature [113]. TCNQ was reacted with a secondary amine to synthesize MORPIP. The CN group acts

as an acceptor that induces electron flow from the benzene ring. On the other hand, the amino group acts as an electron donor which produces an opposite charge flow. This push-pull effect has been used for designing molecules for nonlinear optical applications [104, 119-132].

2.3.3. Commercial Dichroic Dyes `

In order to identify GH effects specific to the highly dipolar dye, three less polar commercially available dyes were selected for comparative studies. The most widely used dichroic dyes in GH displays are azo and anthraquinone dyes [133]. Compared to anthraquinone dyes, azo dyes are, in general, more chemically unstable to UV light, but they posses high dichroic ratios, high order parameters, high extinction coefficients, and good solubility in liquid crystals [42, 58, 68, 73, 84-87, 134, 135]. From a standpoint of colour display requirements, red, blue and black dyes were selected.

D2 is a red azo dye with $\lambda_{mx} = 496$ nm in E7. The colour is very strong, giving a dichroic ratio $(A_{//}/A_{\perp})$ of 10. This is because of its high order parameter of 0.75 (in E7). It has a high extinction coefficient of 3.0×10^4 (in $CHCl_3$). Its melting point is 203°C. The dye is available from Merck Ltd, UK, and the values quoted above are from the data sheets. The measured solubility of D2 in E7 was 3.5 wt% at 21°C. Its chemical structure and normalised absorbance spectra are shown in Figure 2-9.
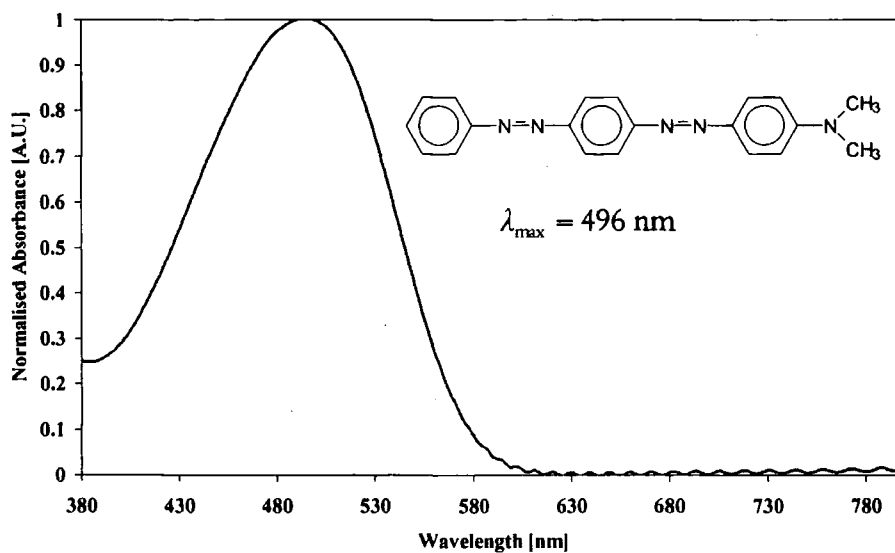
Figure 2-9. Chemical structure and the
normalised absorbance of D2 in E7.
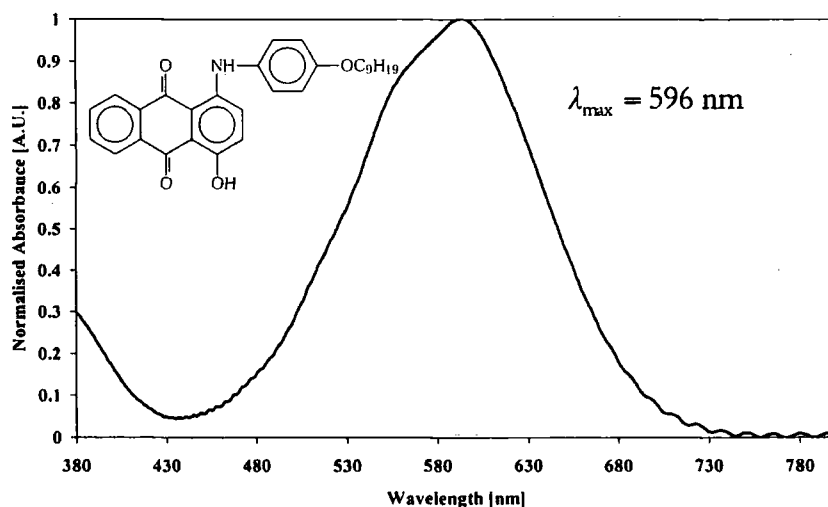
Figure 2-10. Chemical structure and the
normalised absorbance of D16 in E7.

D16 is a blue anthraquinone dye with λ_{max} = 596 nm in E7, also available from

Merck Ltd., UK. The chemical structure and the normalised absorbance are

shown in Figure 2-10. Because of its compact shape the anthraquinone dye

has a smaller order parameter compared to the azo dye. D16 has an order

parameter of 0.63 in E7. The extinction coefficient is 1.24×10^4 in $CHCl_3$. Due

to the lower order parameter, the anthraquinone dye has a lower dichroic

ratio $(A_{//}/A_{\perp})$ of 6.6. Its melting point is 102.5-103 °C. The values were

quoted from the manufacturer's data sheet. The measured solubility was

2.2 wt% in E7 at 25°C.
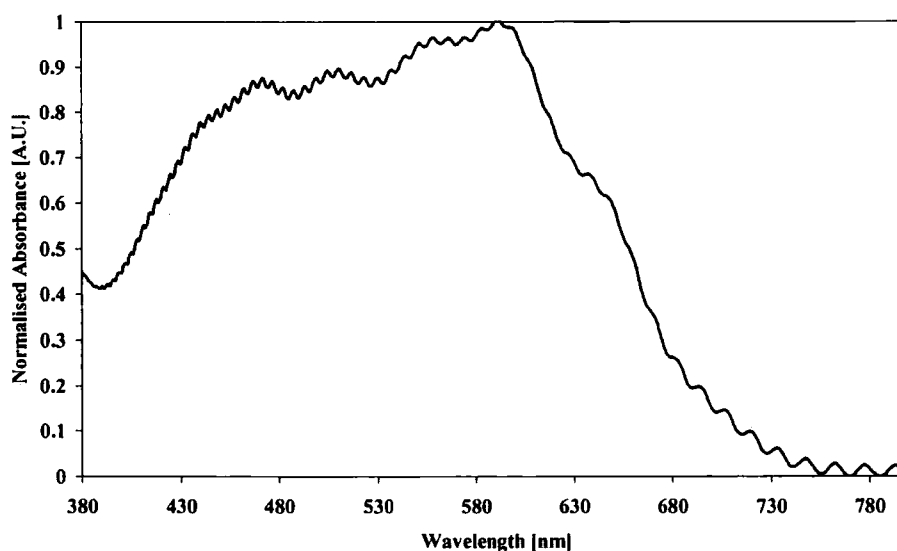
Figure 2-11. Normalised absorbance of B2 in

E7.

B2 (or Black-2) is a black dye that is a mixture of thirteen azo and

anthraquinone dyes, and is available commercially from Mitsubishi Chemical

Corporation, Japan. It has a very high solubility of 11.53 wt% (In ZLI-1565 at

25°). Data of chemical structures and other properties were not available from

the manufacturer. The normalised absorption spectrum is shown in Figure

2-11. The spectrum differs slightly from Figure 2-2 either due to small

difference in the mixing ratio of the component dyes, or due to the solvatochromic shifts for the dyes are different in E7 and the liquid crystal used to obtain the spectrum in Figure 2-2.

2.4. Experiments and Results

2.4.1. Sample Preparation

Cells were prepared by standard methods [136, 137] with variations as described below.

The environment of the cell fabrication was kept constant. In order to minimise the impurity in the sample and to maintain a high resistivity of the liquid crystal, it was ensured that neither metals nor glasses were brought into contact with the materials; spatula and magnetic stirring bars were Teflon coated, and dark coloured plastic sample bottles were used to avoid deterioration by light. All chemicals were kept in the dark in a dry nitrogen filled glove box to avoid absorption of water. MORPIP dye was obtained from our chemist by recrystallisation [108] and was therefore of high purity. The crystals were dried in a vacuum oven at 80 °C for more than a week and then stored in the nitrogen filled glove box afterwards. Other commercial dyes were stored in the glove box at purchase. All of the preparations, apart from weighing dyes and liquid crystals, were carried out in the glove box at room temperature. The environment was kept as dark as possible to minimise dye deterioration.

The empty ITO coated glass sandwich cells with antiparallel homogeneous alignment were purchased from E.H.C Co., Ltd., Japan (KSRP-50/B111PINTS). All the cells were kept in a clean room at 21 °C at purchase. According to the manufacturer's data sheet, the cells were pre-ITO coated on both sides with polyimide (40-50 nm thick, LX-1400 from Hitachi Kasei Ltd, Japan) as surface alignment material, giving the tilt angle of 1-2°, which is the angle between the liquid crystal director and the substrate.

All the cell thickness were measured prior to filling with liquid crystal using a capacitance measurement techinique. HP 4278A 1 kHz/1 MHz Capacitance Meter (Hewlett Packard) was used. The capacitance meter was left on at least 30 minutes to stabilise prior to measurements. It was set to use 1V, 1kHz, 2 m cable length, and average 64 readings. Capacitances of empty glass cells were measured by connecting the capacitor meter's cables to the cell's electrodes, at 21 °C in a clean room environment. The cell's thickness were calculated by using the equation:

$$C = \varepsilon_0 \varepsilon_r \frac{A}{d}$$

Equation 2-2

where C is the capacitance measured, A is the ITO area of 1 cm^2, d is the thickness of the cell (in m), ε_0 is the vacuum permittivity (8.854 × 10^{-12} Fm^{-1}) and ε_r is the reletive permittivity (1.00059 for air). It should be noted that the cell thickness calculated by this method is the average cell thickness over the ITO area and not the exact thickness of one particular spot. Hence the cells

were carefully observed prior to the measurement, i.e. the cell were not used if the ITO area was not overlapping correctly or if the cell contained many and irregular interference pattern (Newton ring). The average cell thicknesses obtained were then used to calculate the average internal electric field (E) for each cell, i.e. $E = V/d$. It was necessary to obtain these data for the response time measurement carried out later in Section 3.4.3.

To obtain a dichroic mixture with the desired concentration, a small amount of dye, typically 0.02 g, was first weighed. Depending on the weight % required, the amount of liquid crystal was controlled. For example, 0.1 g (approximately 0.1 ml) of liquid crystal was added to the 0.02 g dye to make a 5 wt% doped LC solution. The solution was kept in a plastic, dark coloured, centrifuge tube, and it was left stirring for more than a day. After mixing, the solution was centrifuged at 600 rev/min for 5 minutes to eliminate any dust and air bubbles. When the doped LC solution contained undissolved dye that was required to be removed, this centrifuge technique was also used, rather than filtering. This is because filtering caused much solution to be wasted. Finally the cells were filled with the solution by means of capillary action by applying a few drops of the solution to the cell gap. The cells were then heated above the liquid crystal's isotropic temperature (61°C for E7) to remove any alignment defects caused by the filling. The uniformity and the alignment were checked under cross-polarised microscope. When the LC is uniformly aligned, the cell appears black when it is rotated at 0 or 90 ° to one of the polarisers axis. On the other hand, the cell becomes brightest at 45 °. If

the cell used has the homeotropic alignment (Figure 1-4), the cell appears

black at all angles under the cross-polarised microscope. This is because the

liquid crystal does not exhibit birefringent property along the long axis of the

molecule. It was also ensured that no undissolved particles were present at

this stage. Then both open ends of the cell were sealed with epoxy resin to

prevent contamination by surrounding air, and the cells were kept in the glove

box.

2.4.2. Dichroic Ratio and Order Parameter Measurement

Absorbance parallel ($A_{//}$) and perpendicular ($A_{\perp}$) to the director of the liquid

crystals, and hence the maximum and the minimum absorption of the dye

molecules in the liquid crystals, were measured using a Perkin Elmer

UV/VIS/NIR Lambda 19 spectrometer at room temperature. Two identical

Glan-Thompson polarisers were used. As shown in Figure 2-12, the doped

cell was mounted either (a) upright or (b) rotated perpendicular to the

polariser to obtain $A_{//}$ and $A_{\perp}$ respectively.

Cells with large thickness (50 μm) were used in order to measure the strong

enough absorption value of $A_{//}$ and $A_{\perp}$ of the dyes. A typical spectrum of

0.5 wt% D16 dye in E7 liquid crystal is shown in Figure 2-13. Both parallel

and perpendicular absorbances matched above 750 nm (outside the dye

absorption region), indicating that there was no unwanted effect such as

scattering. The reference cell, filled with the undoped liquid crystal, was used

to compensate the losses due to scattering, reflection and absorption from the

cell walls and host molecules. $A_{//}$ and $A_{\perp}$ were measured at λ_{max} [56].
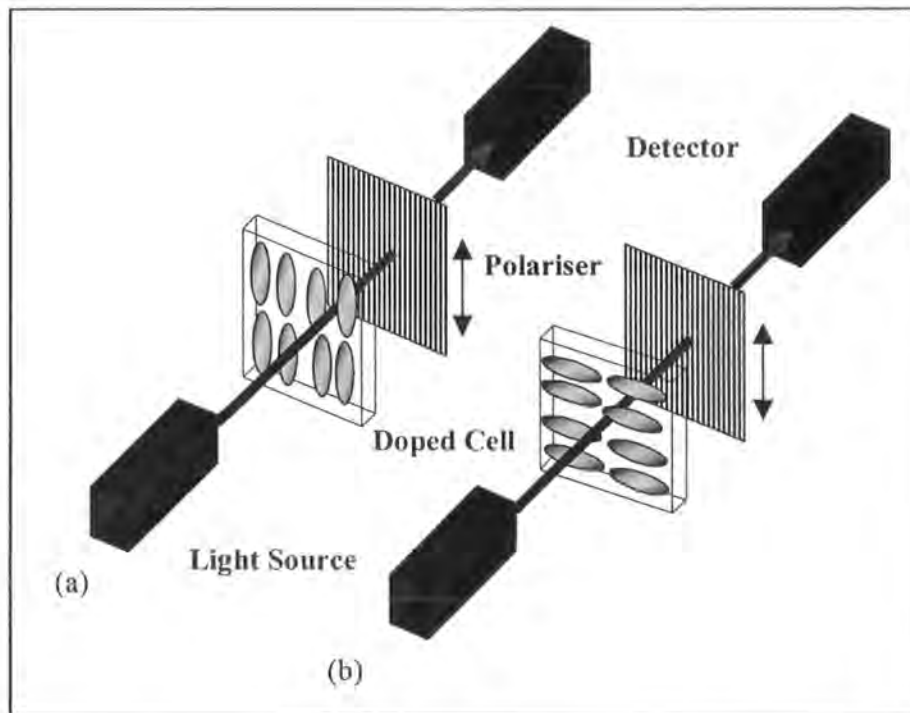
Figure 2-12. Measurement of (a) $A_{//}$ and (b)
$A_{\perp}$ of a dye doped liquid crystal cell.

For D16 dye, λ_{max} was at 596 nm, and $A_{\perp}$=0.1664 when $A_{//}$ was normalised

to unity. Using the Equation 2-1, this data yielded a dichroic ratio of 6.01 and

order parameter of 0.626. Average of 3-5 readings were taken to minimise the

uncertainty in the small deviation of the cell's angle to the polariser axis.

Similarly, dichroic ratios and order parameters of all the other dyes were

calculated and are listed in Table 2-1. The quoted values were obtained from

the manufacturer's datasheet [138], and the error was calculated from small

deviations in the absorbance baseline. For D2 and D16, the obtained values

were consistent with the quoted values within experimental error, assuring the

values obtained for MORPIP and B2. The tendency of the obtained value

being smaller than the quoted values could be because of the weak alignment

due to the thick cell used and also due to inaccurate alignment of cells with

respect to the polarised light. Employment of a cell rotating stage for a precise

angle adjustment against the polariser would increase the accuracy.
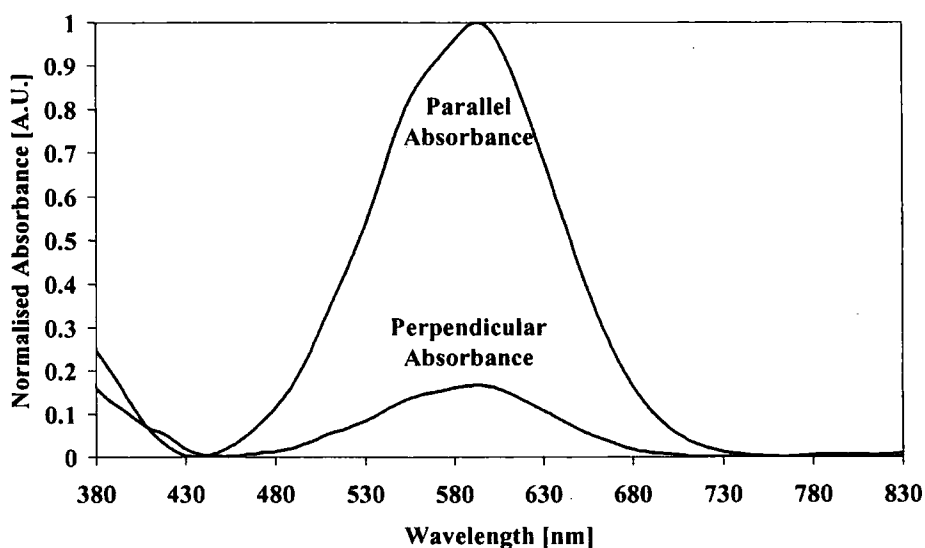
Figure 2-13. Normalised absorption spectra of
D16 dyes at on and off-state.

MORPIP has not been designed specifically for compatibility with the liquid

crystal, thus the molecule was not expected to possess a high dichroic ratio

and order parameter. Indeed, MORPIP was shown to have somewhat lower

values compared with the other commercial dyes.

Dye	Dichroic Ratio	Quoted Dichroic Ratio	Order Parameter	Quoted Order Parameter
MORPIP	2.34 ± 0.40	-	0.309 ± 0.064	-
D2	8.67 ± 1.68	10	0.719 ± 0.044	0.75
D16	6.01 ± 0.76	6.6	0.626 ± 0.035	0.63
B2	11.80 ± 2.17	-	0.783 ± 0.034	-

Table 2-1. Dichroic ratio and order parameter

of dyes.

2.4.3. Photostability
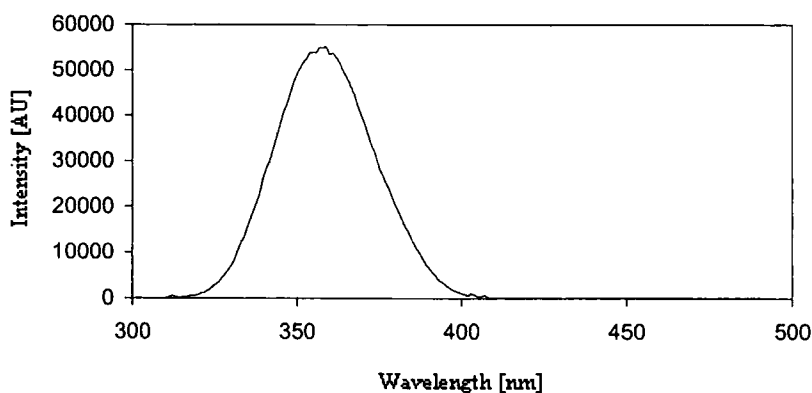
Figure 2-14. Intensity profile of the UV lamp.

As the photostability of the dyes are an important parameter in fabrication of PDLCs (Section 4.2.1), their photostabilities against UV light were monitored. 50 μm cells were used for fabrication of MORPIP, D16 and B2 doped liquid crystal samples. The large thickness allowed the accurate measurement of $A_{//}$ and $A_\perp$ at the λ_{max} of each dye. However, D2 has a very high extinction coefficient (3.0 x 10^4 in CHCl$_3$ [138]) that is too high for 50 μm cell thickness

to be used, thus 10 μm cells were employed. The preparation method was the same as that described in Section 2.4.1. The absorbance obtained for MORPIP, D16 and B2 were divided by 5 to allow direct comparison with D2 absorbance. The dye concentration was 0.3 wt% for MORPIP and 0.5 wt% for D2, D16 and B2. The cells were irradiated by UV light (360 nm, Spectroline, Model EN-180L/F, 230 V, 50 Hz, 0.17A) from a distance of 10 cm at room temperature. This was the same condition that was used for PDLC fabrication described in Section 4.2.1. The measured intensity profile of the UV lamp measured using a Jobin Yvon Horiba Fluoromax 3 is shown in Figure 2-14. The absorbance profile of the glass cell used for this experiment shows that the UV light could transmit through the cell at 360 nm (Figure 2-15).
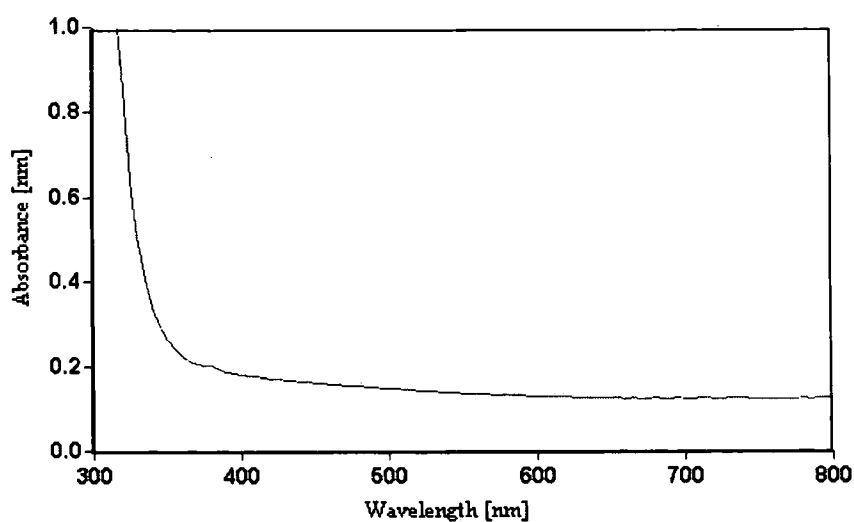
Figure 2-15. Absorbance of the glass cell.

The experimental result (Figure 2-16) shows the constant deterioration of MORPIP absorbance $(A_{//})$ with time. The changes in absorbance were

plotted against time, and the results are shown in Figure 2-17. By assuming that the fading rate is constant [75], the peak absorbance (at constant wavelength) data points were fitted with linear functions against time, and the equations for these were shown next to each line. D2, D16 and B2 show almost no degradation after a 17 hour-long exposure to the UV light. The linear fits of those dyes showed very small negative gradients. The differences were small enough to plot zero gradient lines if the errors were taken into account. A much longer irradiation time or a stronger UV source would reveal more significant deterioration of these commercial dyes.
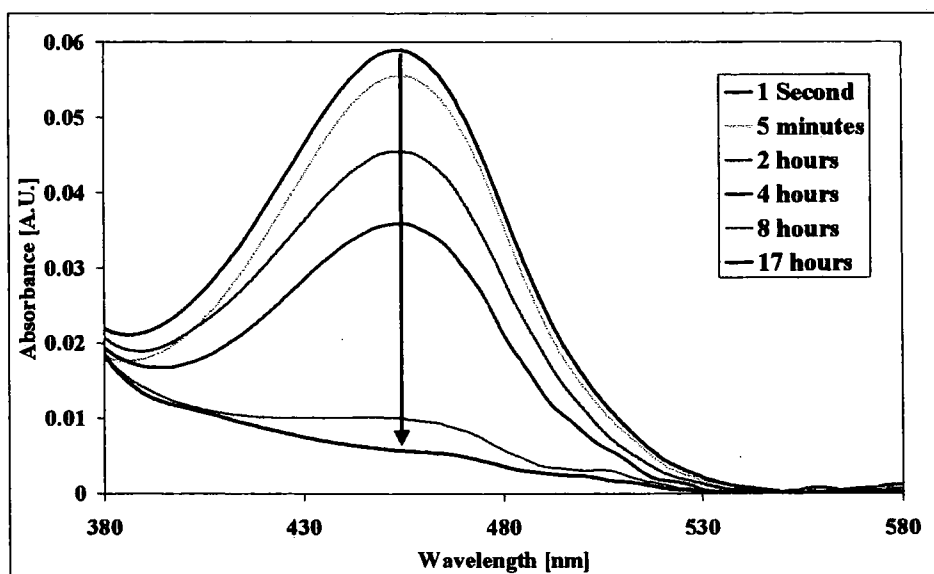
Figure 2-16. Deterioration of MORPIP

absorbance $(A_{//})$ with UV irradiation.

In contrast, a linear fit to the MORPIP data gives the gradient of -8×10^{-7} s^{-1} which is more than 8 times larger than the others. Although the decrease in MORPIP absorbance can be seen in Figure 2-17, the difference is clearer on

observing absorbance spectra of MORPIP as shown in Figure 2-16. The linear gradiant gives the half-life of MORPIP to be 8.56 hours. However, the half-life is clearly not correct as the spectrum at 8 hours in Figure 2-16 shows that it is more than half way through the deterioration. Thus the last "flat spectra" must have been achieved between 8 hours and 17 hours of irradiation. A linear fit of MORPIP without the last data point gives a gradient of $-1 \times 10^{-6}\,\text{s}^{-1}$ with a half-life of 7.153 hours which is more consistent with Figure 2-16. For more accurate measurement of the deterioration rate, thicker cells should be used.
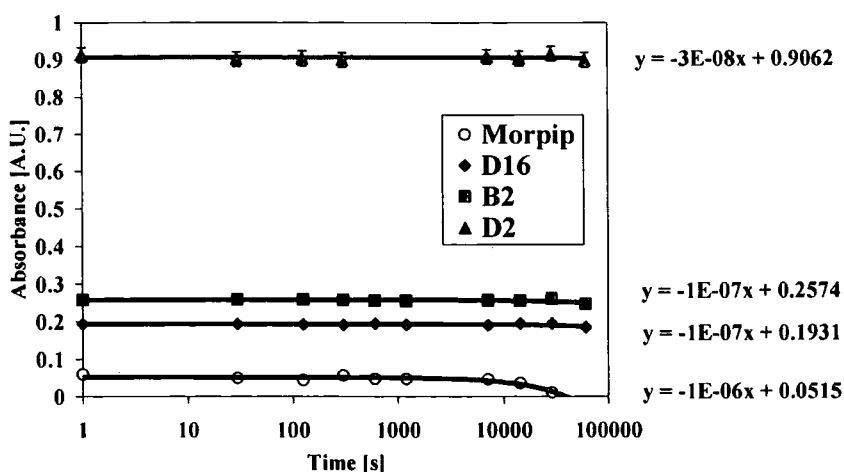
Figure 2-17. Deterioration of absorbance $(A_{//})$
with UV irradiation.

Dichroic ratios and order parameters of each dye during degradation were calculated using Equation 2-1 as in the previous section and are plotted in Figure 2-18 and Figure 2-19 respectively. Symbols identifying dyes are as in Figure 2-17. The results were very similar to the absorbance deterioration

graph (Figure 2-17). MORPIP showed more than an order of magnitude larger negative gradient, while other commercial dyes showed no change within the measurement error. These results imply that MORPIP is not suitable as a dye for a practical GH display.

$y = -1E-06x + 11.104$

$y = -6E-06x + 8.8143$

$y = -6E-07x + 5.9327$

$y = -3E-05x + 2.0474$
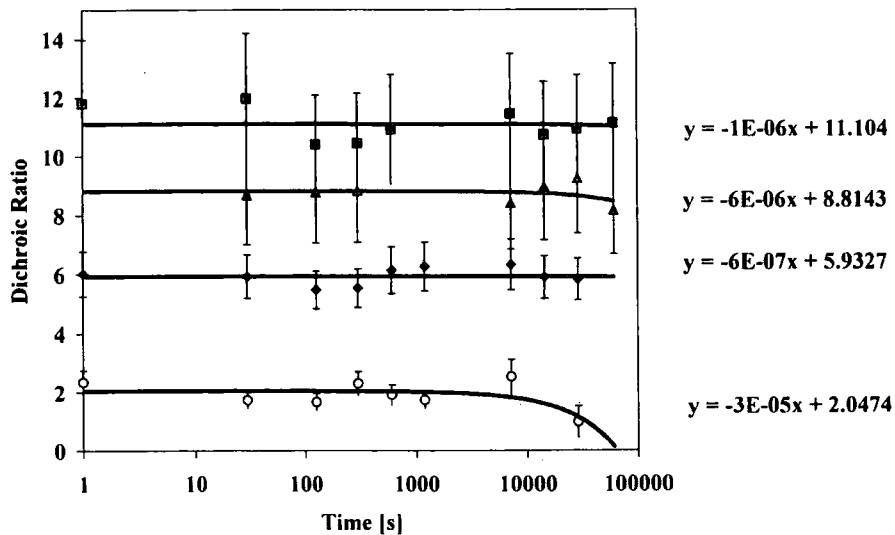
Figure 2-18. Deterioration of dichroic ratio
with UV irradiation.

$y = -1E-08x + 0.7706$

$y = -2E-07x + 0.7226$

$y = -1E-08x + 0.6212$

$y = -8E-06x + 0.2567$
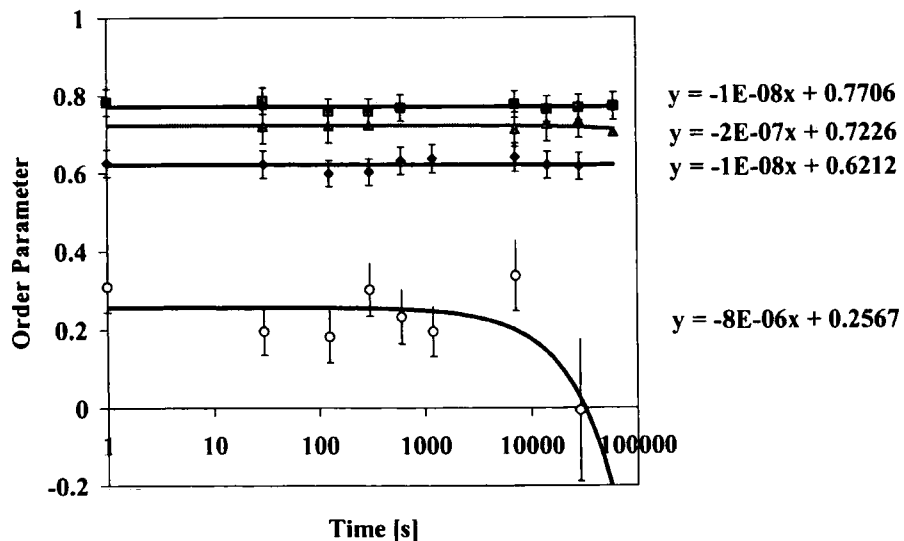
Figure 2-19. Deterioration of order parameter
with UV irradiation.

2.5. Conclusion

In this chapter, basic dye characterisations were performed. The highly dipolar yellow dye MORPIP was compared with commercially available azo and anthraquinone dyes. With the scope of future colour display in mind, a red D2 azo dye, a blue D16 anthraquinone dye and a B2 black dye (mixture of azo and anthraquinone dye) were chosen.

Dichroic ratios and order parameters of the dyes were measured, with D2 and D16 giving consistent results with the manufacturer's data sheet. Those parameters on MORPIP and B2 dyes were also determined. MORPIP was found to give a low dichroic ratio and order parameter compared to other commercial dyes. Although the results were consistent within experimental error, they all tend to be smaller than the quoted value. This is probably due to inaccurate alignment of cells with the plane of polarisation of the light. Employment of a cell rotating stage for a precise angle adjustment against the polariser is expected to increase the accuracy.

The photostability measurement also showed that MORPIP deteriorated faster than other dyes. MORPIP had a half-life of 7.153 hours. The other dyes did not show any significant deterioration over the time span of the experiment. Using a stronger UV source for a longer time might reveal the deterioration of other dyes. The order parameter of the host should be compared with that of the guest using optical birefringence measurements [139].

These results imply that the highly dipolar dye, MORPIP, is not suitable as a dichroic dye for GH displays. Nevertheless, the usefulness of the large molecular dipole of MORPIP is demonstrated in the next chapter. In particular, the increase in response speed of the GH mixture to an applied electric field is investigated in detail.

Chapter 3: Guest-Host LC

3.1. Introduction

Liquid crystal display technology would benefit from reduced switching times and drive voltages. The incorporation of highly dipolar dyes in a liquid crystal host was expected to increase the dielectric anisotropy of the liquid crystal host (see Section 3.2.2) and hence decrease the switching time and driving voltages [9, 140]. This guest-host effect was studied electro-optically; the rise time, decay time and dielectric anisotropy were compared with those for undoped liquid crystal samples. Commercially available dyes described in Section 2.3.3, were also used in this investigation.

The next section describes the backgrounds to the guest-host effect, and the detailed experiments. The results (decay time, rise time and dielectric anisotropy measurements) of the experiments follow.

3.2. Theory

Dyes have been used extensively in nematic [42] and ferroelectric [141] liquid crystal displays, and the GH effect has been studied intensively in the past [56, 68, 92, 134, 142].

Though the use of dyes in nematic liquid crystals to make polarising sheets was proposed in 1946 [143], and the GH effect discovered earlier than TN

displays [21], GH displays did not attain the same market response as TN

displays. Poor dye stability and low contrast made them unsuitable for low

cost, high information content displays. Nevertheless, in the late 1970's, the

technology gained market acceptance for low information content

applications. These displays are widely used in avionics and military displays

that require daylight readability, unrestricted viewing angle, and harsh

environmental stability requirements, especially high temperature operation

and storage [144]. Recently, applications such as automotive dashboards,

multicolour displays [58, 145, 146], electrophotographic printers and optical

storage devices [147, 148] have been developed.

3.2.1. Guest-Host Effect

All GH displays incorporate a small amount of a dichroic dye (guest)

dissolved in a liquid crystal (host). In the case of a *Heilmeier display*, which was

the first proposed GH display [42, 149], pleochroic dyes were added to a

liquid crystal with positive dielectric anisotropy (Figure 3-1). The dye

molecules that are dispersed in the liquid crystal host, tend to arrange in such

a way that their long molecular axis align along the liquid crystal director. This

tendency of alignment between guest molecules and host molecules are called

the *GH effect* [42]. A single polariser is mounted with its polarisation axis

parallel to the long axis of the dyes in liquid crystal. In the unpowered dark

state, the liquid crystal and dye molecules are aligned parallel to the incident

light, which results in maximum absorption of the light. The application of an

electric field in such a system causes reorientation of the liquid crystal molecules. The dye molecules rotate together with the liquid crystal molecules, resulting in a change of colour intensity. This forms the basis of all GH displays [58, 60, 63, 150].
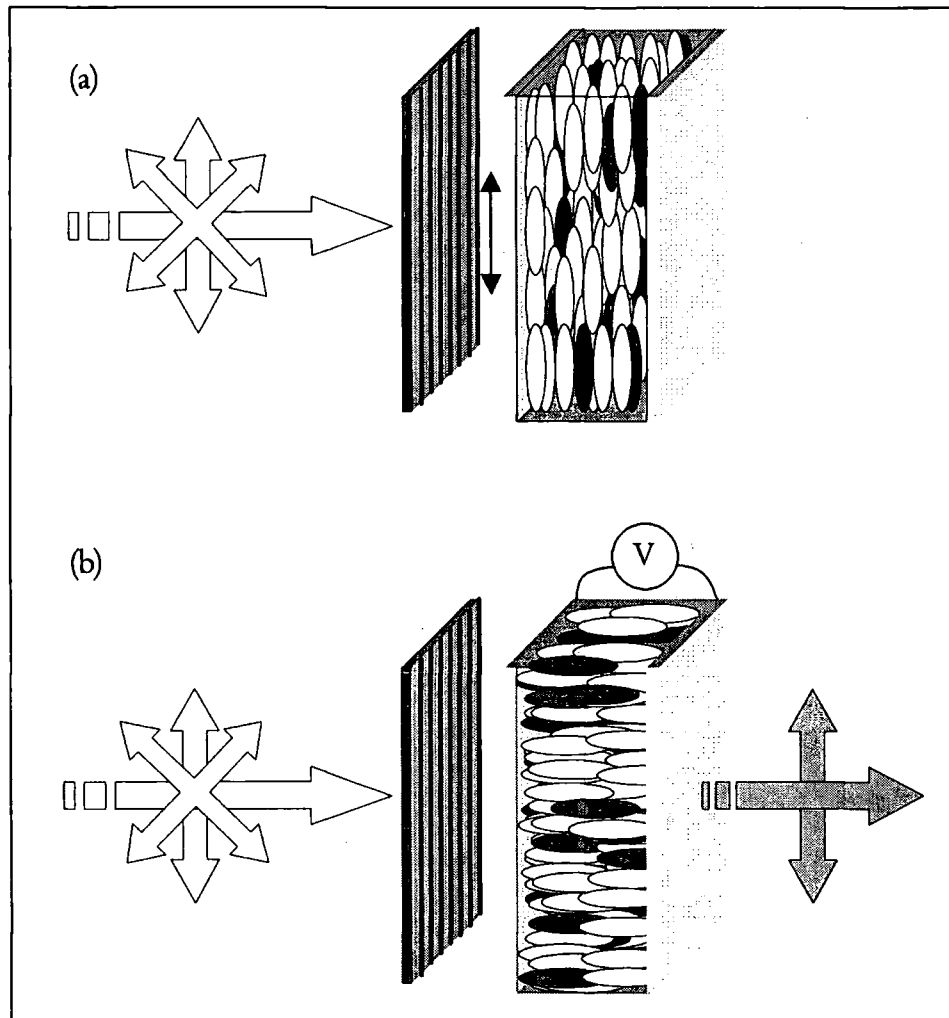
Figure 3-1. Heilmeier display at on- (a) and
off-state (b).

It is known that the small concentration of guest molecules generally does not drastically affect the host properties (e.g. birefringence, dielectric anisotropy, elastic constant, viscosity, order parameter and transition temperature) [69,

72]. Nevertheless, it had previously been found that a higher concentration of a dye affects transition temperature [62, 68, 134, 151-154], order parameter [62, 68, 151] and dielectric properties [120, 155-157].

Heilmeier GH-LCDs [42, 59, 149, 158] have a lower contrast ratio for normal incident light when compared with other LC display mode such as TN-LCDs. However, the Heilmeier GH-LCDs have relatively wide viewing angles, bright colour display, stable hue independent of temperature and high reflectance. Hence Heilmeier display mode is expected to be one of the most promising display modes in future [47].

In the case of a Heilmeier display, the contrast ratio (T_{max}/T_{min}) increases exponentially with an increase in dye concentration while transmittance (T_{min}) shows more or less a linear decrease [72]. This means that with small increase in dye concentration one can obtain a high contrast without a heavy loss in transmittance [72]. The switching time (Section 3.2.3) of the display also increases slightly due to an increase in the viscosity of the liquid crystal. The increase in switching time becomes more significant at lower temperatures and very often restricts the low temperature operation of the display. The threshold voltage (Section 1.3.8) is not affected significantly by increases in dye concentration [59].

3.2.2. Dielectric Anisotropy

As mentioned in the previous section, the dielectric anisotropy does not generally change with a low concentration of dye in a liquid crystal host. However, when the guest dye is polar, it is known to give some noticeable impact on the dielectric anisotropy [155]. Wu *et al* [120] report that the doping with dyes with high solubility and high dielectric anisotropy increases the dielectric anisotropy of the host liquid crystal. This reduces the threshold electric field of the liquid crystal as can be seen from Equation 1-13. It can be shown, see Equation 3-7 below, that this increase in dielectric anisotropy reduces the rise time of the liquid crystal. Hence we have carried out the experiment of adding our highly dipolar MORPIP to a liquid crystal host to see if this is in fact the case.

The change in dielectric anisotropy can be determined by the measurement of the capacitance [159] of homogeneously and homeotropically aligned liquid crystal cells. Then the dielectric anisotropy can be calculated by using the following equations,

$$\Delta\varepsilon = \varepsilon_{//} - \varepsilon_{\perp} \qquad \text{Equation 3-1}$$

where $\varepsilon_{//} = C_{//}/C_0$ and $\varepsilon_{\perp} = C_{\perp}/C_0$. C_0 is the capacitance of empty cell, $C_{//}$ and $C_{\perp}$ are the capacitance of homeotropically and homogeneously aligned cells respectively, $\varepsilon_{//}$ and $\varepsilon_{\perp}$ are dielectric constant of homeotropically and homogeneously aligned cells respectively, and $\Delta\varepsilon$ is the dielectric anisotropy.

3.2.3. Response Time Theory

Homogeneously aligned liquid crystal cells undergo a Freedericksz transition (Section 1.3.8) when the applied electric field, E, is bigger than the critical electric field, E_o. Here equations of the response dynamic of liquid crystal to an electric field are derived and described.

The dynamics of the splay and bend distortions (Figure 1-11) inevitably involve the flow processes, called the backflow effect [160, 161], coupled with the director rotation. Only a pure twist distortion is not accompanied by flow. By assuming a minimal effect due to the backflow, the equation of motion of the director θ (angle variation) for the splay, bend and twist can be expressed by balancing the torques due to the elastic and viscous forces and the external field [162, 163]:

$$\gamma \frac{\partial \theta}{\partial t} = K_{ii} \frac{\partial^2 \theta}{\partial z^2} + \varepsilon_0 \Delta \varepsilon E^2 \sin \theta \cos \theta , \qquad \text{Equation 3-2}$$

where γ is a rotational viscosity, K_{ii} is an elastic constant, ε_0 is a vacuum permittivity ($= 8.854 \times 10^{-12} \, J^{-1}C^2m^{-1}$), z is an axis perpendicular to the cell surface, and $\Delta\varepsilon$ is a dielectric anisotropy.

If the field does not exceed the threshold potential then a small angle approximation can be made on the angle of deviation of the director. Furthermore, approximating the alignment of the director at the cell wall to have no pretilt, the condition $\theta = 0$ can be made at the boundaries. Then a

general solution for θ can be seen as a Fourier series of a superposition of spatial modes [162],

$$\theta = \sum_n c_n(t) \cos[(2n+1)\pi z / d]$$
                                                        Equation 3-3

where d is a layer thickness, n is an integer, and the time dependent amplitudes are small $|c_n(t)| << 1$.

The nature of this equation means that the amplitude of each nth spatial mode will fall off exponentially as a decay time.

Assuming the response requires the least energy then the solution of the above can be taken as being that of the slowest growing harmonic ($n = 0$),

$$\theta = \theta_m(t) \cos\left|\frac{\pi z}{d}\right|$$
                                                        Equation 3-4

where θ_m is the angle of deviation of the director at the centre of the layer. Substituting this result into Equation 3-2 and by integration, the time dependence of θ_m is [37],

$$\theta_m^2(t) = \frac{\theta_m^2(\infty)}{1 + \left[\frac{\theta_m^2}{\delta^2} - 1\right] \exp\left[-\frac{2\varepsilon_0 \Delta \varepsilon E^2}{\gamma}\left(\left(\frac{E-E_0}{E_0}\right)^2 - 1\right)t\right]}$$
                                                        Equation 3-5

where δ^2 is the fluctuation in the director at turn on:

$$\delta^2 = \frac{Tk_B}{\pi d K_{ii}} \log\left(\frac{E-E_0}{E_0}\right) = \langle\theta_m^2(0)\rangle$$
                                                        Equation 3-6

where T is the absolute temperature, k_B is the Boltzmann's constant, $\Delta\varepsilon$ is a dielectric anisotropy, and E_0 is a critical electric field (Equation 1-13).

Assuming the strong anchoring, the time constant in which θ_m tends towards a steady state value can be obtained. This time constant which is the time it takes for the liquid crystal to responds to the field, known as *rise time* τ_{rise}, can be expressed as [37, 164]:

$$\tau_{rise} = \frac{\gamma}{\varepsilon_0 \Delta\varepsilon (E^2 - E_0^{\ 2})} \qquad \text{Equation 3-7}$$

Inverting the Equation 3-7 gives

$$\tau_{rise}^{-1} = \frac{\varepsilon_0 \Delta\varepsilon}{\gamma} E^2 - \frac{\varepsilon_0 \Delta\varepsilon}{\gamma} E_0^{\ 2} \qquad \text{Equation 3-8}$$

showing that the inverse of the rise time is linearly proportional to E^2. Hence the gradients $\varepsilon_0 \Delta\varepsilon / \gamma$ can be used for the comparison of the switching speed of liquid crystals [164]. Additionally, the threshold electric field, E_0, can be calculated using this equation.

The time it takes for the liquid crystal to relax back from its on-state to the initial homogeneous position is known as the *decay time*, τ_{decay}, and it can be obtained by balancing the torques due to the elastic and viscous forces [37].

$$\gamma \frac{\partial \theta}{\partial t} = K_{ii} \frac{\partial^2 \theta}{\partial z^2} \qquad \text{Equation 3-9}$$

As before, the solution can be expressed as Fourier series, with the amplitude of the nth spatial mode falling off exponentially as a decay time, such that for small initial distortions,

$$\tau_{decay}^{-1} = \frac{K_{ii}}{\gamma}\left[\frac{(2n+1)\pi^2}{d}\right]$$

Equation 3-10

If the applied field at turn off was such that $E >> E_0$, then the distribution of the angle of deviation of the director about $\theta(z)$ is given by a series of functions, decaying with time constants in the above equation. The least deformed configuration will decay most slowly, and so the elastic realignment of the director is simply the damped case, described by a single exponential with decay constant, [37]

$$\tau_{decay} = \frac{d^2\gamma}{\pi^2 K_{ii}}$$

Equation 3-11

showing that the decay time is independent of dielectric anisotropy or the applied electric field. In this work, decay time was measured to observe the effect of dopants on the viscosity and elastic constant.

3.3. Experimental Set-up

A suitable method to measure the response time of a GH cell is to observe its dichroism in a *transmittance measurement*. This measurement requires the same configuration as the Heilmeier display described in Figure 3-1. A schematic of the typical intensity output of a transmittance measurement is shown in Figure 3-2. When the voltage is applied (V_{ON}), the transmittance increases as

the liquid crystal rotates with the dye molecules parallel to the incident light (and electric field), resulting in less absorption of the light. This method is simple, but not accurate when the dye does not possess sufficient contrast (Section 1.4.1). Indeed, the highly dipolar dye molecule MORPIP has a very low solubility (0.3 wt% in E7, 2 wt% in 5CB), and it has the extinction coefficient of 0.22×10^4 (in 5CB) with negligible absorption at 632.8 nm which is the wavelength of the He-Ne laser light source. There was a possibility of using other light sources at the λ_{max} of MORPIP, but even with the thickest cell available (50 μm), a sufficient absorption could not be obtained for an accurate measurement to be made by this method.
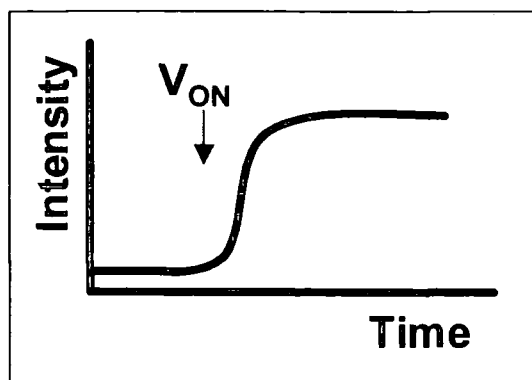
Figure 3-2. Typical schematic intensity output
from transmittance measurement of GH
display.

An alternative method to measure response times is to observe the cell's change in refractive index [165, 166]. This method, called *phase measurement*, allows the observation of the liquid crystal rotation rather than the dye rotation. Since this method works even for a Heilmeier liquid crystal which is

not strongly absorbing, this was the method of choice for the response time measurements in this work.

The set-up of the phase measurement is shown schematically in Figure 3-3. The liquid crystal cell, prepared by the method described Section 2.4.1 was mounted between two crossed polarisers. To maximise the effect of the change in birefringence, the polarisers were set at +45° and –45° respectively to the direction of the liquid crystal director.
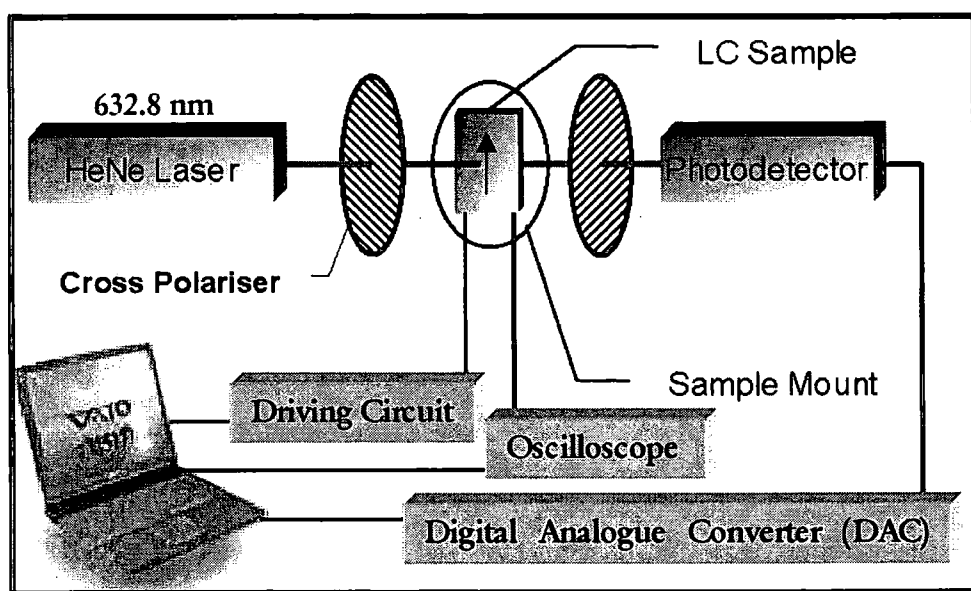
Figure 3-3. Phase measurement set-up used for
the response time measurement of birefringent
liquid crystals.

When polarised monochromatic light propagates through a homogeneously aligned liquid crystal cell with its polarisation axis at an angle 45° to the liquid crystal director, the extraordinary and ordinary rays in the outgoing light will experience a phase difference δ,

$$\delta = \frac{2\pi d}{\lambda}\left(n_{e\!f\!f} - n_o\right)\sin^2\varphi \qquad\qquad \text{Equation 3-12}$$

where d is the liquid crystal cell thickness, λ is the wavelength of the light source, φ is the angle between the liquid crystal director and the light propagation direction, and $n_{e\!f\!f}$ is the effective refractive index

$$n_{e\!f\!f} = \frac{n_e n_o}{\sqrt{n_e^2\cos^2\varphi + n_o^2\sin^2\varphi}}. \qquad\qquad \text{Equation 3-13}$$

When the AC voltage is applied, the birefringence Δn and angle θ change as the liquid crystal rotates parallel to the applied electric field. This produces a change in the phase difference δ, and rotates the incident polarised light. The analyser blocks the light when the light polarisation is perpendicular to the polarisation axis of the polariser. However the light may be transmitted when the light polarisation is parallel to the polarisation axis of the polariser. Hence the detected intensity undergoes a series of oscillations as in Figure 3-4. When enough voltage is applied to rotate the liquid crystal fully parallel to the irradiated light, the output intensity reaches a constant, minimum value because there is no birefringence along the long axis of the molecules; there will be no light transmitted through the crossed polarisers.

In this work, the rise time τ_{rise} is defined as time taken from applying a voltage until the 90% of the waveform saturation. Similarly, decay time τ_{decay} is defined as the time taken from the turn-off of the voltage until it relaxes back to the 90% of the initial position as shown in the Figure 3-4. The number of

oscillation during the τ_{rise} and τ_{decay} were the same for all samples (five peaks for 10 μm thick cell), thus it is possible to directly compare the cells using these quantities.
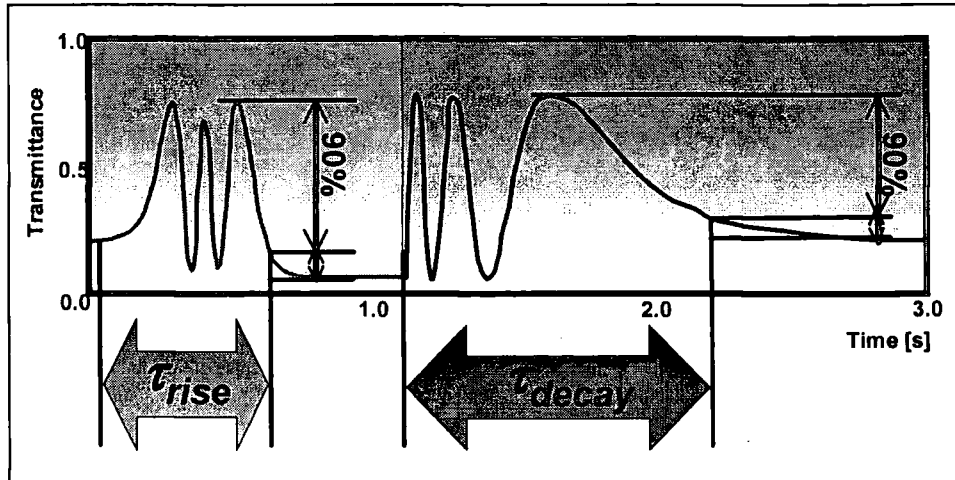
Figure 3-4. Typical output waveform from
phase measurement.

A well collimated 05LHR111 He-Ne laser (class IIIB) with unpolarised output at 632.5 nm was used as the light source. A computer was used as a digital oscilloscope and to drive the liquid crystal cell via DAQ (Data Acquisition) card. DAC-1200 was used for this set-up. Since DAC-1200 saturates at input voltage of 5.0 V, an appropriate neutral density filters was used to reduce the intensity of the laser incident on the photodiode. 20 MHz signal generator was used to feed an envelope frequency to the waveform generation circuit. The drive circuit and the LabWindows drive program (National Instrument) for the liquid crystal cell were constructed by A. Roberts [167]. A separate oscilloscope was used to monitor the operation of the program.

Figure 3-5 is the typical drive waveform used to drive the liquid crystal cell. AC voltage of typically 1 kHz was used to switch the liquid crystal by induced dipole moment, an the square waveform was used to maximise the power of the driving signal.
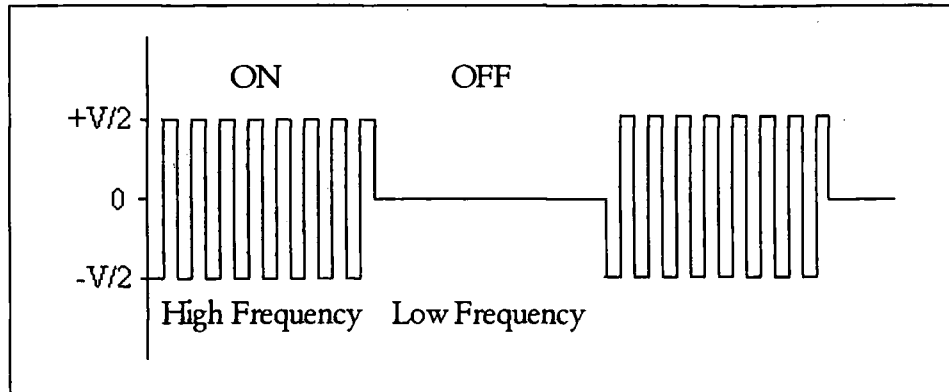
Figure 3-5 Waveform of the drive voltage.

3.4. Experiments and Results

3.4.1. Liquid Crystal Used

As well as the E7 liquid crystal (Section 2.3.1), one of its component liquid crystals 5CB was used as a host to carry out the response time measurement (Section 3.4.3). This is one of the first stable liquid crystals found for application purposes, and this cyanobiphenyl type of liquid crystal is known to possess high dielectric anisotropy which is an important parameter governing the response time of the liquid crystal. Its chemical name is 4'-n-Pentyl-4-cyanobiphenyl, and the structure is shown in Figure 2-6. The material was

purchased from Merck Ltd. (UK), and the values quoted below are from the manufacture's data sheet unless stated.

Ordinary refractive index (n_o) of the liquid crystal is 1.52 and extraordinary refractive index (n_e) is 1.74 (589 nm at 20 °C). Dielectric anisotropy, $\Delta\varepsilon$, is 11.6 $(\varepsilon_{//}=17.8, \varepsilon_{\perp}=6.2, 1\text{ kHz}, 25\text{ °C})$. The material possess a nematic liquid crystal phase between 22.5 to 35 °C [20], and it has a boiling point of ~140 °C. All samples were prepared under the boiling point at room temperature, and all the measurements were taken within the liquid crystal phase range. A density of 1.0 g/ml was used to calculate the weight.

5CB has a resistivity of 5 x 10^{10} Ωcm which is in the desired range of 10^{10} to 10^{11} Ωcm for display applications. The handling was as described in Section 2.3.1. to avoid unnecessary incorporation of impurities.

3.4.2. Decay Time Measurements

Initially an experiment was performed to investigate the effect of highly dipolar guest molecules on the decay time of the liquid crystal. The liquid crystal was doped as described in Section 2.4.1 with different weight concentrations of MORPIP. The voltage was adjusted to give a constant electric field of 2 p-pV/μm for the each cell. The field was calculated using the cell thickness as described in Section 2.4.1. The 1 kHz AC voltage was applied to fully rotate the liquid crystal. The decay time was measured by removing the field and monitoring the transmitted intensity. Up to five cells

of each concentration were used, and their average value of the decay time
was plotted in Figure 3-6.
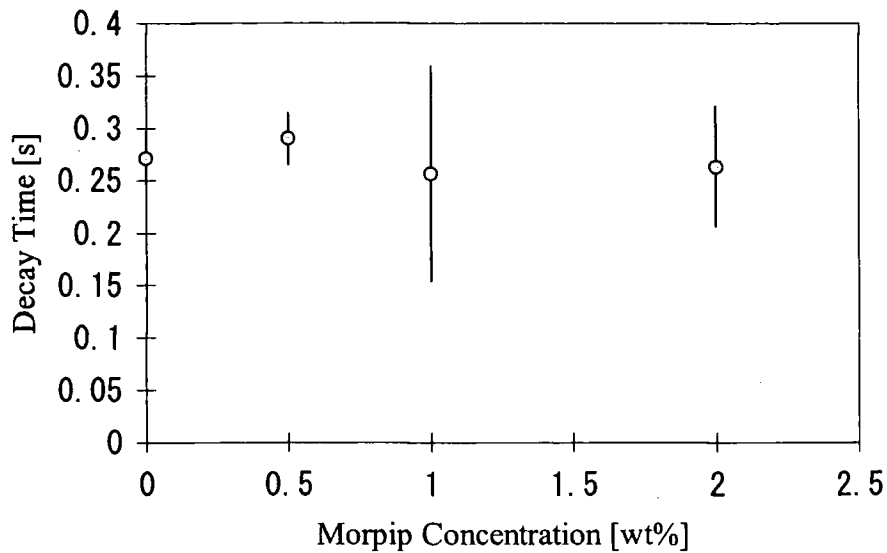
Figure 3-6. Decay time dependency of
MORPIP concentration for 5CB birefringent
LCs.

No change in the decay time was expected since the MORPIP concentration
was too low to increase the viscosity or elastic constant of the host. Indeed
Figure 3-6 (Table 3-1) clearly shows that this was the case from the
experimental results obtained. No change could indicate that either there is no
effect or the fractional effect on the viscosity and the elastic constant is the
same (Equation 3-11). However, the latter seems unlikely since other dyes
affect viscosity more than the elastic constant.

MORPIP Conc. [wt %]	Decay Time	Error
0.0	0.285	0.021
0.0	0.268	0.026
0.0	0.267	0.026
0.0	0.26	0.027
0.5	0.291	0.025
0.5	0.289	0.026
0.5	0.290	0.025
0.5	0.289	0.026
1.0	0.242	0.123
1.0	0.258	0.104
1.0	0.256	0.100
1.0	0.263	0.103
2.0	0.231	0.084
2.0	0.259	0.068
2.0	0.280	0.019
2.0	0.282	0.014

Table 3-1. Decay time versus MORPIP
concentration for 5CB birefringent LCs.

3.4.3. Rise Time Measurements

3.4.3.1. MORPIP doped 5CB LC

Following the decay time measurement described in the previous section, the rise time was measured at different MORPIP concentrations using the same set-up. Unlike the decay time measurement, a decrease in the rise time was observed with increasing dopant concentration.

2 V/μm of 1-10 kHz AC square voltage was applied. The same electric field was applied by varying the applied voltage for each cell whose thickness was determined as described in Section 2.4.1. The same sample cells from the

previous decay time measurement were used. The average rise time was
calculated for all cells with the frequency of the applied voltage from
1~10 kHz. The results (Figure 3-7) show there is little variation of the
measured response time for different cells across this range of frequencies.
Also, the results show that the higher doped 5CB cells respond faster over the
range of frequencies studied.
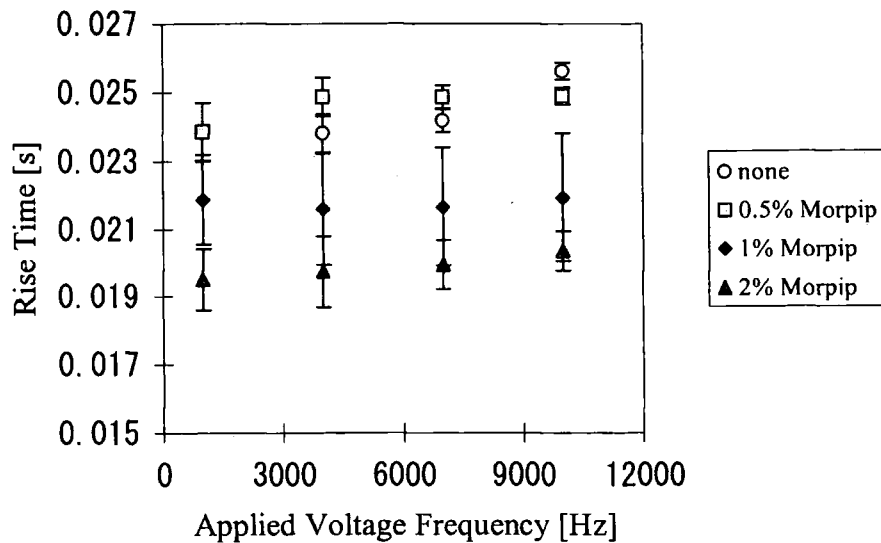
Figure 3-7. Rise time dependency of MORPIP
concentration for 5CB birefringent liquid
crystals over various frequencies.

The values obtained in Table 3-2 were averaged over the frequencies, and
average rise time as a function of MORPIP concentration was plotted as
shown in Figure 3-8. The line was drawn to guide the eye and is the best fit to
the data points. The plot clearly shows a decrease in the rise time with

MORPIP concentration. The averaged rise time with 2 wt% doped 5CB liquid crystal was 18% faster when compared to the undoped samples.

MORPIP Conc. [wt %]	Driving Freq. [Hz]	Rise Time [s]	Error
0.0	1000	0.0238	0.0009
0.0	4000	0.0238	0.0002
0.0	7000	0.0241	0.0002
0.0	10000	0.0256	0.0007
0.5	1000	0.0238	0.0008
0.5	4000	0.0248	0.0005
0.5	7000	0.0248	0.0003
0.5	10000	0.0248	0.0002
1.0	1000	0.0218	0.0013
1.0	4000	0.0215	0.0016
1.0	7000	0.0216	0.0017
1.0	10000	0.0219	0.0018
2.0	1000	0.0194	0.0009
2.0	4000	0.0197	0.0010
2.0	7000	0.0199	0.0007
2.0	10000	0.0203	0.0005

Table 3-2. Rise time variation with MORPIP
concentration for 5CB birefringent liquid
crystals over various frequencies.
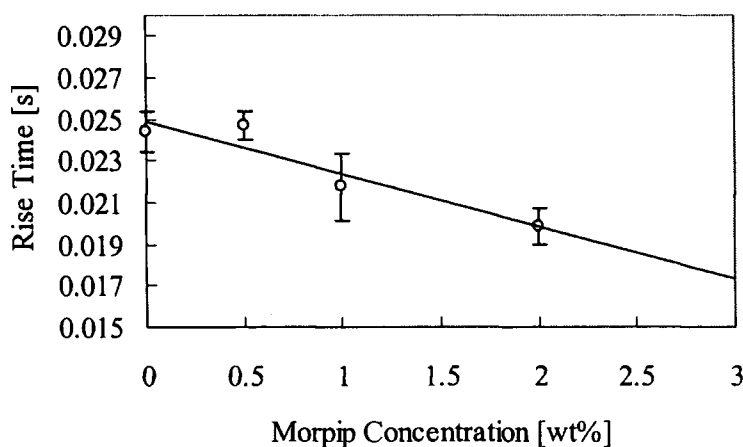
Figure 3-8. Rise time dependency of MORPIP
concentration.

It then remained to determine whether the effect was characteristic of MORPIP, or the same effect could be seen with other dopants. Thus, in the next section, it is demonstrated that the effect was indeed characteristic of MORPIP by undertaking the same experiment using commercially available dyes in the liquid crystal E7. The liquid crystal was changed to E7 from 5CB to investigate whether the same effect could be seen in liquid crystal mixture (E7) rather than a single liquid crystal (5CB). Also, it was favourable to use E7 because the liquid crystal was known to form PDLC

3.4.3.2. MORPIP doped E7 LC

Rise times of the doped E7 liquid crystal mixtures were measured at varying voltages using the same set-up as the previously described in Section 3.3. Dopants used for this experiment were the highly dipolar MORPIP (Section 2.3.2), D2 azo dye, D16 anthraquinone dye and B2 black dye (Section 2.3.3). They were dissolved in E7 at their solubility limit of 0.5 wt%, 3.5 wt%, 2.4 wt% and 3 wt% respectively. B2 has a maximum solubility of 11.53 wt%, and it was the only dye not fully saturated.

The result is shown in Figure 3-9 and it can be seen that MORPIP doped E7 has shorter response time than the undoped E7, but other azo and anthraquinone dyes have small effect that is within the experimental error. Three readings were taken from the MORPIP doped cell. The curves are the best fit to the electric field squared.
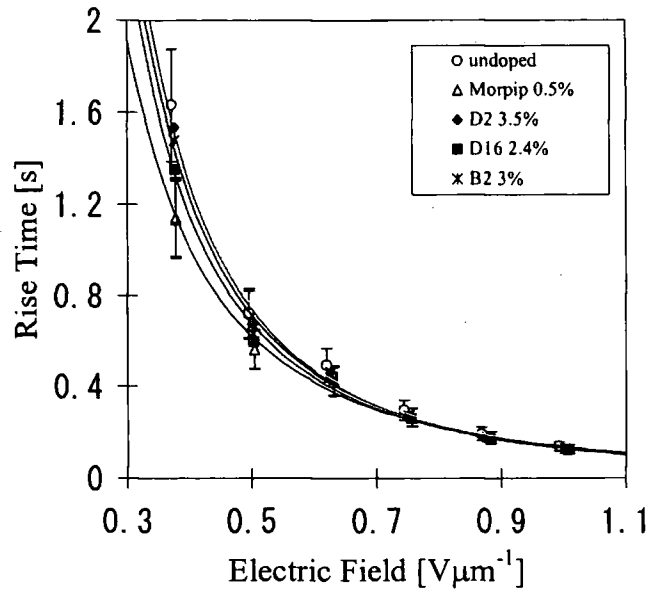
Figure 3-9. Rise time of doped E7 liquid
crystal.

E [Vμm⁻¹]	E^2	Rise time [s]				
		undoped	MORPIP 0.5%	D2 3.5%	D16 2.4%	B2 3%
0.376	0.141	1.629	1.133	1.531	1.353	1.475
0.501	0.251	0.715	0.560	0.672	0.595	0.634
0.626	0.391	0.495	0.426	0.459	0.442	0.462
0.752	0.566	0.296	0.264	0.275	0.260	0.272
0.877	0.769	0.192	0.175	0.175	0.169	0.176
1.002	1.004	0.137	0.125	0.124	0.123	0.128

Table 3-3. Rise time of doped E7 liquid crystal.

To quantify the result using Equation 3-8, the inverse of the rise time was

plotted against the square of the electric field (Figure 3-10). This allows linear

fits to the data points, and from the equation of the fitted line, the response

speed and a threshold electric field could be calculated (Section 3.2.3). The

equations of the fitted line and the threshold equations calculated are shown

in Table 3-4. The E_0 value of MORPIP (0.23 V/μm) was 19% smaller than

that of undoped cell (0.28 V/μm), while the other dyes increased the E_0

values up to 10.7%. Normally the E_0 value is expected to increase with the

dye doping since the mixtures viscosity normally increases. The large

permanent dipole of MORPIP will result in a larger torque due to the applied

field. Thus relative to the host molecules MORPIP will respond at lower

fields as shown by the reduction in E_0. This has the consequence of

shortening the effective rise time. Table 3-4 also shows that the response

speed of the doped LCs are faster compared to the undoped LC. The

effective response time of D2, D16 and B2 doped LCs are slower at low

electric field due to their increased E_0. A possible explanation of the slower

response speed for MORPIP doped LC is that MORPIP carries with it a

surrounding volume of the LC so that the moment of inertia is increased and

the response to the torque is slower.
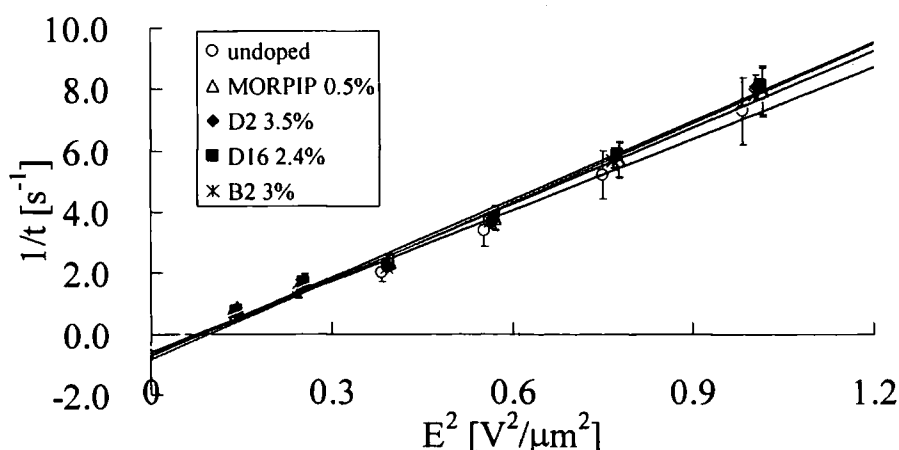
Figure 3-10. Speed factor graph of doped E7
liquid crystal.

Dopant in E7	Equation of the line fit. $y = ax - b$	$E_0 (= \sqrt{b/a}) [V/\mu m]$
Undoped	y = 7.74x - 0.60	0.28
MORPIP 0.5%	y = 7.91x - 0.42	0.23
D2 3.5%	y = 8.57x - 0.84	0.31
D16 2.4%	y = 8.57x - 0.85	0.31
B2 3%	y = 8.28x - 0.71	0.29

Table 3-4. Equation of the fitted line and
threshold equation calculated.

3.4.4. Dielectric Anisotropy Measurements

The dielectric anisotropy of the liquid crystal with different MORPIP concentrations was measured to see if the dielectric anisotropy is increased by the addition of highly dipolar molecules.

Homogeneous alignment cells (50 μm) were prepared as described in Section 2.4.1. Homeotropic cells (50 μm) were prepared similarly to the homogeneous ones, but this time, the cells with surface-active agent (cetyl trimethyl ammonium bromide) layers (KSHH-50/B111PINTS, E.H.C. Ltd., Japan) were used. Due to instability of the layer to heat, the cells were not subject to heat unlike the homogeneous cells. Nevertheless, the observation under cross-polarised microscope confirmed that the cells achieved a homeotropically alignment when they were left over night. The alignment was checked by rotating the cell between cross polarisers: the transmittance of the cell was constant when rotated by 360°.
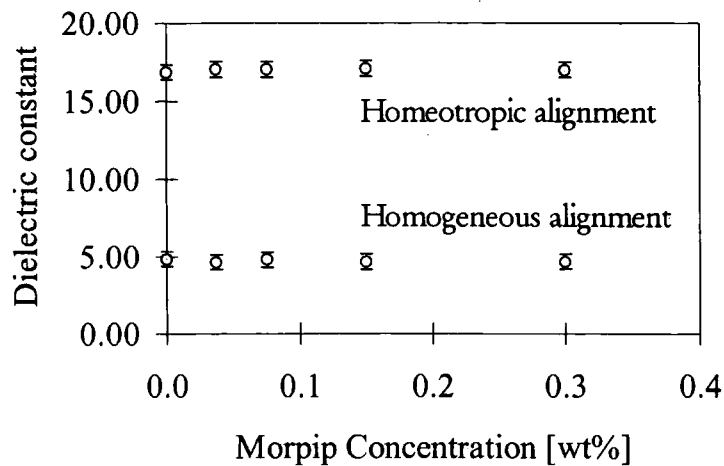
Figure 3-11. Dielectric constants dependency
of MORPIP concentration in E7 liquid crystal.

The capacitance measurements of both homogeneous and homeotropic cells
were carried out as in Section 2.4.1, and dielectric constants were calculated
from the capacitances of unfilled and filled cell using Equation 2-2. The
results were plotted in Figure 3-11.

The data sheet from Merck gave the values of $\varepsilon_{//}$=19.0 and $\varepsilon_{\perp}$=5.0, which

agreed for experimental value obtained for $\varepsilon_{\perp}$ within error, but for $\varepsilon_{//}$, the

experimental value was smaller by approximately 10%. This was thought to

be because the homeotropic alignment was not perfectly achieved for the cells

used in this work. Nevertheless, the results showed no change in the dielectric

constants and, hence no change in the dielectric anisotropy of the system.

The result obtained in Section 3.4.3.2 showed a 20% decrease in the rise time.

In order to achieve this change, $\Delta\varepsilon$ must increase a 20% increase according to

the Equation 3-7. Since such a big change could not be observed, the increase

in response speed could not be due to the increase in dielectric anisotropy.

MORPIP Conc. [wt%]	Alignment	Empty C [pF]	Filled C [pF]	Dielectric Constant ($=C_{filled}/C_{empty}$)
0.000	homeotropic	19.09	319.65	16.74
0.000	homeotropic	19.16	322.66	16.84
0.000	homeotropic	20.24	328.90	16.25
0.038	homeotropic	19.87	337.94	17.01
0.075	homeotropic	20.35	346.29	17.02
0.150	homeotropic	20.34	347.08	17.06
0.300	homeotropic	20.30	344.99	16.99
0.000	homogeneous	19.16	92.35	4.82
0.000	homogeneous	19.08	92.30	4.84
0.000	homogeneous	19.30	89.21	4.62
0.000	homogeneous	19.60	89.09	4.55
0.038	homogeneous	18.97	87.65	4.62
0.075	homogeneous	18.97	90.62	4.78
0.150	homogeneous	19.00	88.37	4.65
0.300	homogeneous	19.00	88.76	4.67

Table 3-5. Dielectric constants variation with
MORPIP concentration.

This is in contradiction to the report from Wu *et al.* [120], who observed an

increase in the dielectric anisotropy by the addition of compounds possessing

both high dielectric anisotropy and low elastic constant. One such molecule is

shown in Figure 3-12, which increased the dielectric anisotropy of E63 liquid

crystal to 65±5 by 3% doping. The undoped E63 has $\Delta\varepsilon$ of 14.6 at 2 kHz

[168]. The order parameter of this dipolar molecule is 0.35 which is

comparable to 0.309 of MORPIP (Section 2.4.2). The difference may be due to the low solubility limit of MORPIP, which is only up to approximately 0.5 wt%. Measurement of MORPIP's dielectric anitosropy in a more soluble liquid crystal host may reveal the effect more clearly.
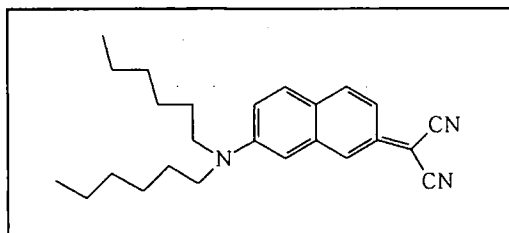
Figure 3-12 Chemical structure of the
molecule employed by Wu *et al.*

3.5. Conclusion

In this chapter, the effects of guest dyes on liquid crystal hosts have been investigated. The response time of both 5CB and E7 has been successfully reduced by ~20% by doping at low concentrations with the highly dipolar MORPIP dye which was originally synthesized for nonlinear optical applications (Section 3.4.3.1). The decrease in rise time of MORPIP was compared with those of commercially available dyes, D2, D16 and B2 when doped in E7. The large decrease in rise time was observed for MORPIP doped E7. Interestingly, a small effect was also observed for D16 dye, but it should be noted that the concentration of this dye was approximately 4 times that of MORPIP doped concentration. Therefore we conclude that the results indicated that the effect was unique to MORPIP. The response speed and the threshold electric field were calculated using Equation 3-8. The E_0 value of

MORPIP (0.23 V/μm) was 19% smaller than that of undoped cell

(0.28 V/μm), while the other dyes increased the E_0 values up to 10.7%. The

large dipole of MORPIP reduced E_0 and shorted the effective rise time

especially at low electric field (Section 3.4.3.2).

As a mechanism of the decreased threshold voltage, an increase in the

dielectric anisotropy was suspected. Dielectric anisotropies of doped and

undoped liquid crystals (Section 3.4.4) were measured, but no observable

change was detected.

Since the dielectric anisotropy did not change with MORPIP concentration,

there must be another mechanism of decreasing the threshold voltage of the

doped liquid crystals. According to Equation 1-13, the threshold voltage can

be reduced by a decrease in the elastic constant. MORPIP and adjacent LC

molecules has a large inertia since MORPIP cannot follow AC even though it

has a permanent dipole; the rotational diffusion constant must be drastically

reduced by interaction with LC. The dragging of the liquid crystal by the

dipolar molecule would look like an effective decrease in elastic constant (i.e.

decrease in threshold voltage) but does not affect the relaxation when there is

no field present (i.e. no change in decay time). The field would exert a large

torque on the highly dipolar dyes. These would rotate faster and drag the

surrounding LC with them.

A small order parameter of MORPIP could be due to the formation of nano-

scale aggregates that would not be visible and would be randomly oriented

[109]. This implies that the steric factors control orientation rather than dipole-dipole interaction, hence small effect on the dielectric anisotropy. The similar effect had been reported for the optical control of LC alignment using cis-trans isomerisation of azobenzene, known as a *command surface* [169-171]. This photochromic reaction is a switching activity at the molecular level whereby the molecular structure changes photochemically; the orientation of nematic liquid crystal changes by photochemical reaction of an organic molecule (e.g. azobenzene) membrane formed on the substrate surface.

Wu *et al.* has reported [140] an observation of a decrease in the elastic constant and increase in dielectric anisotropy for liquid crystals when doped with molecules with large dielectric anisotropy (Figure 3-12). They suggested that the mechanism may be due to changes of short range order, size and arrangement of steric units, steric hindrance or dipole-dipole interactions induced by the dopants. Although the increase in dielectric anisotropy could not be observed in this work, if K_{11} is decreased by addition of highly dipolar dye, and the rotational viscosity is also decreased by the same amount, this could explain the decrease in the rise time with no change in the decay time (Equation 3-11). However, the above hypothesis seems unlikely since viscosity normally increases with the increase of dye concentration.

The exact nature of this mechanism can be explored by further investigations. Direct measurements of the elastic constant, dielectric anisotropy and rotational viscosity may help to clarify the hypothesis given above. More accurate dielectric anisotropy measurements at elevated temperatures where

MORPIP solubility is higher, may be performed. This is because there is a possibility that the MORPIP concentration was too low to observe any noticeable effect. A systematic response time measurement of various dipolar and non-dipolar liquid crystals incorporating other dipolar and non-dipolar dyes, dyes with various shapes, and dyes similar to Wu *et al.* (Figure 3-12) would help obtaining the broader picture of the effect. Synthesis of molecules with higher dipole moments, increased solubility and better compatibility with liquid crystals will allow us to investigate the effect further.

Chapter 4: Dichroic PDLC

4.1.Introduction

The PDLC technique is one of the most promising candidates for future electronic paper-like displays which have high brightness, a wide viewing angle and are flexible. Following the investigation of GH liquid crystal presented in the previous chapter, GH effect of PDLC was explored, in order to assess its potential in the development of a multicolour reflective type PDLC display. The study included fabrication of the undoped PDLCs and dye doped PDLCs, along with their characterisation. However, these conventional PDLCs showed insufficient contrast for display applications due to dye deterioration by UV radiation and dye trapping in the polymer matrix. To overcome these problems, two new fabrication techniques were proposed and the novel PDLCs with improved contrast and fast response times were successfully fabricated.

The conversion between reflectance (R), transmittance (T) and absorbance (A) were carried out using Equation 4-1 and Equation 4-2 where I is the intensity of the original light, I' is the intensity of the light after passing through the cell once, and I'' is the intensity of the light after passing through the cell twice (Figure 4-1).

$$-A = \log(I/I') = \log T$$

$$\text{And } R = I/I'' = (I/I')^2 = T^2.$$

Equation 4-1 is from the Beer-Lambert law [172] where I is the intensity of the incident light, and I' is the light transmitted through a sample. Since a reflectance measurement was unavailable, R was converted in to T (Equation 4-2) by assuming that the light is reflected by a perfect mirror as shown in Figure 4-1. The quantity R does not refer to the intensity reflected by the substrate surface, i.e. in this sense, the normal description of $A' + R + T = 1$ does not hold. A' is an absorption factor of the medium, which is different from the absorbance, A, in Equation 4-1. The surface reflection is neglected for the simplicity, hence $A' + TA' + R = 1$. For undoped PDLCs, the backscattering from the PDLC droplets contributes to R. However, for the dye doped PDLCs, the backscattering is neglected due to the strong internal absorption by dyes. Hence the target aims described in Table 1-2 were converted as 86% transmittance at on-state, and 31% transmittance at off-state. These values will be used as the target values from here on.

The next section describes the background of the PDLC, including fabrication, contrast and response time. Detailed experimental characterisation and results follow.
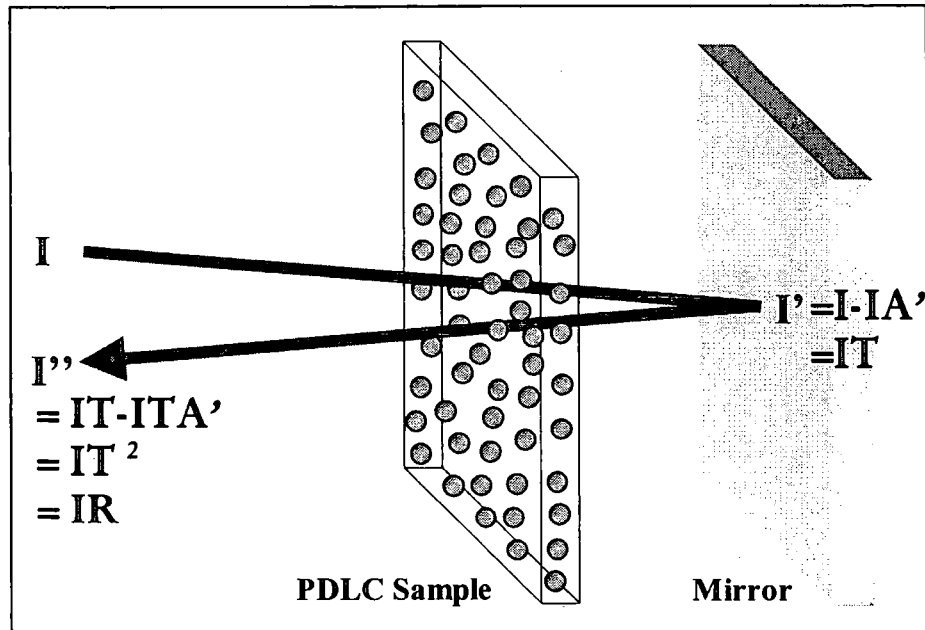
Figure 4-1 Reflection of light by a perfect
mirror

4.2. Fabrication and Properties

This section describes various fabrication techniques, and parameters affecting contrast and response time of PDLCs.

4.2.1. Fabrication Techniques

There are two basic methods developed for preparing PDLC [44]: *encapsulation* and *phase separation*. Furthermore, the phase separation method has three different techniques within it. Each one of them, along with its advantages and disadvantages, are described below.

Encapsulation is a technique that has been applied to obtain small capsules of drugs for controlled release, of drug and food products and even of

cholesteric liquid crystals in temperature indicating devices [173]. The encapsulation technique starts with an inhomogeneous solution and involves emulsifying a nematic liquid crystal in an aqueous mixture containing the encapsulating medium. The method uses mechanical shear to disperse the liquid crystal into an aqueous solution of a film-forming polymer. The droplets are formed during the emulsification process before the film is coated and allowed to dry. In the method used by Fergason [1], a nematic liquid crystal is mixed with a water-borne polymer such as polyvinyl alcohol (PVA) and the mixture mechanically stirred to form an emulsion [3]. Other materials such as ammonium polyacrylate and gelatin have been used as the encapsulating medium for liquid crystals [174]. Scanning electron microscope studies of encapsulated material generally indicate that the droplets can be interconnected and often are not very uniform in size. The product of this technique is sometime called *nematic curvilinear aligned phase (NCAP)*.

The phase separation technique involves first forming a homogeneous solution of polymer or prepolymer with a liquid crystal; during processing, the liquid crystal separates from the solution, and forms droplets, with subsequent polymer gelation or solidification occuring [49, 175]. Phase separation methods can be classified into three types: *temperature-induced phase separation (TIPS)*, *solvent-induced phase separation (SIPS)*, and *polymerisation-induced phase separation (PIPS)*.

TIPS involves the cooling of a homogeneous liquid crystal and thermoplastic polymer mixture to induce phase separation [175]. Thus, this process is useful

for thermoplastics which melt below their decomposition temperature. Thermoplastic materials such as epoxy systems, polymethymethacrylate (PMMA) and polyvinylformal (PVF) can form droplet dispersions with cyanobiphenyl liquid crystal materials [175, 176]. The morphology (droplet size, droplet density, and composition) is dependent upon several factors such as system viscosity, the rate of cooling, and the initial proportion of liquid crystal to polymer. In general, a larger proportion of liquid crystals is required for TIPS compared to PIPS method. However, aligned droplets can be made with TIPS if a field is applied during the droplet formation process [177]. After the droplets are formed and the field removed, droplets with bipolar alignment have been found to remain oriented. This offers one form of thermal memory for use in irreversible thermometers.

SIPS is useful with thermoplastics which melt above the decomposition temperature of the thermoplastic or the liquid crystal. The technique involves the evaporation of a solvent from a homogeneous mixture of liquid crystal, polymer, and solvent. As the solvent evaporates, phase separation occurs. The morphology depends on the rate of solvent evaporation and the initial proportion of liquid crystal to polymer. SIPS can be used in conjunction with TIPS when solvent coating techniques are used. Films can be formed on a suitable substrate using standard film coating techniques, and the solvent is rapidly removed with no concern for droplet size or density. The film can then be warmed to redissolve the liquid crystal in the polymer and cooled at a rate chosen to give the desired droplet size and density. This combination of

SIPS followed by TIPS adds flexibility and the ease to the production of commercial PDLC films.

PIPS is useful when the prepolymer materials are miscible with the liquid crystal compounds [4, 175, 178]. The process begins with a homogeneous mixture of liquid crystal and monomer or pre-polymer. Polymerisation is initiated to induce phase separation. Droplet size and morphology are determined by the rate of polymerisation, the types of liquid crystal and polymers used, viscosity, rate of diffusion, and solubility of the liquid crystal in the polymer [175, 177, 179, 180]. For thermally cured polymers, the rate of polymerisation can be controlled by the curing temperature. For ultraviolet light (UV) initiated polymerisation, the rate of polymerisation may be changed independent of the curing temperature by changing the light intensity [106]. PIPS method using free-radical polymerisation is by far the most studied, and the majority of free-radical polymerisation systems are initiated by UV light. The process has several advantages over other methods such as, better phase separation, uniform droplet size, and better control of the droplet size. A very large choice of monomers is possible because the only restrictions are solubility of the monomers in the liquid crystal and refractive index matching. The variety of possible systems gives access to a wide range of properties. Moreover, a wide range of liquid crystal concentration can be used because of the possibility of crosslinking the polymer [181]. Therefore, this work used the PIPS technique for doped and undoped PDLC preparation. The drawback of the PIPS method was shown to be the photodegradation of dyes

by the UV radiation (Section 4.3.7), however the problem could be avoided
by the new fabrication method proposed in Section 4.4.

4.2.2. Phase Separation

Phase separation processes are an important and well-studied problem in
many areas of material science [182-184]. The process determines the
morphology of the PDLC film, which ultimately controls the electro-optical
properties of these devices.
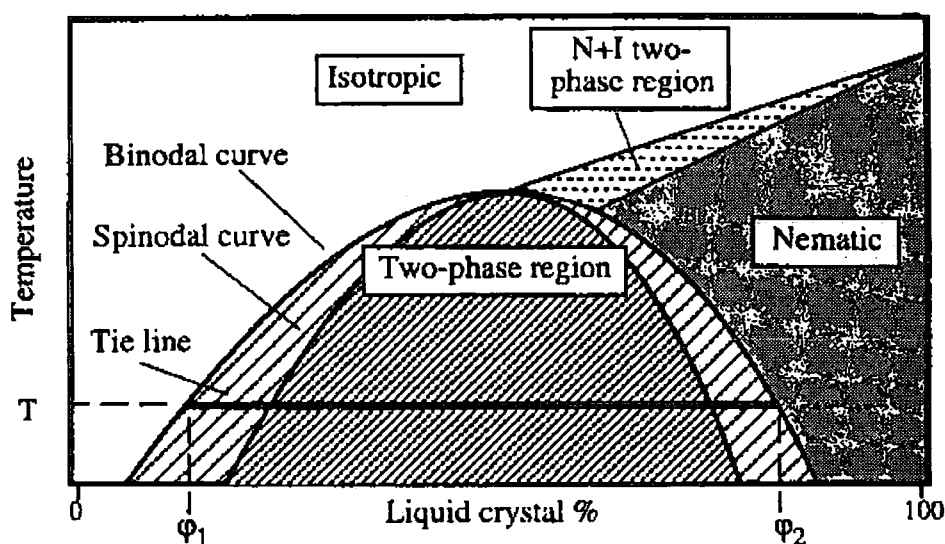
Figure 4-2 Schematic illustration of a binary
phase diagram.

The morphology of a PIPS formed PDLC film depends on the chemical
nature of the liquid crystal and polymer constituents and on the kinetics of
the processes. To understand the process, the *phase diagram* (Figure 4-2) [175,
185, 186] is used. By simplifying the PDLC system to possess a binary

mixture, i.e. a single liquid crystal molecule and a single monomer, a simple phase diagram can be drawn.

As shown in Figure 4-2, a single phase is stable at high temperatures. Miscibility decreases with decreasing temperature, and phase separation can occur in the mixture at low temperatures. At the extremes of concentration, the two components may be completely miscible and not phase separate at any temperature. The *tie line* illustrates the concentrations of liquid crystal in the two phases at temperature T: one phase is liquid crystal deficient with concentration φ_1, while the other phase is liquid crystal rich with concentration φ_2. The N-I two-phase region is where the liquid crystal is not fully misssible in the monomer, hence nematic and isotropic phases co-exist.

The *bimodal* curve marks the temperature/concentration where phase separation becomes thermodynamically allowed. Between the bimodal and *spinodal* curves the system is metastable. Phase separation is thermodynamically allowed but requires a certain activation energy, and the phase separation proceeds by a *nucleation and growth* mechanism. The nucleation and growth mechanism leads to isolated domains of one phase within a continuous phase of the other phase: either the liquid crystal or the polymer forms nearly-discrete domains. Nucleation is the process of generating a new and more stable phase within the initial metastable phase [182], hence requires an activation energy. The domains grow in size initially by molecular diffusion, and later by coalescence of neighbouring domains. Under the spinodal curve, the system spontaneously decomposes into two

phases without the need for activation energy. Here, the phase separation proceeds by a *spinodal decomposition* [182, 183]. The mechanism leads to interpenetrating networks of the two phases. The examples of different PDLC morphologies will be shown later in Section 4.3.2.

Many theoretical works regarding the phase separation have been carried out. Flory-Huggins theory [182, 184, 187], Maier-Saupe theory [188-190], Maier-Saupe-McMillan theory [191] have been shown to be useful in explaining the observed PDLC phase diagrams. The ability to calculate phase diagrams allows the simulation of the phase diagram change as curing proceeds [192]. For example, as polymerisation proceeds the area of the two-phase region broadens and moves to higher temperatures. This change follows from the decreased entropy of mixing that larger molecular weight species possess, which lowers the solubility of the growing chains in the liquid crystal solvent. Phase separation occurs when this change in the position of the phase boundary line moves the system into a two-phase regime, even though the temperature and overall composition of the system does not change. It is now known that the phase separation process depends not only the concentration of liquid crystal in the initial mixture and the temperature of the curing, but also on the size of the gap separating the bimodal and spinodal curves, the size of the activation barrier within the metastable region, whether nucleation sites are available, and the rapidity with which the system crosses the phase boundary lines.

4.2.3. Contrast

Contrast is a very important property for display applications. Dye addition is known to increase contrast of reflective type PDLCs [193]. This is because the scattering of PDLC increases the optical path length by a factor of 2 to 3, resulting in increase of absorption by the dye [5, 193-195].
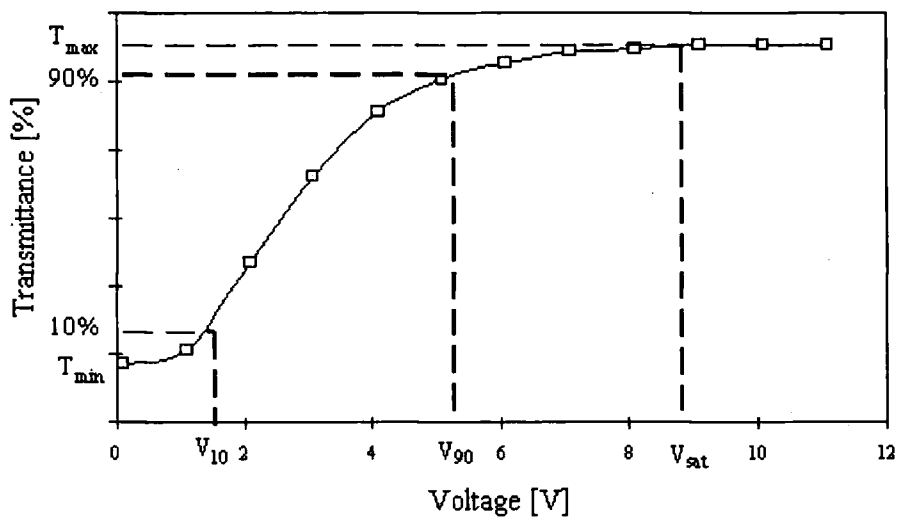
Figure 4-3. Typical electro-optical curve of
PDLC

Contrast can be calculated by measuring the transmittance of a PDLC in its on and off-states as shown in Figure 4-3. Several other properties are indicated in the figure: Minimum transmittance T_{min}; maximum transmittance T_{max}; V_{10}, V_{90} and V_{sat} are the voltages necessary to obtain fractions of 10%, 90% and 100% of the total transmittance change, respectively. There are several definitions of contrast [178], but the most widespread definition is as

contrast $= T_{max}/T_{min}$ which was used in this work. Increasing the transparency in the on-state and scattering in the off-state increase contrast.

A highly transparent on-state can be achieved by adjusting the polymer refractive index (n_p) to match the ordinary refractive index of the liquid crystal (n_o) [180]. A highly scattering off-state can be achieved by increasing refractive index anisotropy (i.e. birefringence) of the liquid crystal, so that the extraordinary refractive index of the liquid crystal (n_e) is bigger than n_o and n_p. [196, 197]. The off-state scattering is a function of refractive index differences between a liquid crystal droplet and the polymer; between two adjacent droplets [198]; within a droplet of liquid crystal [199].

Adjusting refractive indices is not straightforward, because they are a function of miscibility of the polymer in the liquid crystal and vice versa. As much as 53% of the liquid crystal is known to remain dissolved in the polymer binder [178, 200, 201]. Oligomers from the binder can remain dissolved in the liquid crystal [202]. Because of the liquid crystal present in the polymer, the refractive index of the composite is increased, so that it is necessary to choose n_p slightly lower than n_o [203, 204]. It has been reported [6] that the scattering efficiency of the doped PDLC film is less than that of the undoped film, because the dye affects the refractive indices of the liquid crystal in the droplets. Also, dye remaining in the polymer matrix decreases the contrast of the system.

Temperature can modify the solubility of the liquid crystal in the polymer [200] and thus the refractive indices. Nevertheless, these variations can be avoided if a high *nematic to isotropic temperature transition* (T_{N-I}) liquid crystal is used [196]. The off-state scattering increases with decreasing temperature, because n_o decreases while n_e increases, i.e. the birefringence $\Delta n = n_e - n_o$ increases with decreasing temperature (Figure 4-4 [202]) [180, 205-207]. These variations are very significant close to the T_{N-I} [180].
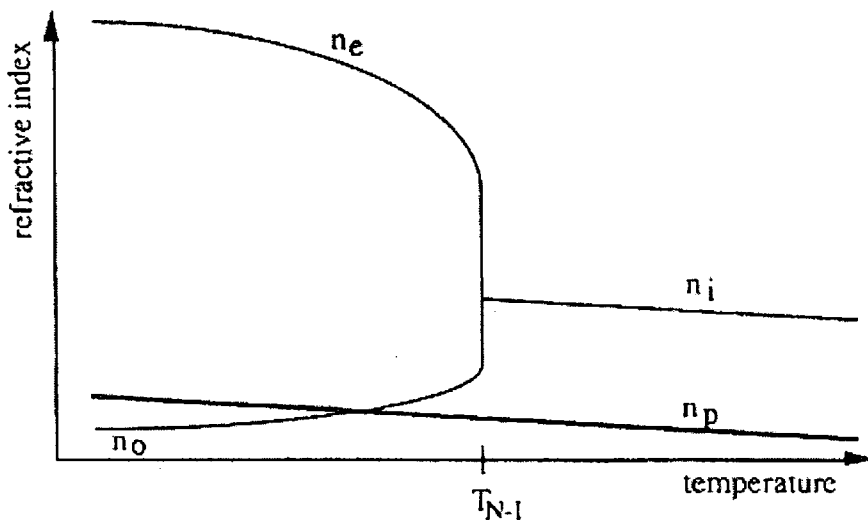
Figure 4-4. Qualitative temperature
dependence of refractive indices of the
polymer and the liquid crystal.

A very large or very low proportion of liquid crystal to polymer leads to PDLCs that do not scatter efficiently. Several authors have reported that the optimum composition to maximise scattering is in the range of 60 wt% liquid crystal for their systems [208]. In this work, 44.3 wt% liquid crystal is used for making PDLC cells.

Similarly, very large or very small droplets do not scatter light efficiently. Transmittance electron microscopy has confirmed that it is possible to prepare materials with droplets 0.01-10 µm in radius [177, 209, 210]. For a maximum scattering and contrast, the optimum size of the droplets is calculated to be $5 \times \lambda$ (~3 µm) [44, 211, 212]. The uniform shape of droplets is also important, as even a slightly elongated droplet is known to decrease transparency in the on-state [213]. Also, the broad size distribution was found to induce the slow change in transmittance (broadness of driving voltage) and hysterisis [214].

The variation of scattering as a function of thickness is close to an exponential law [198, 205, 215, 216]. On the other hand, on-state transparency is nearly independent of thickness. However, the contrast measured by absorbance for a dye doped PDLC was reported to be independent of thickness when the dichroic response is not strongly affected by scattering within a film [5].

4.2.4. Response Time

Rise time (τ_{rise}) is usually defined as the time needed for the composite to reach 90% of the on-state transmittance when an alternating voltage of amplitude V is applied (Figure 4-3). Similarly, the decay time (τ_{decay}) is the time needed for a composite in the on-state to reach 10% of the on-state transmittance, i.e. 10% of $(T_{max}-T_{min})$, when the voltage is set to zero. As in the case of GH liquid crystal (Section 3.2.3), PDLC rise time is inversely

proportional to the applied voltage V^2, and decay time is independent on V [205].

The droplet size and shape are significant factors in determining the response time [217]. The rise and decay times can be calculated for the case where only the droplet shape anisotropy determines the elastic contribution to the free energy density. For the case of an ellipsoidal droplet elongated along the film plane, and ignoring potential depolarisation effects, rise and decay time can be expressed as [218]:

$$\tau_{rise} = \frac{\gamma}{\varepsilon_0 \Delta \varepsilon E^2 - \frac{K_{ii}(l^2 - 1)}{a^2}}$$

          Equation 4-3

$$\tau_{decay} = \frac{\gamma a^2}{K_{ii}(l^2 - 1)}$$

          Equation 4-4

Where γ is a rotational viscosity, K_{ii} is an elastic constant, a is the length of the ellipsoid semi-major axis (half of longest axis of the ellipsoid) and l is the shape anisotropy. Unfortunately, both equations are of limited utility because the elastic contribution to the torque ignores anchoring effects.

Small droplets enhance the liquid crystal's elastic deformation energy, and there is an increase in anchoring by the increased surface area of liquid crystal-polymer wall relative to the bulk. This leads to a higher threshold voltage (V_{10} in Figure 4-3), a longer rise time and a shorter decay time [211]. Decay time has been shown to increase moderately while rise time is dramatically reduced

by an increase of droplet size. Decay time is proportional to the liquid crystal droplet size, and it reduces dramatically when the droplets are elongated in shape [219]. Similarly, Wu *et al.* have shown [218] that a small amount of polymer forming a web-like network in the liquid crystal droplets reduces decay time, probably through an increase in anchoring. Numerous experimental results show that increasing temperature reduces rise time [196, 205, 206], probably through a decrease in liquid crystal viscosity.

4.3. Conventional PDLCs

4.3.1. Polymer

One of the most widely used UV curable polymer, NOA65, was chosen for PDLC fabrication. It was purchased from Norland Product Inc., US. The material consists of a modified backbone polymer (urethane acrylate), photoinitiator (benzophenone) and crosslinking oligomers (trimethylolpropane diallyl ether, trimethylolpropane tris thiol, isophorone and di-isocyanate ester) [220].

NOA65 is a colourless liquid. The use of NOA65 eliminates premixing, drying, and heat curing operations common to other optical adhesive systems. According to the manufacturer's data sheet, the refractive index of the cured polymer is 1.524, which matches well with the ordinary refractive index of E7 (1.5216). The cured adhesive is very flexible and was designed to minimise strain. NOA65 has enough elasticity to keep strain to a minimum even when

dissimilar materials with different coefficients of expansion are bonded together. These properties make NOA65 a promising candidate for use in a flexible PDLC display.

NOA65 is cured by UV light within the range of 350 to 380 nm. For the clean-up of the adhesive, acetone can be used if the cure has not progressed too far. If fully cured, methylene chloride can be used to soak assemblies apart.

4.3.2. Sample Fabrication

The fabrication process of PDLC cells in this work differs only a little from liquid crystal cell fabrication described in Section 2.4.1. The major difference in the procedure is the addition of the UV curing step.

First, a polymer-LC mixture was prepared by mixing the equal volume of the UV curable polymer, NOA65, and the doped liquid crystal prepared with the method described in Section 2.4.1. The mixture was stirred using a Teflon coated magnetic stirrer for at least one hour in the dark. A 10 μm empty glass cell with no alignment layer (KSSZ-10/B111PINTS from E.H.C Co., Ltd., Japan) was filled with the solution at 70°C. Immediately after filling, the cell was cooled to room temperature of 21°C, the cell was irradiated by means of UV light (360 nm, Spectroline, Model EN-180L/F, 230 V, 50 Hz, 0.17A). The intensity required for the curing is 4.8 mW/cm^2 according to the manufacture's datasheet [221]. The duration of the irradiation required was

later determined, in Section 4.3.4, to be 2 minutes when the distance from the sample to the UV lamp was 10 cm.
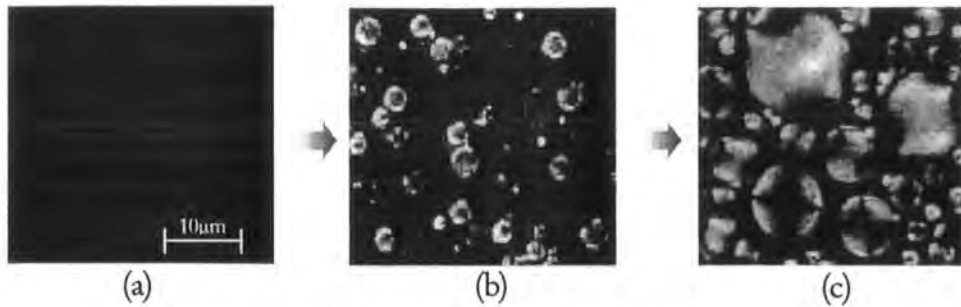
Figure 4-5. Curing of polymer-LC mixture
observed under the cross-polarised
microscope.
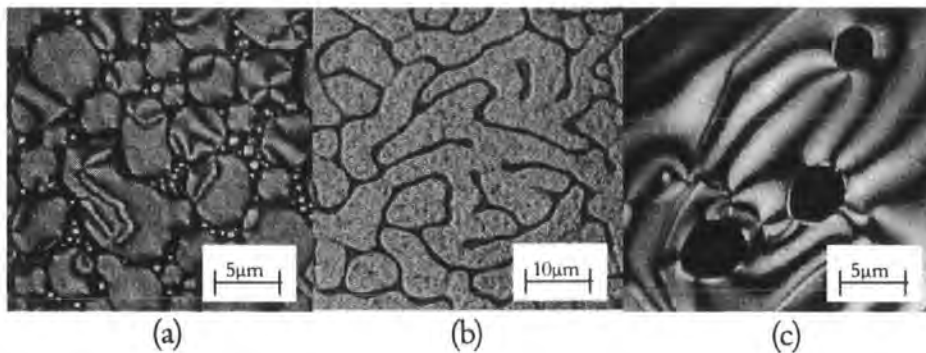
Figure 4-6. 80% PDLC (a), 90% polymer
network type PDLC (b), and 90% polymer
ball type PDLC (c).

This UV curing process initiates the cross-linking of the polymer, making the liquid crystal insoluble in the polymer. The phase separated liquid crystal forms droplets, they merge and grow bigger until the polymer matrix locks its morphology. This curing process was observed under a cross-polarised microscope, and the captured images are shown in Figure 4-5. This shows that as the UV initiates the cross-linking of polymer chains, the liquid crystal

phase separates from the polymer phase (Figure 4-5 b) and merges to form bigger droplets (Figure 4-5 c). The morphology was typical of the nucleation and growth mechanism (Section 4.2.2). The size of the droplets can be controlled by the speed of the curing process [49, 222].

PDLCs with different morphologies of the droplet type could be made by varying the E7-NOA65 composition and curing conditions. When the proportion of liquid crystal to polymer was 80 % by volume (80% PDLC), the liquid crystal droplets were no longer spherical in shape but deformed as shown in Figure 4-6 (a). According to the phase diagram (Figure 4-2), this mixture was in the isotropic regime and undergone the nucleation and growth mechanism. This is still the same mechanism for the ordinary PDLC described in this work. However, when the liquid crystal proportion was increased to 90%, the mixture has undergone the spinodal decomposition, i.e. enclosure of liquid crystal in polymer matrix has disappeared, and a network of polymer was formed in the liquid crystal matrix (Figure 4-6 b). On the other hand, when the same 90% PDLC is cured with a stronger intensity of UV light (e.g. 1 cm from the UV lamp to the sample), the reverse "nucleation and growth" occurred, forming polymer droplets as shown in Figure 4-6 (c). These latter two types of PDLC are known as *network type PDLC* and *polymer ball type PDLC*, and they have been studied in detail previously [197, 216, 223, 224]. The characteristic director configuration around spherical particles seen in Figure 4-6 (c) was studied in detail by Stark [225] and Fukuda *et al.* [226].

4.3.3. Droplet Size

The droplet size of the PDLC is known to depend on the speed of curing [49, 222] since the faster curing locks the polymer matrix before the droplets can merge and grow. Faster curing can be achieved by irradiating the cell with greater UV intensity, i.e. by either using more powerful UV lamp or curing at a closer distance.

		Distance from the sample to the UV lamp			
		5 cm	15 cm	50 cm	120 cm
Proportion of E7 to NOA65 by weight	50%	3 ± 1 μm	5 ± 1 μm	18 ± 2 μm	30 ± 5 μm
	60%	10 ± 2 μm	20 ± 3 μm	30 ± 5 μm	110 ± 10 μm
	70%	30 ± 5 μm	40 ± 5 μm	80 ± 10 μm	150 ± 10 μm

Table 4-1. Droplet size dependency with
distance to the UV lamp. PDLCs with
different liquid crystal densities were made.
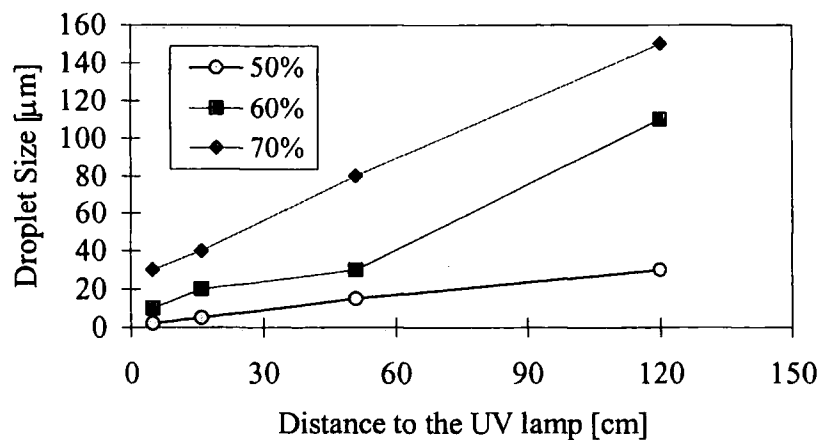
Figure 4-7. Droplet size dependency with
distance to the UV lamp.

To find out the optimum curing conditions to achieve the maximum contrast, undoped PDLC cells with different proportions of liquid crystal to polymer were cured at a variety of UV strengths, i.e. distance between the UV source and the uncured cell was varied. The droplet sizes were measured under a cross-polarised microscope.

Figure 4-8. Example of a PDLC display
sample.

The result (Figure 4-7) confirms that the droplet size increases with the distance from the UV lamp as the curing rate falls. The size also increases with the liquid crystal volume density in the PDLC. The limited cell thickness of 10 μm deformed droplets bigger than 10 μm. The cure distance of 5 cm for PDLC with 50% liquid crystal density (50% PDLC) gave a droplet size of 3 μm which was desirable for the maximum scattering [44, 211]. The 50% PDLC composition was the only mixture which reliably formed droplets with an approximately spherical shape. It can also form the optimised droplet size of 3 μm. Hence the rest of the PDLC characterisations were performed with 50% PDLC cured at 10 cm. An example of the undoped PDLC is shown in

Figure 4-8. The cell was placed on a black background. The ITO coated region becomes transparent when the voltage was applied, showing the black background. The white colour is due to the back scattering of the liquid crystal droplets.

4.3.4. Cure time
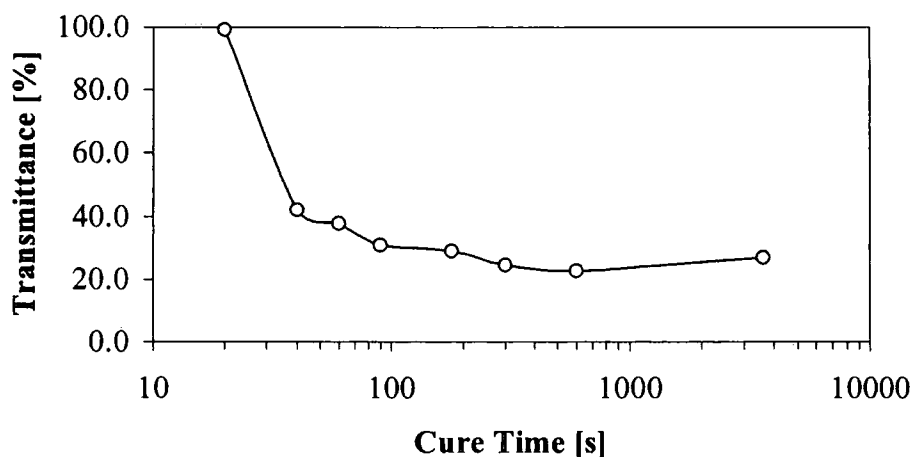
Figure 4-9. Transmittance variation of PDLC
with cure time.

The time needed for the curing of PDLC was measured to avoid over and under curing. The transmittance was measured during the curing process, using the set-up similar to the one used for the GH liquid crystal (Figure 3-3). However, the polarisers and the driver were not used, and the uncured cell was simply placed between the He-Ne laser and the photo diode. The photo diode was not sensitive to the UV light used to initiate polymerisation. Irradiation of the UV light from 10 cm away made the cell become more

scattering, reducing the detected intensity with time. This was recorded using an oscilloscope, giving a typical profile shown in Figure 4-9. The thickness of the cell was 20 µm, and the result showed that more than 90% curing was achieved within two minutes.

Cure time [s]	Transmittance [%]
0	100.0
20	99.1
40	42.1
60	37.7
90	30.7
180	28.9
300	24.6
600	22.8
3600	27.0

Table 4-2. Transmittance variation of PDLC
with cure time.
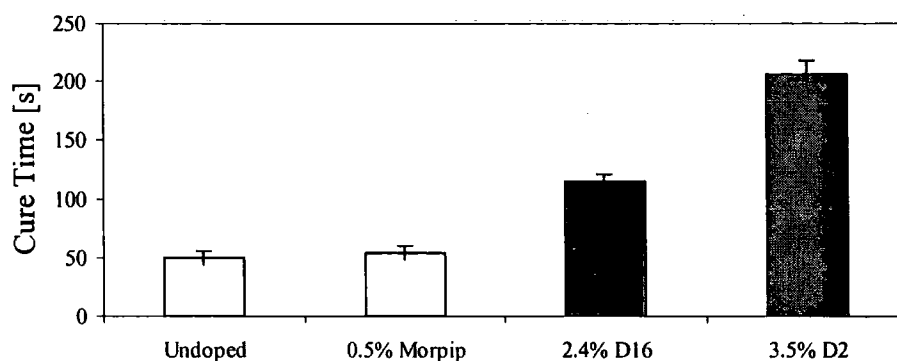
Figure 4-10. Cure time for dichroic PDLCs.

The same experiment was carried out for doped and undoped PDLCs. This time, 10 μm cells were used because this thickness was believed to be the best candidate for commercial display use. Each dye was dissolved to its maximum solubility into the E7 liquid crystal host as in Section 3.4.3.2, and then an equal volume of doped liquid crystal was mixed with NOA65 to form 50% PDLCs. The result shown in Figure 4-10 shows that the time needed for cure depends heavily on the nature of the dyes used.

The long cure time, most probably due to absorption of dyes, make the droplets size bigger (Figure 4-11). This is an undesirable effect because the bigger droplets cause less scattering. Also the absorption of UV means that there might be a degree of dye deterioration such as shown in Section 2.4.3.

⊢20μm⊣

Figure 4-11 MORPIP, D2 and D16 doped
PDLCs (from left), observed under the cross
polarised microscopes.

4.3.5. Cure Problems Associated with Dyes

Attempts have been made to make PDLCs doped with light sensitive [227] blue TCNQ derivatives named DEMI and ULTRA [130, 131]. They were explored because of their high dipole (>30 D [131]) hence they were expected

to show the dipolar effect more than MORPIP. Additionally their blue colour was attractive as one of the three colour components required for colour displays. The structures and spectras of both DEMI and ULTRA are shown in Figure 4-12.
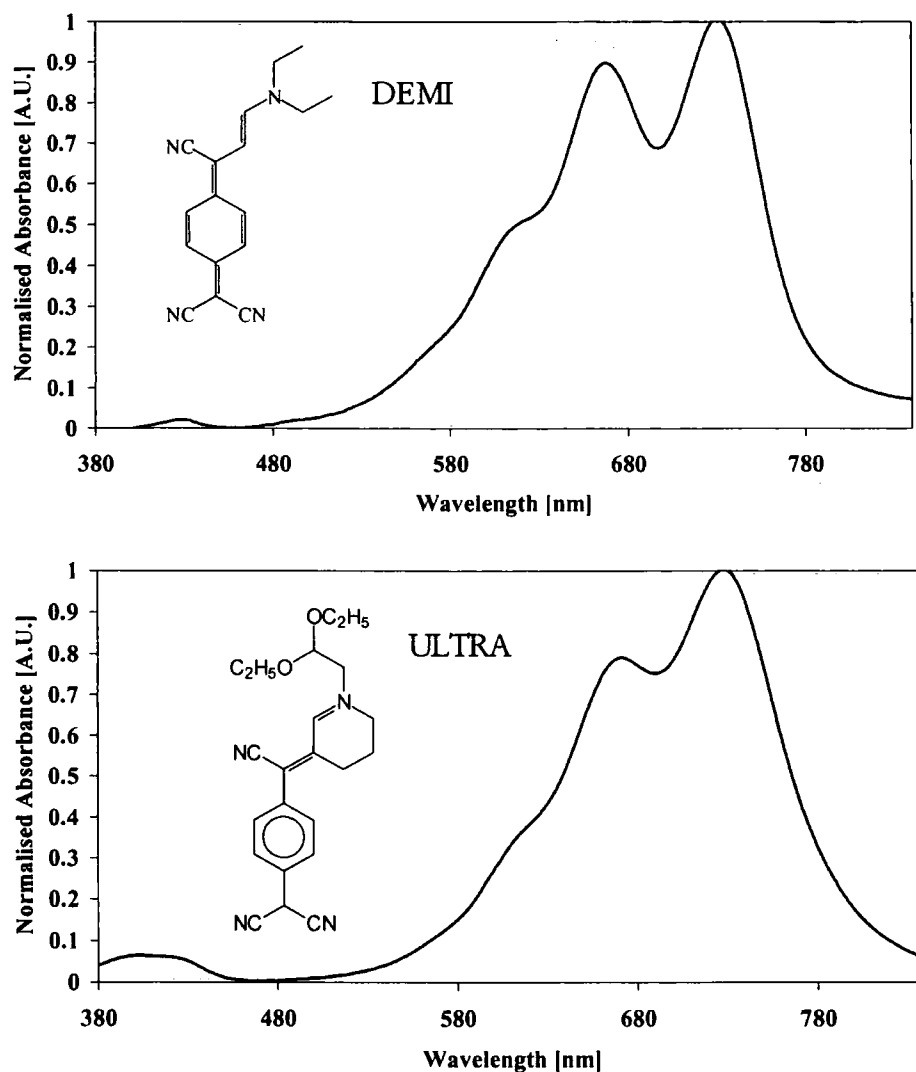
Figure 4-12 Chemical structures and the normalised absorbance of DEMI and ULTRA

DEMI and ULTRA have low absorption at the UV irradiation wavelength and were anticipated to be not sensitive to UV degradation. However, when the UV was irradiated on a mixture of NOA65 and DEMI/ULTRA doped E7, the phase separation could not be initiated until most of the colour had disappeared; the doped PDLCs made were only slightly blue indicating most of the dye had deteriorated. The result suggests that these dyes may be susceptible to attack by the initiator present during polymerisation. Despite the need for a blue dye in a colour display, the lack of stability of these dyes meant that they were not investigated further.

4.3.6. Response Time of MORPIP doped PDLCs

Highly dipolar MORPIP showed a decrease in the switching time of a GH liquid crystal compared to an undoped liquid crystal cell (Section 3.4.3.2), and it was interesting to see whether the same effect was evident for the MORPIP doped PDLCs. It is not simple to compare doped PDLCs because the response time depends on droplet size and shape.

No significant difference in the droplet morphologies and sizes were observed under the cross polarised microscope for MORPIP doped and undoped PDLC compared to D2 or D16 doped PDLCs. The droplet sizes of undoped and MORPIP doped PDLC were both in the order of 3-5 μm, D16 doped PDLC had 5-10 μm droplets and the D2 doped cell did not have uniformly sized droplets. The similarity in droplet size of the undoped and MORPIP doped PDLC makes sense since they both showed little difference

in the cure time (Figure 4-10). Unfortunately, the size of 3-5 μm was too small to be measured accurately under the cross polarised microscope, hence the use of the scanning electron microscope would be useful for the further investigation of the droplet size and morphology of PDLCs.

In this experiment, the response times of PDLCs doped with different MORPIP concentrations were measured. The experimental set-up was the same as for the response time measurement of GH liquid crystal (Section 3.3), but the polarisers were not used. The applied voltage was set to give 90% transmittance of the on-state transmittance $(1.67 \times 10^6 V/m = 25V/15\mu m)$. The measurements were taken at room temperature (24°C).
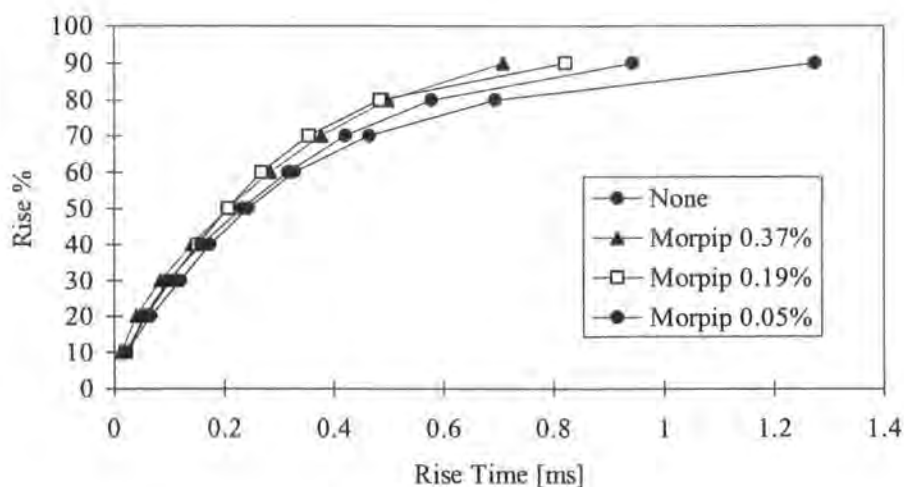
Figure 4-13. Rise time dependency of
MORPIP doped PDLCs.

The result of rise time measurement is shown in Figure 4-13 and Table 4-3. As in the case of MORPIP doped GH liquid crystal (Section 3.4.3.2), a decrease in rise time was observed as the concentration of MORPIP

increased (Figure 4-14). As much as a 45% decrease in rise time was recorded

with 0.37 wt% of MORPIP, which was considerable improvement compared

to the 21% for the GH liquid crystal (0.5%wt MORPIP). One possible reason

for such an improved rise time is the slight increase in droplet size: since

MORPIP has some absorption at 360 nm, the cure times required for

MORPIP doped PDLC are slightly longer (Section 4.3.4). The decay time

experiment (Figure 4-15) showed the increase in decay time with 0.1 wt%

MORPIP. If the droplet size was increased as suspected by the rise time

measurement, the increase in the decay time makes sense because the polymer

walls of the bigger droplets are expected to have a smaller anchoring energy.
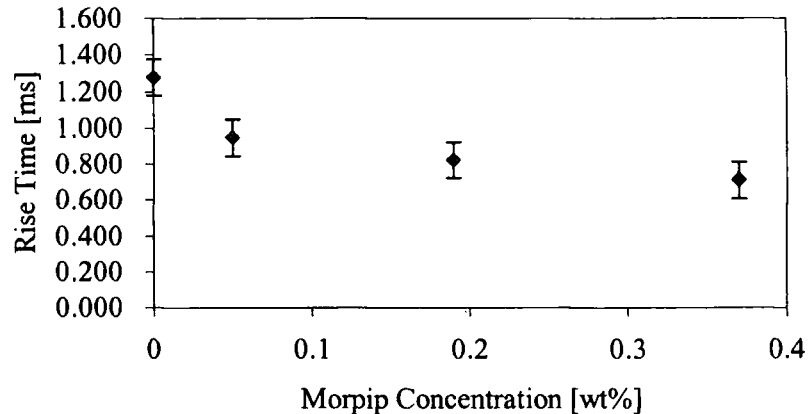
Figure 4-14. Rise time dependency of
MORPIP concentration for PDLCs.
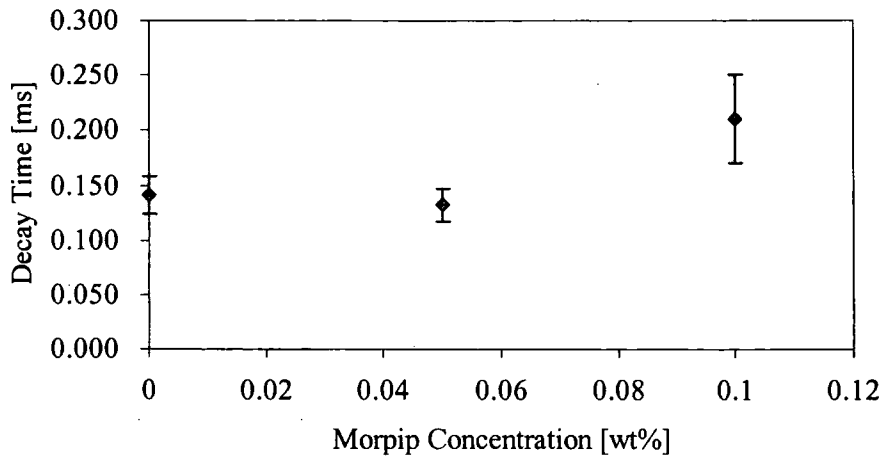
Figure 4-15 Decay time dependency of
MORPIP concentration for PDLCs.

Rise time [ms]	10%	20%	30%	40%	50%	60%	70%	80%	90%
undoped	0.0220	0.0663	0.1207	0.1746	0.2443	0.3295	0.4654	0.6948	1.2739
Error	0.0129	0.0216	0.0176	0.0227	0.0283	0.0315	0.0432	0.0924	0.2853
Morpip 0.37wt%	0.0128	0.0401	0.0852	0.1421	0.2072	0.2849	0.3775	0.4995	0.7099
Error	0.0077	0.0205	0.0343	0.0390	0.0351	0.0309	0.0256	0.0275	0.0431
Morpip 0.19wt%	0.0216	0.0589	0.1022	0.1510	0.2072	0.2691	0.3549	0.4853	0.8225
Error	0.0132	0.0247	0.0334	0.0292	0.0280	0.0336	0.0659	0.0912	0.2246
Morpip 0.05wt%	0.0230	0.0553	0.0994	0.1578	0.2326	0.3172	0.4213	0.5790	0.9442
Error	0.0147	0.0367	0.0509	0.0613	0.0494	0.0432	0.0575	0.0795	0.1803
Decay time [ms]	10%	20%	30%	40%	50%	60%	70%	80%	90%
undoped	1.7554	-	1.7054	1.6929	1.6841	1.6778	1.6734	1.6704	1.6682
Error	0.0243	-	0.0121	0.0080	0.0047	0.0025	0.0011	0.0005	0.0002
Morpip 0.10wt%	1.7646	-	1.7109	1.6971	1.6873	1.6799	1.6750	1.6715	1.6688
Error	0.0376	-	0.0161	0.0100	0.0053	0.0024	0.0011	0.0006	0.0003
Morpip 0.05wt%	1.7693	-	1.7095	1.6959	1.6863	1.6793	1.6745	1.6711	1.6685
Error	0.0380	-	0.0162	0.0100	0.0055	0.0027	0.0013	0.0007	0.0004

Table 4-3. Rise and decay time versus
MORPIP concentration for PDLCs

4.3.7. Contrast

The transmittance of doped PDLCs was measured. The cells were fabricated using the appropriate cure times determined in Section 4.3.4. The transmittance spectrum of each cell was measured using Perkin Elmer UV/VIS/NIR Lambda 19 spectrometer. The minimum transmittance at λ_{max} of each dye was recorded for both the on and off-state, and the result is shown in Figure 4-17.

As expected (Section 4.2.3), the experiments showed the successful decrease in off-state transmittance by addition of dyes (Figure 4-16). For example, off-state transmittance of D2 doped PDLC had decreased by 51% compared to undoped PDLC at 493nm. However, the on-state transmittance had also decreased by 40%. Unfortunately, this decrease in on-state transmittance occurred for all doped PDLCs (Figure 4-17). Their measurement were taken at 500nm for undoped PDLC, and at the respective absorption maximum for the dye doped PDLC, i.e. 454.5nm for MORPIP, 496nm for D2 and 596nm for D16. A very clear on-state is necessary to achieve a good contrast for the display application, especially for the three-layered structure (Section 1.4.4) suggested by Sony.

Figure 4-18 shows each of the doped PDLCs placed over some text. The middle section, where text is seen clearly, is the ITO coated area. The doped PDLCs are at on-state within this middle section. The other parts of the cells are in the off-state. The contrasts of the cells are clearly not satisfactory for

display use. D2 and D16 doped PDLCs appeared less scattering at their off-states because of their longer cure time (Section 4.3.4). This problem could be solved by using a chemical accelerator to increase the curing speed [228].
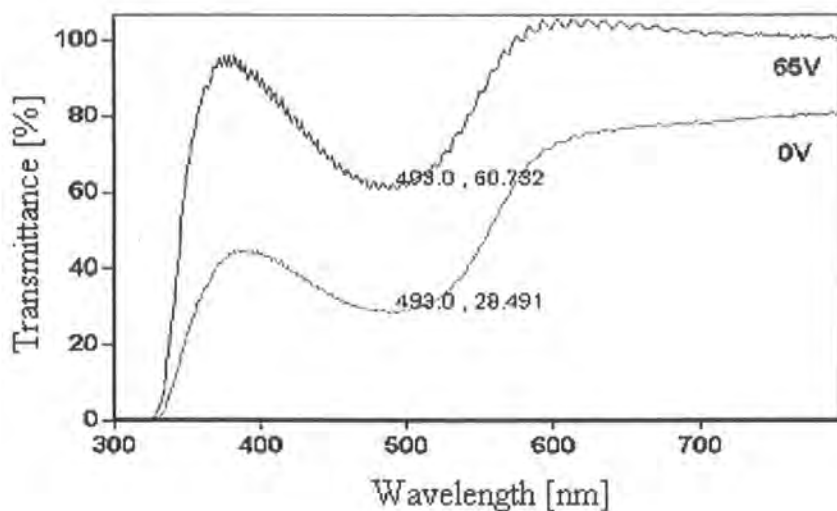
Figure 4-16 Transmittance at on and off-state
of 3.5 wt% D2 doped PDLC.
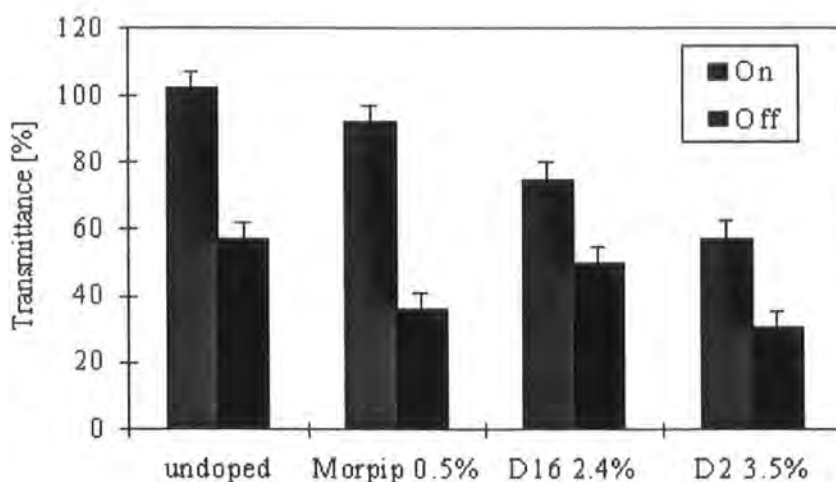
Figure 4-17. Transmittance at on and off-state
of doped PDLCs.
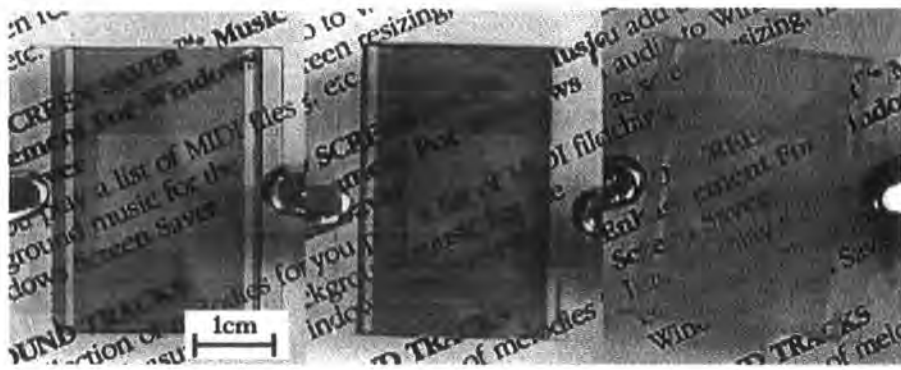
Figure 4-18. D16, D2 and MORPIP doped
PDLC cells at on-states (left to right).

The on-states of all cells appeared coloured. This indicates that the dyes are trapped in the polymer matrix together with liquid crystal.

As described previously (Section 4.2.3), as much as 53% of the liquid crystal can remain dissolved in the polymer binder [178, 200, 201]. In fact, by using an IR spectra, as much as 14% of E7 liquid crystal was found to stay in the NOA65 polymer matrix [167].

4.4. Novel PDLCs

To overcome the low contrast problem due to dye deterioration and dye trapping, two new dichroic PDLC fabrication techniques were developed [10]. For convenience, the PDLCs made by the first method were named *Dispersed PDLC (DPDLC)*, and the second ones were named *Sponge PDLC (SPDLC)*. Their fabrication and properties are described below.

4.4.1. Dispersed PDLC

The first method involves forcing doped liquid crystal "in", and consequently pushing undoped liquid crystal "out" from a ready-made PDLC cell. This method may be applied only when the liquid crystal phase in the PDLC is interconnected as in Figure 4-6. For the liquid crystal-polymer combination used in this work, the liquid crystal proportion in the PDLC must be more than 80% to achieve the continuous liquid crystal phase.

Pictures of DPDLC taken under cross-polarised microscopy are presented in Figure 4-19. The picture (a) shows polymer balls in the nematic liquid crystal. The refilling process did not sweep the polymer balls out from the cell, therefore they were probably attached to either side of the substrates. This cell was made by curing 90% PDLC for 2 minutes with the UV source placed 10 cm away from the cell. The picture (b) shows the same cell after being refilled with 2.5 wt% B2 doped liquid crystal. The nematic liquid crystal appears dark due to the B2 dye absorbing light.

(a)   (b)
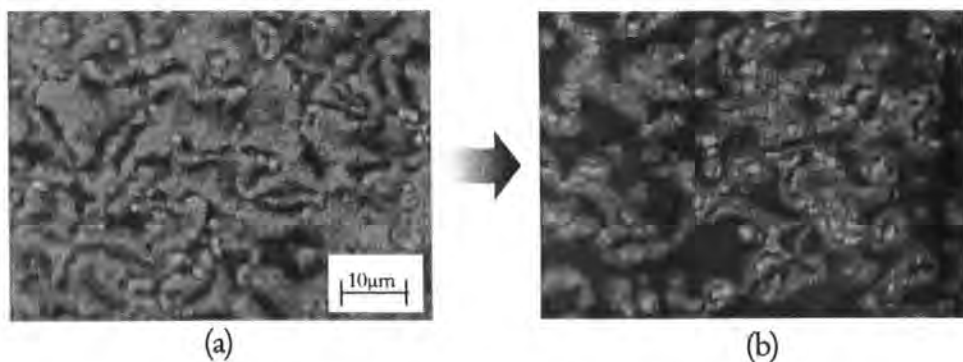
Figure 4-19. PDLC with 90% liquid crystal.
Undoped PDLC (a) and DPDLC doped with
B2 dye (b).
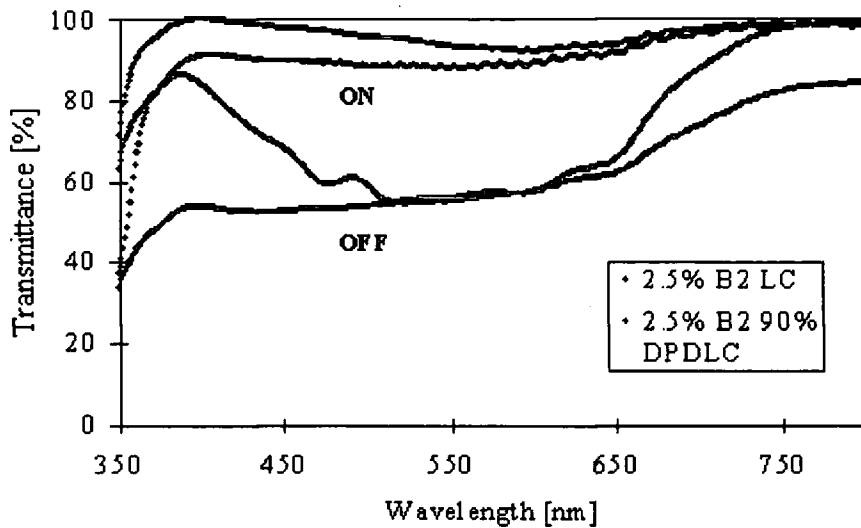
Figure 4-20. Transmittance measurement of
dichroic DPDLC with Heilmeier liquid crystal.

Further, the transmittance of the DPDLC was compared with a Heilmeier

liquid crystal doped to same concentration of dye to see how scattering has

improved the absorption of the dye. The result (Figure 4-20) showed a

transmittance decrease at 800 nm, which indicates that more scattering was

present in DPDLC compared to Heilmeier liquid crystal. Even though the

DPDLC has 10% less dye present compared to the Heilmeier liquid crystal,

the transmittance at 550 nm stays the same (54%), implying the increase in

dye absorption due to scattering. Unfortunately, the DPDLC contrast ratio

was 1.63 (T_{max}/T_{min}=88%/54%) at 530 nm, which was still too weak for

display applications that requires a contrast ratio of 2.7 or more (Section 1.4.4).

It was not possible to increase the contrast ratio much more by using the

same liquid crystal (E7) and polymer (NOA65) combination, as the mixture

starts forming droplets under 80% PDLC. The network type PDLC or

polymer ball type PDLC [197, 216], which has continuous liquid crystal, with very high scattering would further improve the contrast of DPDLC.

4.4.2. Sponge PDLC

This second new fabrication technique, which gives an increased contrast compared to DPDLC introduced in the previous section, makes use of the fact that E7 liquid crystal is highly soluble in acetone, while NOA65 polymer is only slightly soluble [221]. When a ready-made undoped PDLC cell (Section 4.3.2) was soaked in acetone, E7 liquid crystal and uncured monomer and oligomer in the PDLC cell slowly dissolve in the solution (Figure 4-21).

The cell became less scattering when E7 mixes with acetone, but it became weakly scattering again as the E7 is fully washed out. The duration of this process depends on the size and proportion of liquid crystal droplets (Section 4.3.3). When the droplet sizes are in order of 1 μm, and the liquid crystal proportion is 50%, the washing process takes a few weeks. If the droplet sizes are in order of 100 μm, and the liquid crystal proportion is 90%, i.e. all the liquid crystal is connected together, the process takes only a few days.

After fully removing the E7, slow heating in the drying cabinet evaporated the acetone in the remaining acetone-polymer system (Figure 4-22 bottom right). A sponge of polymer matrix with air cavities (Figure 4-22 top left) remained.

Observation of the polymer sponge under a microscope did not show any noticeable difference in the matrix structure.
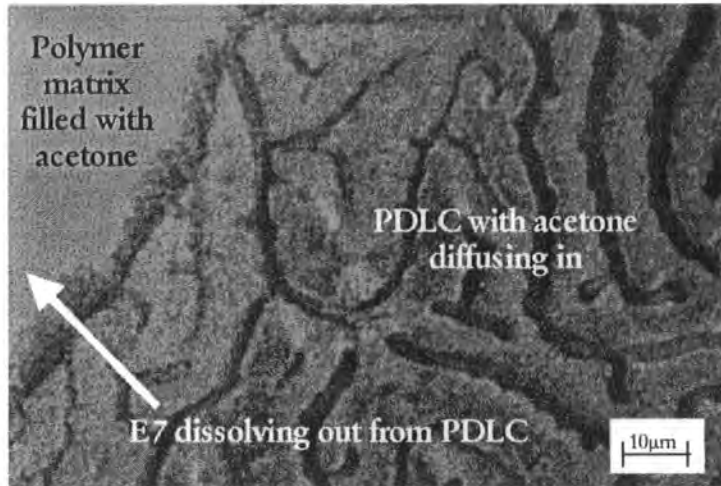
Figure 4-21. Photo taken under microscope.
Acetone (top left) is slowly diffusing into a
PDLC (bottom right), dissolving E7.
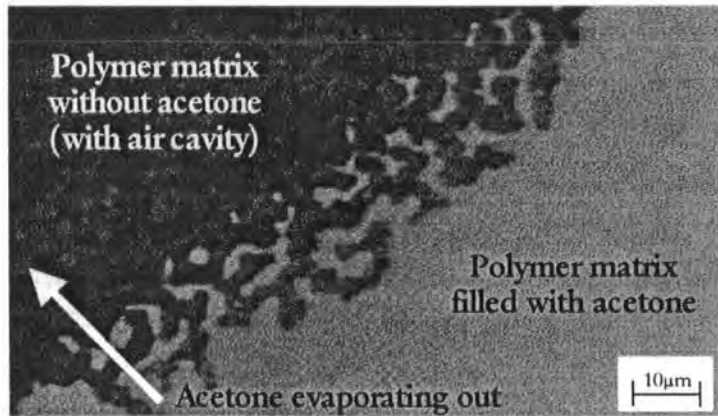
Figure 4-22. Photo taken under microscope.
Drying of acetone from polymer matrix.
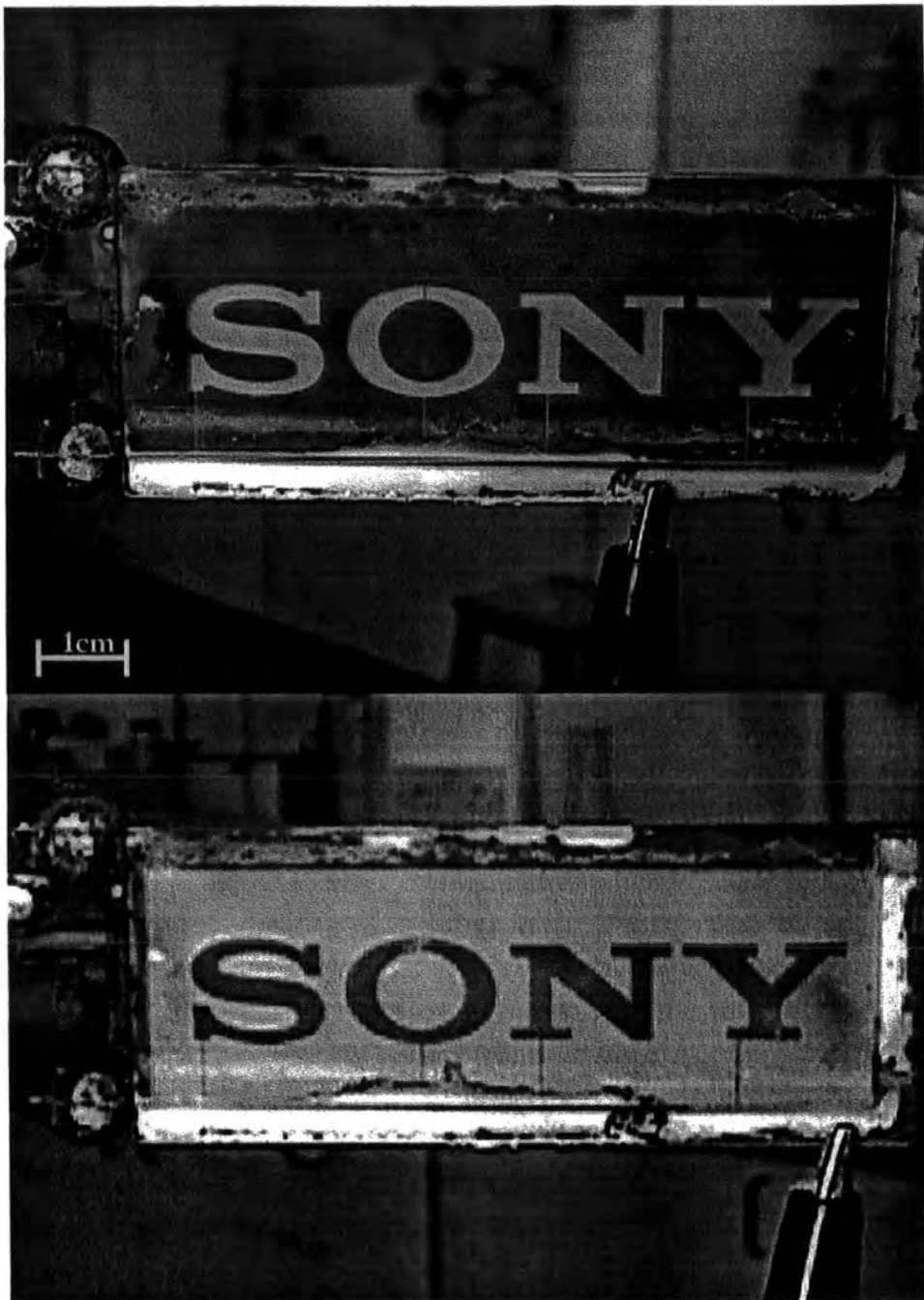
Figure 4-23 2% B2 doped 70% SPDLC cell

Then the cell was stood upright in a small beaker filled with the desired dye

doped liquid crystal, leaving one open-end of the cell open to air, i.e. not

soaked in the liquid crystal. Then the beaker was quickly placed in a vacuum oven at 40 °C. This refilling method [229] in vacuum avoids any air left in the matrix after filling with the doped liquid crystal. Finally, when the cell is refilled, it was taken out of the beaker, and both open-ends of the cell were sealed with epoxy. As an example, an SPDLC cell made using this method is shown in Figure 4-23. The cell is normally black with scattering state. When the electric field is applied, the cell becomes transparent and shows the white background. The cell has an ITO patterned as "SONY", and one can selectively switch the letter part ON (Figure 4-23 above) or the non letter part ON (Figure 4-23 below).

4.4.3. Contrast Measurement

Off-state transmittance of doped SPDLC and a conventional Heilmeier liquid crystal cells were compared to investigate whether the contrast was better than that observed with doped PDLC (Figure 4-17). Both cells contained 2.5 wt% B2 in the liquid crystal. The liquid crystal proportion to polymer in SPDLC was 70%.

The result in Figure 4-24 shows that the Heilmeier liquid crystal transmittance of 55% was decreased to 30% for SPDLC. This is surprising considering that the SPDLC has 30% less liquid crystal, and hence 30% less dye concentration. At 520 nm, doped SPDLC achieved a contrast ratio of 3.0 compared to 1.7 for the Heilmeier liquid crystal. The decrease in transmittance was clearly achieved by the scattering effect, as can be observed by the decrease of

transmittance at 800 nm where there is no absorption by the dye. The effect of the scattering can be seen by a further decrease in the SPDLC transmittance at 400 nm. This is because the scattering efficiency decreases rapidly with increasing wavelength [210].
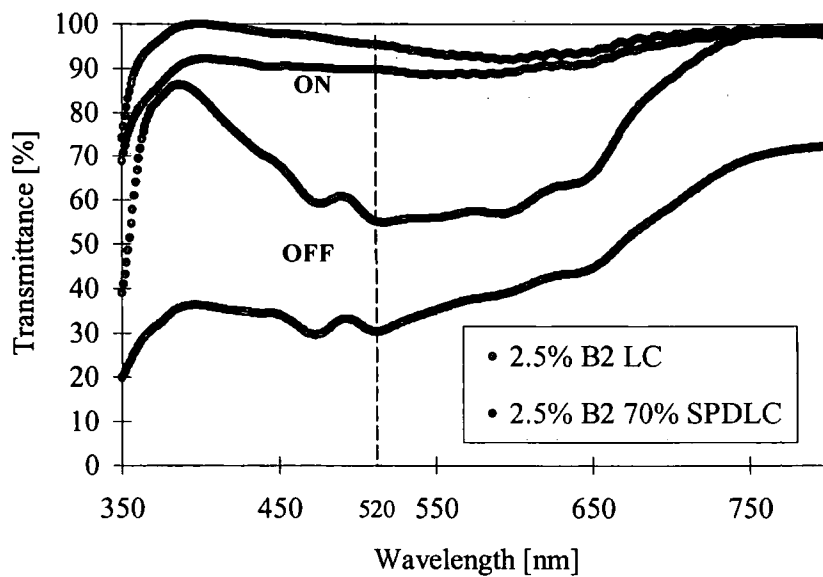
Figure 4-24. Transmittance of a SPDLC and a
conventional GH cell.

4.4.4. Threshold Characteristics of SPDLC

Following the successful contrast result from the previous section, the SPDLCs were investigated further by comparing the electro-optic properties of undoped SPDLC with undoped PDLC. Two identical undoped PDLC cells were made under the same conditions. The liquid crystal proportion of the PDLC's was 60%, and the cells were irradiated with UV from 10 cm away for 2 minutes (Section 4.3.4). Both cells were 10 μm thick without any prior

alignment treatment. Then one of these cells was converted to an undoped SPDLC sample by the method described previously (Section 4.4.2). The E7 was simply washed away as described in Section 4.4.2, and the polymer sponge was filled with undoped E7 LC. Transmittance variation with applied voltage was measured using the same setup described in Section 4.3.4 (He-Ne laser, 632.8 nm), and the result shown in Figure 4-25 was obtained.

The result shows that the V_{10} (Section 4.2.3) is 2.5±0.3 V for PDLC, and 3.5±0.3 V for SPDLC. V_{90} for PDLC is 7.5±0.3 V and 12±0.3 V for SPDLC. Both V_{10} and V_{90} were increased by approximately 34% by transforming the PDLC into SPDLC. The increase indicates an increase in anchoring energy at the polymer walls, caused by the removal of the uncured monomer and oligomer or drying, or combination of both.
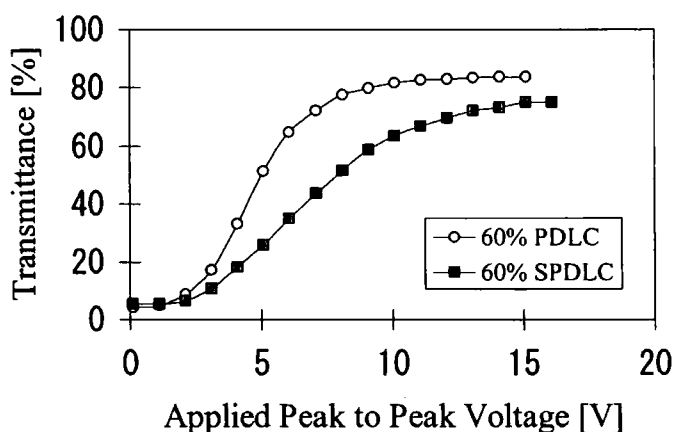
Figure 4-25. Transmittance measurement of undoped
PDLC and undoped SPDLC.

Applied Voltage [V]	PDLC Transmittance [%]	SPDLC Transmittance [%]
0.1	4.1	5.2
1.1	4.8	5.2
2.1	8.7	6.2
3.1	17.0	10.8
4.1	33.1	18.1
5.1	51.2	25.8
6.1	64.8	34.8
7.1	72.1	43.5
8.1	77.4	51.6
9.1	79.8	58.5
10.1	81.6	63.4
11.1	82.6	66.9
12.1	83.0	69.7
13.1	83.3	72.1
14.1	83.7	73.2
15.1	83.7	74.9
16.1	–	74.9

Table 4-4. Transmittance measurement of
undoped PDLC and undoped SPDLC

4.4.5. Response Time Measurement

To further characterise the SPDLC, the response times of undoped PDLC and undoped SPDLC were measured using the same set-up used in the previous section. All cells tested were 10 μm thick without any surface alignment. Rise and decay time results are shown in Figure 4-26 and Figure 4-28 respectively.

The inconsistent results at lower voltage, under 8V, for the SPDLC was due to the liquid crystal not reaching full alignment. Nevertheless, the trend, that

the undoped SPDLC responds slower to the electric field compared to undoped PDLC, can be seen when higher voltages are applied. This difference is shown more clearly when the rise time variation is plotted with inverse square of the electric field (Section 3.4.3.2) as shown in Figure 4-27. Assuming that the PDLC responds to an electric field as the liquid crystal does (Section 3.4.3.2), a straight line through the origin was fitted to the data points, and the gradient calculated. The gradients of the PDLC and SPDLC samples were 0.016 ± 0.002 sV^2 μm^{-2} and 0.031 ± 0.002 sV^2 μm^{-2} respectively. Even though the lines do not fit the data points perfectly due to the larger threshold electric field, E_0, for PDLCs (Equation 3-7), the difference in gradients clearly indicates that the SPDLC is approximately twice as slow as the PDLC. Nevertheless, they are both well within the targeted range of 100 ms under an applied field of 10V for display application.
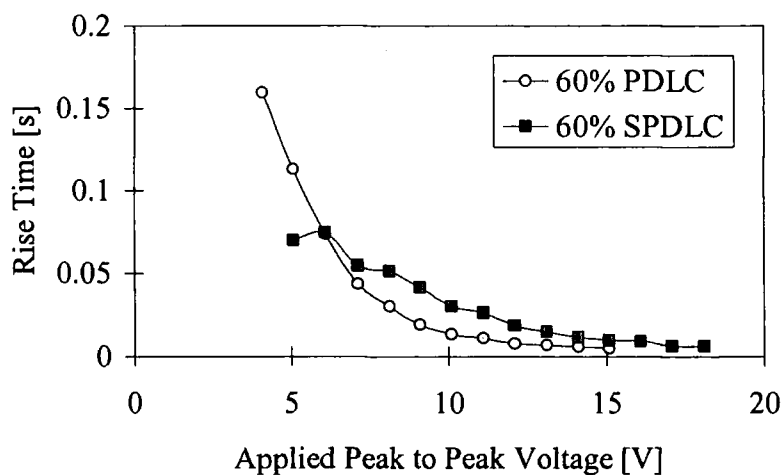
Figure 4-26. Rise time measurements of undoped PDLC
and undoped SPDLC.

Applied Voltage [V]	SPDLC Rise Time [s]	PDLC Rise Time [s]
4.1	-	0.159
5.1	0.069	0.112
6.1	0.074	0.073
7.1	0.054	0.043
8.1	0.050	0.030
9.1	0.041	0.019
10.1	0.030	0.013
11.1	0.025	0.010
12.1	0.018	0.007
13.1	0.014	0.006
14.1	0.011	0.005
15.1	0.009	0.004
16.1	0.008	–
17.1	0.006	-
18.1	0.006	-

Table 4-5. Rise time measurements of
undoped PDLC and undoped SPDLC
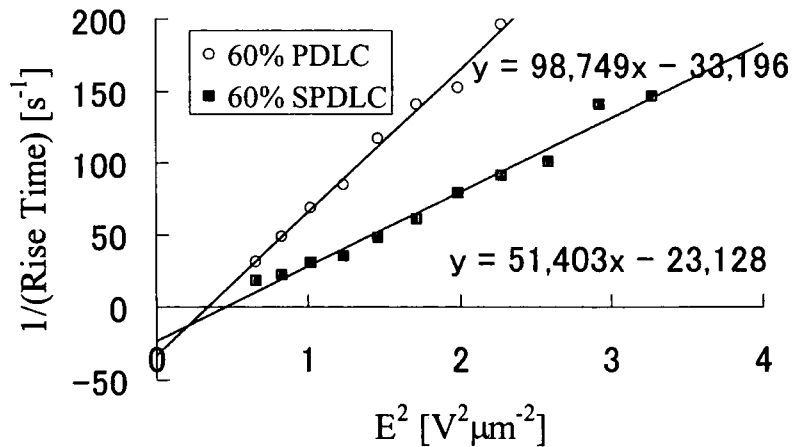
Figure 4-27. Rise time variation with inverse electric field
square for PDLC and SPDLC

E^2 [$V^2\mu m^{-2}$]	SPDLC Inverse Rise Time [s^{-1}]	PDLC Inverse Rise Time [s^{-1}]
0.6561	18	31
0.8281	22	48
1.0201	30	68
1.2321	35	84
1.4641	47	116
1.7161	60	140
1.9881	78	152
2.2801	91	196
2.5921	100	-
2.9241	140	-
3.2761	146	-

Table 4-6. Rise time variation with inverse
electric field square for PDLC and SPDLC.

It is interesting to note that the rise times of the PDLC and the SPDLC are approximately 0.013 s and 0.03 s respectively at 10V ($=1V/\mu m$), while the GH LCs investigated at Section 3.4.3 showed the rise time of approximately 0.15 s (Figure 3-9). This slower switching of the homogeneously aligned GH LCs are probably due to the full 90° orientation required, while most LC droplets in the PDLCs require the orientation of less than 90°.

The same PDLC and SPDLC cells were used to measure decay time (Section 3.4.2), and the result is shown in Figure 4-28. The decay time of the SPDLC cell is only 73% of the decay time obtained for the PDLC cell. The SPDLC cell switches off as fast as it switches on, and this can be useful since the slow decay time of liquid crystals is one of the problems suffered by liquid crystal displays. The measured decay time for 10 μm Heilmeier liquid crystal

in Section 3.4.2 was 250 ms, which is considerably longer than the 30 ms for

SPDLC.
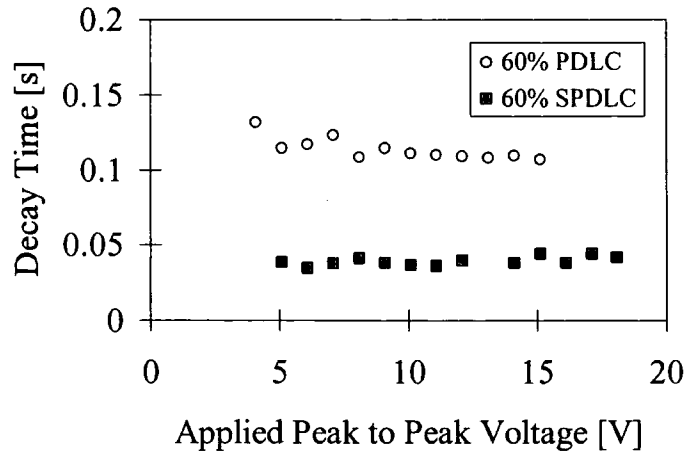
Figure 4-28. Decay time of undoped PDLC
and undoped SPDLC.

Increases in the rise time and decreases in the decay time, together with the

increased threshold voltage measurement from the previous section, are

common effects observed when the anchoring energy of the polymer wall is

increased (Section 4.2.4). Further measurements of anchoring energy would

reveal if this is the origin of the observed effect.

Owing to the long fabrication time required, it was not possible to

characterise dye doped SPDLCs within the time scope of this project. A

development of improving the fabrication speed is underway, and the full

characterisation of dye doped SPDLCs will be carried out in the near future.

Applied Voltage [V]	SPDLC DecayTime [s]	PDLC Decay Time [s]
4.1	-	0.131
5.1	0.038	0.114
6.1	0.034	0.116
7.1	0.037	0.123
8.1	0.041	0.108
9.1	0.037	0.114
10.1	0.036	0.111
11.1	0.036	0.110
12.1	0.039	0.108
13.1	-	0.107
14.1	0.038	0.109
15.1	0.044	0.106
16.1	0.037	-
17.1	0.044	-
18.1	0.041	-

Table 4-7. Decay time of undoped PDLC and
undoped SPDLC

4.5. Conclusion

In this chapter, GH effects of PDLC were explored in order to evaluate the potential for a reflective type PDLC display. The conventional PDLCs were made successfully using the UV initiated phase separation method (Section 4.3.2). Other morphologies, such as polymer network type and polymer droplet type PDLC, could also be made by varying the proportion of liquid crystal to the polymer. Although these morphologies were interesting in themselves, they did not scatter sufficiently for display use. The liquid crystal

proportion of 50% with rapid curing provided the most scattering PDLC (Section 4.3.3).

While measuring the optimum time needed for the PDLC curing, it was found that the doped PDLCs required far longer, as much as four times, than the cure time required for the undoped PDLC (Section 4.3.4). The reason was believed to be the UV absorption by the dye, preventing the polymer curing. Also deterioration of dyes was encountered for light sensitive dyes supporting this conclusion. Nevertheless, the cure time required for MORPIP doped PDLC was the same as undoped PDLC, implying that changes in the morphologies, such as droplet size, were minimal for MORPIP doping. Indeed, no observable change in droplet size and morphologies could be seen under the polarising microscope for MORPIP doped PDLC. Hence the response time of the PDLCs with different concentrations of MORPIP could be compared. The result showed that the rise time decreases with increasing concentration of MORPIP (Section 4.3.6), which was consistent with the result obtained in the previous chapter (Section 3.4.3). A 45% decrease in rise time was recorded with 0.37 wt% of MORPIP. One of the possible reasons for a difference in the rise time compared to the 21% decrease of the simple GH liquid crystal is the slight increase in droplet size: MORPIP has some absorption at 360 nm, making the cure time required for MORPIP doped PDLC slightly longer and hence making the droplet size bigger than the undoped PDLC (Section 4.3.4). Small droplets enhance the liquid crystal's elastic deformation energy, and there is an increase in anchoring by the

increased surface area of liquid crystal-polymer wall. The anchoring energy of such MORPIP doped PDLC is smaller because the droplets are slightly larger, and consequently contributing to the further decrease of the rise time.

The contrast measurement of the doped PDLCs showed an insufficient contrast for practical purposes (Section 4.3.7). The sources of the problem were determined as poor off-state scattering due to long cure time, and poor on-state transmittance due to the dyes trapped in the polymer matrix. The poor off-state scattering could be improved by using a chemical accelerator to increase the curing speed [228]. The poor on-state transmittance could be improved by chemical synthesis of dyes and liquid crystal which do not dissolve in the polymer matrix well. Otherwise different fabrication techniques of PDLC such as NCAP systems are preferred [193, 195]. However, two new fabrication methods were developed to overcome all the problems of long curing, dye trapping, as well as dye deterioration.

The first fabrication method (Section 4.4.1) was named Dispersed PDLC (DPDLC). It involves forcing doped liquid crystal "in", and consequently pushing undoped liquid crystal "out" from a ready-made PDLC cell. The technique avoided the UV irradiation of dyes as well as the trapping of dyes. The method was simple, and it proved to increase dye absorption by an increase in scattering. However, this method could only be applied when a liquid crystal droplets are interconnected to each other, and it was not possible to fabricate a high scattering network type PDLC [197, 216] with E7-NOA65 combination. It is possible to obtain a contrast 3 times as large as

that of the droplet type PDLC [197, 216, 230], thus application of the method to a high scattering polymer network or ball type PDLC would further improve the contrast of DPDLC.

The second fabrication method (Section 4.4.2) was named Sponge PDLC (SPDLC). It involves washing out the liquid crystal "out" from undoped PDLC to make a sponge of polymer, and forcing the doped liquid crystal "in" to the open porous polymer. This method allowed the use of more scattering 50% PDLC, achieving the higher contrast ratio of 3 (Section 4.4.3) compared to any of the dichroic PDLC made in this study. The preliminary results showed that undoped SPDLC has 34% increased threshold voltage of 12V (Section 4.4.4), 100% longer rise time of 30 ms, but 73% shorter decay time of 30 ms (Section 4.4.5) compared to the conventional PDLC. Although the threshold voltage and rise time were slightly increased, the considerably shorter decay time would be useful for the display [231, 232]. This indicates that the process lead to an increase in surface anchoring by modification of polymer surfaces by washing out and refilling the liquid crystal. The voltage was high (5-10V) compared to the target voltage (5V), but the response time (rise time + decay time) was kept within the targeted 0.1s due to the decrease in decay time. Decreasing the cell thickness could lower the driving voltage, but this may decrease the contrast ratio of the cell too. Further optimisation is required to balance these parameters.

The only disadvantage of the SPDLC was the slow fabrication owing to the diffusion of acetone into the PDLC. Nevertheless, there is scope for

improvement in the fabrication speed by (1) modifying the diffusion process, (2) using different materials, (3) using different polymer matrix structures, and (4) by opening up the cell.

Some researchers have performed the removal of liquid crystal to investigate the structure of PDLC under scanning electron microscopy [3, 107, 197, 216, 233, 234]. Also, there is one researcher who made the polymer matrix first using emulsion method (Section 4.2.1), and filled the matrix with undoped liquid crystal afterwards [229]. Although the techniques of DPDLC and SPDLC seems to involve somewhat similar processes and ideas, the methods are unique in the sense that the droplet size can be controlled easily, and they allow a more detailed study of PDLC doped with light sensitive dye and LC. Moreover, the fast decay time proves the method to be of scientific and commercial interest.

Chapter 5: Conclusions

In Chapter 2, the dichroic ratio and order parameter of the highly dipolar MORPIP dye, D2 azo dye, D16 anthraquinone dye, and B2 dye mixture were first determined (Section 2.4.2). D2 and D16 dyes were used as reference materials, and the values obtained from the measurements were consistent with the manufacturer's data sheet. MORPIP was found to give a dichroic ratio of 2.34 ± 0.404 and an order parameter of 0.309 ± 0.064, which are low values for dichroic dyes, but not surprising given the molecular shape. However, B2 was found to have a dichroic ratio of 11.8 ± 2.173, and an order parameter of 0.783 ± 0.034. Both of these values were higher than the values for D2 dye which is known to posses relatively high values for its dichroic ratio and order parameter compared with other commercially available dyes. The photostability of the dyes were tested, and it was found that MORPIP was the least stable dye with a half-life of 7.153 days under the specific condition of UV irradiation employed. No significant deterioration of the other dyes was observed, and the use of a stronger UV light source and a long term irradiation is expected to determine the deterioration rates for those commercial dyes.

Despite the unfavourable dichroic ratio and order parameter results for MORPIP, Chapter 3 revealed the usefulness of this highly dipolar dye. MORPIP decreased the rise time of 5CB liquid crystals by 18% with 2.0 wt%

doping (Section 3.4.3.1). The decay time of MORPIP doped 5CB showed no change (Section 3.4.2). Moreover, the rise time of E7 was decreased by 21% with the doping of a mere 0.5 wt% (Section 3.4.3.2). The response speed and the threshold electric field were calculated. The E_0 value of MORPIP (0.23 V/μm) was 19% smaller than that of undoped cell (0.28 V/μm), while the other dyes increased the E_0 values up to 10.7%. The large dipole of MORPIP reduced E_0 and shorted the effective rise time especially at low electric field (Section 3.4.3.2). An enhancement in dielectric anisotropy was thought to be a possible reason for the decrease in E_0, but no change in dielectric anisotropy has been detected (Section 3.4.4).

Since the dielectric anisotropy did not change with MORPIP concentration, there must be another mechanism of decreasing the rise time of the doped liquid crystals. A steric interaction, rather than dipole-dipole interaction, due to a large inertia between adjacent LC molecules and MORPIP may be the cause of this effect; dragging the liquid crystal molecules by the dipolar molecule leading to an effective decrease in elastic constant. The similar effect had been reported for the optical control of LC alignment *command surface*. A further direct measurement of the elastic constant, dielectric anisotropy and rotational viscosity may help to clarify the effect.

A systematic response time measurement of various dipolar and non-dipolar liquid crystals incorporating molecules with various dipole moments, increased solubility, better compatibility with liquid crystals, dyes with various

shapes, and dyes similar to Wu *et al.* (Figure 3-12) would help in obtaining the broader picture of the effect.

Following the investigation of the GH effects in the previous chapters, Chapter 4 was devoted to the exploration of the GH effect in PDLCs, in order to explore the possibility of a reflective type PDLC display. Conventional PDLCs were made successfully using the UV initiated phase separation method (Section 4.3.2). By varying the proportion of liquid crystal to the polymer, other morphologies could also be made, such as polymer network type and polymer droplet type PDLC. For the PDLC system employed in this work, the optimised scattering of the undoped PDLC was found to be achieved by setting the curing distance of 10 cm from a cell to the UV lamp (Section 4.3.3) and curing for 50 ± 7 seconds (Section 4.3.4) Furthermore, the cure time required for MORPIP doped PDLC was the same as undoped PDLC. However, the time required to cure most doped PDLCs was much longer: 120 seconds for D16 doped PDLC, and 210 seconds for D2 doped PDLC. The droplet sizes of MORPIP doped PDLC were observed by the polarising microscope to be unaffected by the cure time, hence the response time of the PDLCs with different concentrations of MORPIP were able to be compared. It was therefore shown that the rise time decreases by as much as 45% with increasing concentration of MORPIP (Section 4.3.6). This was similar to the result obtained with a MORPIP doped Heilmeier type liquid crystal cell (Section 3.4.3). Red, yellow and blue PDLCs were made successfully, but they showed very poor contrast (Section 4.3.7).

The sources of the problems were determined to be a poor off-state scattering (due to long cure time) and poor on-state transmittance (due to the dyes trapped in the polymer matrix). Hence two unique fabrication methods were proposed to overcome the problems of long curing and trapping. These methods overcame the problem of dye deterioration during curing, and they were further developed. Some of this work was carried out in collaboration with Mr. Tony Roberts [167].

The first fabrication method (Section 4.4.1) was named Dispersed PDLC (DPDLC). This method involves forcing doped liquid crystal "in", and consequently pushing undoped liquid crystal "out" of a pre-formed PDLC. This technique avoids exposing the dyes to UV, as well as the trapping of dyes in the matrix. The method is simple, and it proved to increase dye absorption by increasing effective path length of light due to scattering. However, this method can only be applied when the liquid crystal droplets are interconnected with each other, and it was not possible to fabricate a high scattering network type PDLC with E7-NOA65 combination.

The second fabrication method (Section 4.4.2) was named Sponge PDLC (SPDLC). It involves using a suitable solvent to wash the liquid crystal "out" from undoped PDLC to create a porous polymer matrix "sponge", and forcing the doped liquid crystal "in" to the empty porous polymer. This method allowed using a 50:50 mixture of PDLC in order to maximise scattering. This resulted in achieving the higher contrast of 3 (Section 4.4.3) compared to any of the dichroic PDLC made in this study. The preliminary

results show that, compared to the conventional PDLC, an undoped SPDLC has a 34% increase in the threshold voltage to 12V (Section 4.4.4), a 100% longer rise time of 30 ms, but a 73% shorter decay time of 30 ms (Section 4.4.5). Although the threshold voltage and rise time were slightly increased, these drawbacks are considerably out weighed by the notably shorter decay time, thus making this method useful for display applications. The only disadvantage of the SPDLC method was its week-long fabrication time owing to the slow diffusion of acetone into the PDLC. It is essential to improve this fabrication speed, and carry out a thorough study of doped SPDLCs.

Using these methods for fabricating Dispersed PDLC and Sponge PDLC opens up a wide selection of materials. It is now possible to use dyes with high solubilities in polymer. These two methods are unique in the sense that the droplet size can be controlled easily, and they allow a more detailed study of the PDLC doped with a light sensitive dye and liquid crystal. Using these fabrication techniques, it is now possible to make PDLCs doped with light sensitive, highly dipolar dyes such as DEMI and ULTRA (Section 4.3.5). It is possible to study how the absorption of the PDLC is affected by the scattering for a range of dyes without the problems of dye stability and solubility in the polymer matrix. Moreover, the fast decay time of the method is of scientific and commercial interest. For future work, the effect of the anchoring should be first explored by trying different solvents to wash-out the LC to establish whether the solvent is causing the change in the wetting of

the polymer wall. There is a possibility that the monomer left in the LC may be acting as a lubricant at the polymer wall. This idea could be tested further by the intentional incorporation of a monomer in the LC. For the development of a paper-like display incorporating SPDLC, viewing angle measurement using reflection studies, and fabrication of a dye doped PDLC on a flexible substrate [235] must be carried out in the future. It is necessary to investigate material selection, LC/Polymer composition, curing conditions and matrix morphology for further optimisation of PDLCs and SPDLCs. For example, synthesis of TCNQ molecules with a long alkyl chain may be carried out in order to increase the dye compatibility to liquid crystal molecules and observing the GH effect more clearly. Different kinds of liquid crystal such as fluorinated ones rather than those with cyano groups may show different GH effects. The SPDLC method can be applied to PDLCs prepared by different fabrication techniques such as the emulsion method, which allows investigation of the anchoring effect with different types of polymers. These works would provide the basis for on-going research.

BIBLIOGRAPHY

1. Fergason, J.L., *SID Int. Symp. Digest of tech. Papers*, 1985. **16**: p.68.

2. Fergason, J.L., 1984, 4 435 047, US Patent.

3. Drzaic, P.S., *J. App. Phys.*, 1986. **60** (6): p.2142-2148.

4. Doane, J.W., Vaz, N.A., Wu, B.G., and Zumer, S., *App. Phys. Lett*, 1986. **48** (4): p.269-271.

5. Drzaic, P.S., *Pure App. Chem*, 1996. **68** (7): p.1435-1440.

6. Wu, J.J., Wang, C.M., and Chen, S.H, *Jpn. J. App. Phys. Pt. 1 - Reg. Pap.*, 1996. **35** (5A): p.2681-2685.

7. Zharkova, G.M., Streltsov, S.A., and Khachaturyan, V.M., *Mol. Cryst. Liq. Cryst. Tech. Sec. a*, 1995. **265**: p.435-444.

8. Zharkova, G.M., Streltsov, S.A., and Khachaturyan, V.M., *J. Struct. Chem*, 1993. **34** (6): p.930-933.

9. Yasuda, A., Bloor, D., Cross, G.H, Love, G.D., and Masutani, A., 2000, 01110255.5, European Patent.

10. Masutani, A., Yasuda, A., Bloor, D., Cross, G.H, and Love, G.D., 2002, under application, European Patent.

11. Reinitzer, F., *Montash Chem*, 1888. **9**: p.421.

12. Lehmann, O., Z. *Krist.*, 1890. **18**: p.464.

13. Williams, R., *Nature*, 1963. **199**: p.273.

14. Williams, R., *J. Chem Phys.*, 1963. **39** (2): p.384.

15. Williams, R., May 30 1967, 3,322,485, US Patent.

16. Heilmeier, G.H, *App. Phys. Lett*, 1968. **13**: p.46.

17. Heilmeier, G.H, *Proc. IEEE*, 1968. **56**: p.1162.

18. Heilmeier, G.H, *App. Eng*, 1968. **11**: p.21.

19. Kelker, H, *Angew Chem - Int. Edit Engl.*, 1969. **8** (11): p.884.

20. Gray, G.W. Liquid Crystals and Ordered Fluids, ed. J.F. Johnson and R.S. Porter. Vol. 2. 1974: Plenum.

21. Schadt, M. and Helfrich, W., *App. Phys. Lett.*, 1971. **18**: p.127.

22. *Merck (UK) Ltd., E7 datasheet*, 1999.

23. de Gennes, P.G., *The physics of liquid crystals*. 1974, London: Oxford University Press.

24. Gray, G.W. and Winsor, P.J., *Liquid crystals and plastic crystals*. 1974, Chichester: Ellis Horwood.

25. Chandrasekhar, S., *Liquid crystals*. 1977, London: Cambridge University Press.

26. Brown, G.H., *Advances in liquid crystals*. Vol. I, II, III, IV and V. 1975-82, New York and London: Academic Press.

27. Saeva, F.D., *Liquid crystals - The fourth state of matter*. 1979, New York: Marcel Dekker, Inc.

28. Friedel, G., *Ann. Phys.*, 1922. **9** (18): p.273.

29. Gray, G.W. and Goodby, J., *Smectic liquid crystals: Textures and structures*. 1984: Leonard Hill.

30. Greenfield, M.S., *Properties of BL001 and 5CB*, 1999, private communication.

31. Pohl, L., *Physical Properties of Liquid Crystals*. Liquid Crystals Applications and Uses, ed. B. Bahadur. Vol. 1. 1990, Singapore: World Scientific. 139.

32. Chatelain, P., *Bull. Soc. Min.*, 1943. **66**: p.105.

33. Zocher, H. and Birstein, K., *Z. Phys. Chem*, 1973. **24**: p.59.

34. Haas, W., *Phys. Rev. Lett.*, 1970. **25**: p.1326.

35. Kahn, F., *App. Phys. Lett.*, 1973. **22**: p.386.

36. Frank, F.C., *Discussions Faraday Soc*, 1958. **25**: p.19.

37. Blinov, L.M., *Electro-optical and magneto-optical properties of liquid crystals*. 1983: John Wiley & Sons. 116-118.

38. De Gennes, P.G., *Solid State Comm*, 1968. **6**: p.163.

39. Freedericksz, V. and Zolina, V., *Trans. Faraday Soc*, 1933. **29**: p.931.

40. Trufanov, A.N., Blinov, L.M., and Barnik, M.I., *Zhurnal Eksperimentalnoi I Teoretioheskoi Fiziki*, 1980. **78**: p.622.

41. Blinov, L.M. and Chigrinov, V.G., *Electrooptic Effects in Liquid Crystal Materials*. 1993, New York: Springer-Verlag.

42. Heilmeier, G.H. and Zanoni, L.A., *App. Phys. Lett.*, 1968. 13 (3): p.91-92.

43. Hilsum, C., 1976, 1,442,360, UK Patent.

44. Doane, J.W., *Polymer Dispersed Liquid Crystal Displays*. Liquid Crystals Applications and Uses, ed. B. Bahadur. Vol. 1. 1990, Singapore: World Scientific. 361.

45. Park, N.H., Park, S.I., and Suh, K.D., *Coll. Poly. Sci.*, 2001. **279** (11): p.1082-1089.

46. Craighead, H.G., Cheng, J., and Hackwood, S., *App. Phys. Lett.*, 1982. 40 (1): p.22-24.

47. West, J.L., *Acs Sym Series*, 1990. **435**: p.475-495.

48. Kitzerow, H.S., *Liq. Cryst.*, 1994. 16 (1): p.1-31.

49. Doane, J.W., Golemme, A., West, J.L., Whitehead, J.B., and Wu, B.G., *Mol. Cryst. Liq. Cryst.*, 1988. **165**: p.511-532.

50. Bai, Y., Chen, X., Wan, X., Zhou, Q.F., Liu, H., Zhang, B., and Gong, Q., *App. Phys. B*, 2001. **73** (1): p.35-37.

51. *Polymers & Liquid Crystals*, 1999.
    http://plc.cwru.edu/tutorial/enhanced/files/pdlc/droplet/droplet.htm.

52. Yamaguchi, R., Waki, Y., and Sato, S., *J. J. App. Phys. Pt. 1*, 1997. **36** (5A): p.2771-2774.

53. Kim, B.K., Hong, E.Y., and Ok, Y.S., *Korea Polymer Journal*, 1997. 5 (2): p.77-83.

54. Park, N.H., Cho, S.A., Kim, J.Y., and Suh, K.D., *J. App. Poly. Sci.*, 2000. 77 (14): p.3178.

55. Yasuda, A., *Sony International (Europe) GmbH*, 1999, private communication.

56. Bahadur, B., Sarna, R.K., and Bhide, V.G., *Mol. Cryst. Liq. Cryst.*, 1981. 75 (1-4): p.121-132.

57. Seki, H., Uchida, T., and Shibata, Y., *Mol. Cryst. Liq. Cryst.*, 1986. **138** (1-4): p.349-365.

58. Ivashchenko, A.V. and Rumyantsev, V.G., *Mol. Cryst. Liq. Cryst.*, 1987. **150**: p.3-167.

59. Bahadur, B., *Dichroic Liquid Crystal Displays*. Liquid Crystals: Applications and Uses, ed. B. Bahadur. Vol. 3. 1992, Singapore: World Scientific. 65-208.

60. Uchida, T. and Wada, M., *Mol. Cryst. Liq. Cryst.*, 1981. **63** (1-4): p.19-43.

61. Rumyantsev, V.G., Ivashchenko, A.V., Muratov, V.M., Lazareva, V.T., Prudnikova, E.K., and Blinov, *Mol. Cryst. Liq. Cryst.*, 1983. **94** (1-2): p.205-212.

62. Bauman, D., *Mol. Cryst. Liq. Cryst.*, 1989. **172**: p.41-50.

63. Scheffer, T.J., *J. App. Phys.*, 1982. **53** (1): p.257.

64. Mitsubishi-Chemical-Corporation, *Dichroic Dyes for Colored Liquid Crystal - Technical Information*, 2000.

65. Seki, H., Shishido, C., Yasui, S., and Uchida, T., *Jpn. J. App. Phys. Pt. 1*, 1982. **21** (1): p.191-192.

66. Cognard, J., Phan, T.H., and Basturk, N., *Mol. Cryst. Liq. Cryst.*, 1983. **91** (3-4): p.327-340.

67. Basturk, N., Cognard, J., and Phan, T.H., *Mol. Cryst. Liq. Cryst.*, 1983. **95** (1-2): p.71-89.

68. Bauman, D., *Mol. Cryst. Liq. Cryst.*, 1988. **159**: p.197-218.

69. Raj, D., *Mat. Chem. Phys.*, 1996. **43** (3): p.204-211.

70. Salamon, Z. and D., B., *Mol. Cryst. Liq. Cryst.*, 1982. **82** (4): p.115.

71. Hasse, W., *Gen. Rel. Grav*, 1987. **19** (5): p.515.

72. Bahadur, B., *Mol. Cryst. Liq. Cryst.*, 1991. **209**: p.39-61.

73. Pellatt, M.G., Roe, I.H.C., and Constant, J., *Mol. Cryst. Liq. Cryst.*, 1980. **59**: p.299.

74. Aftergut, S. and Cole, H.S., *Mol. Cryst. Liq. Cryst.*, 1982. **89** (1-4): p.37-45.

75. Seki, H., Uchida, T., and Shishido, C., *Jpn. J. App. Phys.*, 1980. **19** (8): p.L501-L503.

76. Aftergut, S. and Cole, H.S., *Mol. Cryst. Liq. Cryst.*, 1990. **188**: p.147-153.

77. White, D.L. and Taylor, G.N., *J. App. Phys.*, 1974. **45**: p.4718.

78. Rumyantsev, V.G., Blinov, L.M., and Kizel, V.A., *Kristallografiya*, 1973. **18**: p.1101.

79. Baur, G., Stieb, A., and Meier, G., *Mol. Cryst. Liq. Cryst.*, 1973. 22: p.261.

80. Matsui, M., Tanaka, N., Andoh, N., Funabiki, K., Shibata, K., Muramatsu, H., Ishigure, Y., Kohyama, E.N., Abe, Y., and Kaneko, M., *Chem. Mat.*, 1998. 10 (7): p.1921-1930.

81. Cox, R.J., *Mol. Cryst. Liq. Cryst.*, 1979. 55: p.1.

82. Gray, G.W., *Chimica*, 1980. 34: p.47.

83. Ivashchenko, A.V. and Rumyantsev, V.G., *Mol. Cryst. Liq. Cryst.*, 1987. 150A: p.1.

84. Bloom, A. and Hung, P.L.K., *Mol. Cryst. Liq. Cryst.*, 1977. 40: p.213.

85. Constant, J., Kirton, J., Raynes, E.P., Shanks, I.A., Coates, D., Gray, G.W., and McDonell, D.G., *Electron. Lett.*, 1976. 12: p.514.

86. Cognard, J. and Phan, T.H., *Mol. Cryst. Liq. Cryst.*, 1981. 68: p.207.

87. Jones, F. and Reeve, T.J., *Mol. Cryst. Liq. Cryst.*, 1980. 60: p.99.

88. Cognard, J. and Phan, F.H.T., *Mol. Cryst. Liq. Cryst.*, 1981. 70 (1-4): p.1279.

89. Uchida, T., Shishido, C., Seki, H., and Wada, M., *Mol. Cryst. Liq. Cryst. Lett.*, 1977. 34: p.153.

90. Uchida, T., Shishido, C., Seki, H., and Wada, M., *Mol. Cryst. Liq. Cryst.*, 1977. 39: p.39.

91. Hung, P.L.K. and Bloom, A., *Mol. Cryst. Liq. Cryst.*, 1980. 59: p.1.

92. Jones, F. and Kirby, F.A., *Mol. Cryst. Liq. Cryst.*, 1984. 108 (1-2): p.165-175.

93. Pelzl, G., Zaschke, H., and Demus, D., *Displays*, 1985: p.141.

94. Pelzl, G., Schubert, H., Zaschke, H., and Demus, D., *Kristall and Technik*, 1979. 14: p.817.

95. Imazeki, S., Mukoh, A., Yoneyama, T., and Kaneko, M., *Mol. Cryst. Liq. Cryst.*, 1987. 145: p.79.

96. Praefcke, K., Schmidt, D., and Naturforsch, Z., *Z. Naturforsch*, 1981. 86b: p.375.

97. Yano, S., Kato, S., Kano, M., and Kamijo, Y., *Mol. Cryst. Liq. Cryst.*, 1985. 123 (1-4): p.179.

98. Bloom, A. and Hung, P.L.K., *Mol. Cryst. Liq. Cryst.*, 1978. 44: p.323.

99. Iwanaga, H., Naito, K., Sunohara, K., and Okajima, M., *Bull. Chem. Soc. Jpn*, 1998. 71 (7): p.1719-1723.

100. Veghely, T., *Mol. Cryst. Liq. Cryst.*, 1982. 80: p.35.

101. Bahadur, B., *Display parameters and requirements*. Liquid Crystals: Applications and Uses, ed. B. Bahadur. Vol. 2. 1991, Singapore: World Scientific. 1-120.

102. Sceuble, B.S., Weber, G., Pohl, L., and Jubb, R.E., *SID digest*, 1983: p.176.

103. Prasad, P.N. and Williams, D., *Introduction to nonlinear optical effects in molecules and polymers*. 1991, New York: Wiley-Interscience. 306.

104. Kanis, D.R., Ratner, M.A., and Marks, T.J., *Chem. Rev*, 1994. 1994 (94): p.195-242.

105. Heeger, A.J., Orenstein, J., and Ulrich, D.R., *Nonlinear optical properties of polymers*. Materials research society symposium proceedings, ed. A.J. Heeger, J. Orenstein, and D.R. Ulrich. Vol. 109. 1987, Pittsburgh: Materials Research Society. 390.

106. Whitehead Jr, J.B., Gill, N.L., and Adams, C., *Proc SPIE*, 2000. 4107: p.189.

107. Kalkar, A.K., Kunte, V.V., and Deshpande, A.A., *J. App. Poly. Sci.*, 1999. 74 (14): p.3485.

108. Kagawa, Y., *New Tetracyanoquinodimethane Chromophores, Synthesis and Physical Properties*. Department of Physics. 1998, Durham: University of Durham, PhD Thesis.

109. Palsson, L.O., Kay, A.J., Szablewski, M., Roberts, A., Masutani, A., Love, G.D., Cross, G.H., Woolhouse, A.D., Yasuda, A., and Bloor, D., *Mol. Cryst. Liq. Cryst.*, 2002. in preparation.

110. Bloor, D. and Kagawa, Y., in preparation.

111. Chemla, D.S. and Zyss, J., *Nonlinear Optical Properties of Organic Molecules and Crystals*. 1987, New York: Academic.

112. Kepler, R.G., Bierstedt, P.E., and Merrifield, R.E., *Phys. Rev Lett.*, 1960. 5 (11): p.503.

113. Acker, D.S., Harder, R.J., Hertler, W.R., Mahler, W., Melby, L.R., Benson, R.E., and Mochel, W.E., *J.A.C.S.*, 1960. 85: p.6408.

114. Acker, D.S. and Blomstrom, D.C., 1963, 3,115,506, US Patent.

115. Acker, D.S., Waynesboro, V.A., and Blomstrom, D.C., 1964, 3,162,641, US Patent.

116. Acker, D.S. and Hertler, W.R., *J.A.C.S.*, 1962. **84**: p.3370-3374.

117. Melby, L.R., Harder, R.J., Hertler, W.R., Mahler, W., Benson, R.E., and Mochel, W.E., *J.A.C.S.*, 1962. **84**: p.3374-3387.

118. Hertler, W.R., Harzler, H.D., Acker, D.S., and Benson, R.E., *J.A.C.S.*, 1962. **84**: p.3387-3390.

119. Fouquey, C., Lehn, J.M., and Malthete, J., *J. Chem Soc - Chem Comm*, 1987 (19): p.1424-1426.

120. Wu, S.T., Margerum, J.D., Ho, M.S., and Fung, B.M., *App. Phys. Lett.*, 1994. **64** (17): p.2191-2193.

121. Kamada, K., Ueda, M., Nagao, H., Tawa, K., Sugino, T., Shmizu, Y., and Ohta, K., *J. Phys. Chem*, 2000. **A 104**: p.4723-4734.

122. Blanchard-Desce, M., Alain, V., Midrier, L., Wortmann, R., Lebus, S., Glania, C., Kraemer, P., Fort, A., Muller, J., and Barzoukas, M., *J. Photochem Photobio. A: Chem*, 1997. **105**: p.115-121.

123. Verbiest, T., Houbrechts, S., Kauranen, M., Clays, K., and Persoons, A., *J. Mat. Chem*, 1997. **7** (11): p.2175-2189.

124. Meyers, F., Marder, S.R., Pierce, B.M., and Bredas, J.L., *Chem Phys. Lett.*, 1994. **228**: p.171-176.

125. Sheng, Y. and Jiang, Y., *J. Chem Soc, Faraday Transactions*, 1998. **94** (13): p.1823-1828.

126. Boldt, P., Bourhill, G., Brauchle, C., Jim, Y., Kammler, R., Muller, C., Rase, J., and Wichern, J., *Chem Comm*, 1996 (6): p.793-795.

127. Lambert, C., Stadler, S., Bourhill, G., and Brauchle, C., *Angew Chem - Int. Edit Engl.*, 1996. **35** (6): p.644-646.

128. Bourhill, G., Bredas, J.L., Cheng, L.T., Marder, S.R., Meyers, F., Perry, J.W., and Tiemann, B.G., *J.A.C.S.*, 1994. **116** (6): p.2619-2620.

129. Szablewski, M., *Multi-Functional D-p-A Materials for Molecular Electronics.* Cranfield Institute of Technology. 1991, Cranfield: Cranfield Institute of Technology. 244, Ph.D. Thesis.

130. Szablewski, M., *J. Org Chem*, 1994. **59**: p.954-956.

131. Szablewski, M., Thomas, P.R., Thornton, A., Bloor, D., Cross, G.H., Cole, J.M., Howard, J.A.K., Malagoli, M., Meyers, F., Bredas, J.L., Wenseleers, W., and Goovaerts, E., *J.A.C.S.*, 1997. **119** (13): p.3144.

132. Szablewski, M., Ravi, M., Cole, J.M., Teat, S.J., and Maclean, E.J., in Preparation.

133. Ivashchenko, A., *Dichroic dyes for liquid-crystal displays*. 1994: CRC Press, Inc.

134. Bauman, D., Moryson, H., and Jadzyn, J., *Acta Physica Polonica a*, 1994. **85** (3): p.553-562.

135. Seki, H., Shishido, C., Uchida, T., and Wada, M., *Mol. Cryst. Liq. Cryst.*, 1981. **66** (1-4): p.529-538.

136. Morouzmi, S., *Materials and Assembling Process of LCDs*. Liquid Crystals: Applications and Uses, ed. B. Bahadur. Vol. 1. 1990, Singapore: World Scientific. 171.

137. Bahadur, B., *Mol. Cryst. Liq. Cryst.*, 1984. **109** (1): p.1-93.

138. Merck, *Liquid crystals - Advanced Material Division Datasheet 12 - Dichroic Dyes*.

139. Bauman, D. and Moryson, H., *J. Mol. Str.*, 1997. **404** (1-2): p.113-120.

140. Wu, S.T., Zhang, Q.T., and Marder, S., *Jpn. J. Appl. Phys. Pt. 2 - Lett.*, 1998. **37** (10B): p.L1254.

141. Coles, H.J., Gleeson, H.F., and Kang, J.S., *Liq. Cryst.*, 1989. **5** (4): p.1243-1252.

142. Bauman, D., Kuball, H. G., *Chem Phys.*, 1993. **176** (1): p.221.

143. Dreyer, F., 1946, 2,400,877, US Patent.

144. Bahadur, B., *Mol. Cryst. Liq. Cryst.*, 1983. **99** (1-4): p.345-374.

145. Bauman, D., Skibinski, A., and Stolarski, R., *Mol. Cryst. Liq. Cryst.*, 1986. **138** (1-4): p.367.

146. Wolarz, E., Moryson, H., and Bauman, D., *Displays*, 1992. **13** (4): p.171-178.

147. Simoni, F., Di Bella, S., Lucchetti, L., Cipparrone, G., and Mazzulla, A., *Mat. Res. Soc. Symp. Proc*, 1999. **559**: p.65.

148. Blinov, L.M., Kozlovsky, M.V., Ozaki, M., and Yoshino, K., *Mol. Cryst. Liq. Cryst. Sci. Tech. C- Mol. Mat.*, 1996. **6** (4): p.235-252.

149. Heilmeier, G.H., Castellano, J.A., and Zanoni, L.A., *Mol. Cryst. Liq. Cryst.*, 1969. **8**: p.293.

150. Bauman, D. and Z., S., *Opt. Comm*, 1984. **48** (5): p.306.

151. Kozielski, M., D., B., M., D., and Z., S., *Mol. Cryst. Liq. Cryst.*, 1987. **142** (1-4): p.1.

152. Bauman, D., Fan, Z.X., and Haase, W., *Act. Phys. Pol. A*, 1991. **80** (4): p.545-552.

153. Bauman, D., Martynski, T., and Mykowska, E., *Liq. Cryst.*, 1995. **18** (4): p.607-613.

154. Diot, P., Jk, F., and W., H., *Rev. Phys. App.*, 1985. **20** (3): p.121.

155. Bauman, D. and Haase, W., *Mol. Cryst. Liq. Cryst.*, 1989. **168**: p.155-168.

156. Bauman, D., *Mol. Cryst. Liq. Cryst.*, 1989. **174**: p.1.

157. Bauman, D., Czechowski, G., and Jadzyn, J., *Act. Phys. Pol. A*, 1989. **75** (5): p.697-703.

158. Scheffer, T.J., *Philos. Trans. R. Soc. Lond. Ser. A-Math. Phys. Eng. Sci.*, 1983. **309** (1507): p.189.

159. Wu, S.T. and Wu, C.S., *Phys. Rev. A*, 1990. **42** (4): p.2219.

160. van Dooorn, C.Z., *Phys. Lett. A*, 1973. **42A**: p.537.

161. Shiekel, M., Fahrenschon, K., and Gruler, H., *Appl. Phys.*, 1975. **7**: p.99.

162. Brochard, F., Pieranski, P., and Guyou, E., *Phys. Rev. Lett.*, 1972. **28** (26): p.1681.

163. Pieranski, P., Brochard, E., and Guyon, E., *J. Phys. France*, 1973. **34**: p.35.

164. Jakeman, E. and Raynes, E.P., *Phys. Lett.*, 1972. **39A** (1): p.69.

165. Saupe, A. and Naturforsch, Z., *J. App. Phys.*, 1960. **15a**: p.815.

166. Wu, S.T., Efron, U., and Hess, L.D., *App. Opt.*, 1984. **23** (21): p.3911.

167. Roberts, A., *in preparation.* Physics. 2001: University of Durham, Ph.D. Thesis.

168. Wu, S.T., Hsu, C.S., and Shyu, K.F., *App. Phys. Lett.*, 1999. **74** (3): p.344.

169. Ichimura, K., Suzuki, Y., Seki, T., Holoki, A., and Aoki, K., *Langmuir*, 1988. **4**: p.1214.

170. Ichimura, K., *Chem. Rev*, 2000. **100**: p.1847.

171. O'Neill, M. and Kelly, S.M., *J. Phys. D - App. Phys.*, 2000. **33** (10): p.R67-R84.

172. Atkins, P.W., *Physical Chemistry*. Fourth Edition ed. 1990: Oxford University Press. 502.

173. Vandegaer, J.E., *Microencapsulation; Processes and Applications*. 1974: Plenum Press.

174. Elliot, G., January 5 1973, 2,139,537, France Patent.

175. West, J.L., *Mol. Cryst. Liq. Cryst.*, 1988. **157**: p.427-441.

176. Wu, B.G., West, J.L., and Doane, J.W., *J. App. Phys.*, 1987. **62** (9): p.3925-3931.

177. Golemme, A., Zumer, S., Doane, J.W., and Neubert, M.E., *Phys. Rev A*, 1988. **37** (2): p.559-569.

178. Vaz, N.A., Smith, G.W., and Montgomery, G.P., *Mol. Cryst. Liq. Cryst.*, 1987. **146**: p.17-34.

179. Smith, G.W. and Vaz, N.A., *Liq. Cryst.*, 1988. 3 (5): p.543-571.

180. Vaz, N.A. and Montgomery, G.P., *J. App. Phys.*, 1987. **62** (8): p.3161-3172.

181. Yamaguchi, R. and Sato, S., *Jpn. J. App. Phys. Pt. 2-Lett*, 1991. **30** (4A): p.L616-L618.

182. Olabisi, O., Robeson, L.M., and Shaw, M.T., *Polymer-Polymer Miscibillity*. 1979, New York: Academic Press.

183. Cahn, J.W., *Trans. Metallurgical Soc. AIME*, 1968. **242**: p.166-180.

184. Nishi, T., *J. Macromol. Sci.-Phys.*, 1980. **B17**: p.517-542.

185. Hirai, Y., Niiyama, S., Kumaim, H., and Gunjima, T., *Proc SPIE*, 1990. **1257**: p.2-8.

186. Drzaic, P.S., *Liquid crystal dispersions*. Series on liquid crystals, ed. H.L. Ong. Vol. 1. 1995, Singapore: World Scientific Publishing.

187. Flory, P.J., *Principles of polymer chemistry*. 1953, Ithaca: Cornell University Press.

188. Maier, W. and Saupe, A., Z. *Naturforsch*, 1959. **Teil A** (14): p.882.

189. Maier, W. and Saupe, A., Z. *Naturforsch*, 1960 (15): p.287.

190. deGennes, P.G., *The Physics of Liquid Crystal*. 1993, London: Oxford Scientific Publications, Oxford University Press.

191. McMillan, W.L., *Phys RevA*, 1971. **4**: p.1238.

192. Kyu, T. and Chiu, H.W., *Polymer*, 2001. **42** (21): p.9173-9185.

193. Drzaic, P.S., Wiley, R.C., and McCoy, J., *Proc SPIE*, 1989. **1080**: p.41.

194. West, J.L., Tamura-Lis, W., and Ondris, R., *Proc SPIE*, 1989. **1080**: p.48.

195. Drzaic, P.S., *Displays*, 1991. **12** (1): p.2-13.

196. Coates, D., *Displays*, 1993. **14** (2): p.94-103.

197. Yamaguchi, R. and Sato, S., *Liq. Cryst.*, 1993. **14** (4): p.929-935.

198. Drzaic, P.S. and Gonzales, A.M., *SPIE Liquid Crystal Materials, Devices and Applications*, 1992. **1665**: p.32.

199. Drzaic, P.S. and Gonzales, A.M., *Mol. Cryst. Liq. Cryst.*, 1992. **222**: p.11-20.

200. Smith, G.W. and Vaz, N.A., *Mol. Cryst. Liq. Cryst. Sci. Tech. Sec. A - Mol. Cryst. Liq. Cryst.*, 1993. **237**: p.243-269.

201. Rout, D.K. and Jain, S.C., *Jpn. J. App. Phys. Pt. 2 - Lett.*, 1991. **30** (8A): p.L1412-L1414.

202. Bouteiller, L. and LeBarny, P., *Liq. Cryst.*, 1996. **21** (2): p.157-174.

203. Coates, D., Greebfield, S., Goulding, M., Brown, E., and Nolan, P., *SPIE Liquid Crystal Materials, Devices and Applications*, 1993. **1911**: p.2.

204. Nolan, P., Tillin, M., and Coates, D., *Liq. Cryst.*, 1993. **14** (2): p.339-344.

205. Choi, C.H., Kim, B.K., Kikuchi, H., Kajiyama, T., Amaya, N., and Murata, Y., *J. App. Poly. Sci.*, 1993. **50** (12): p.2217-2222.

206. Fuh, A.Y.G., Ko, T.C., Chyr, Y.N., Huang, C.Y., Tzen, B.W., and Sheu, C.R., *Jpn. J. App. Phys. Pt. 1 - Reg. Pap.*, 1993. **32** (8): p.3526-3529.

207. Fuh, A. and Caporaletti, O., *J. App. Phys.*, 1989. **66** (11): p.5278-5284.

208. Yamaguchi, R. and Sato, S., *Jpn. J. App. Phys. Pt. 2 - Lett.*, 1992. **31** (3A): p.L254-L256.

209. Golemme, A., Zumer, S., Allender, D.W., and Doane, J.W., *Phy. Rev Lett.*, 1988. **61** (26): p.2937-2940.

210. Montgomery, G.P., West, J.L., and Tamuralis, W., *J. App. Phys.*, 1991. **69** (3): p.1605-1612.

211. Lackner, A.M., Margerum, J.D., Ramos, E., and Lim, K.C., *SPIE Liq. Cryst. Chem, Phys. and App.*, 1989. **1080**: p.267.

212. Montgomery, G.P. and Vaz, N.A., *Applied Optics*, 1987. **26** (4): p.738-743.

213. Whitehead, J.B., Zumer, S., and Doane, J.W., *Proc SPIE*, 1989. **1080**: p.250.

214. Ono, H. and Kawatsuki, N., *Kobunshi Ronbunshu*, 1995. **52** (4): p.195-206.

215. Akins, R.B. and West, J.L., *Proc SPIE*, 1992. **1665**: p.280.

216. Yamaguchi, R. and Sato, S., *Jpn. J. App. Phys. Pt. 1 - Reg. Pap.*, 1994. **33** (7A): p.4007-4011.

217. Drzaic, P.S., *Liq. Cryst.*, 1988. 3 (11): p.1543-1559.

218. Wu, B.G., Erdmann, J.H., and Doane, J.W., *Liq. Cryst.*, 1989. **5** (5): p.1453-1465.

219. Erdmann, J., Doane, J.W., Zumer, S., and Chidichimo, G., *Proc SPIE*, 1989. **1080**: p.32.

220. Smith, G.W., *Mol. Cryst. Liq. Cryst.*, 1991. **196**: p.89-102.

221. Norland Products, I., *Norland Optical Adhesive 65 data sheet.*

222. Vaz, N.A., Smith, G.W., and Montgomery, G.P., *Mol. Cryst. Liq. Cryst.*, 1987. **146**: p.1-15.

223. Braun, D., Frick, G., Grell, M., Klimes, M., and Wendorff, J.H., *Liq. Cryst.*, 1992. **11** (6): p.929-939.

224. Yamagishi, F.G., Miller, L.J., and van Ast, C.I., *Proc SPIE*, 1989. **1080**: p.24.

225. Stark, H., *Eur. Phys. J. B*, 1999. **10** (2): p.311-321.

226. Fukuda, J. and Yokoyama, H., *Eur. Phys. J. E*, 2001. 4 (3): p.389-396.

227. Ren, Y.T., Szablewski, M., and Cross, G.H., *App. Opt.*, 2000. **39** (15): p.2499.

228. Montgomery, G.P., Vaz, N.A., and Smith, G.W., *Mol. Cryst. Liq. Cryst.*, 1993. **225**: p.131-151.

229. Andreau, A., Farhi, R., Tarascon, J.M., and Gisse, P., *Liq. Cryst.*, 2000. **27** (1): p.1.

230. Chang, S.J., Lin, C.M., and Fuh, A.Y.G., *Liq. Cryst.*, 1996. **21** (1): p.19-23.

231. Kim, J.B., Lee, M.G., and Choi, J.H., *Poly. Bull.*, 1998. **41** (1): p.37-43.

232. Kim, J.B., Lee, M.G., and Choi, J.H., *Poly. Bull.*, 1998. **41** (6): p.701-705.

233. Kajiyama, T., Kikuchi, H., Miyamoto, A., Moritomi, S., and Hwang, J.C., *Chem. Lett.*, 1989 (5): p.813-816.

234. Shimada, E. and Uchida, T., *Jpn. J. App. Phys. Pt. 2 - Lett.*, 1992. **31** (3B): p.L352-L354.

235. Kim, J.Y., Sohn, D., and Kim, E.R., *App. Phys. A*, 2001. **72** (6): p.699-704.